SYNTHESIS, CHARACTERIZATION AND APPLICATIONS OF ZnO NANOSTRUCTURES

Thesis submitted in the fulfillment for the requirements of the degree of

DOCTOR OF PHILOSOPHY

IN

Physics

BY

RICHA KHOKHRA

(Enrollment No. 116901)

DEPARTMENT OF PHYSICS AND MATERIALS SCIENCE

JAYPEE UNIVERSITY OF INFORMATION TECHNOLOGY
WAKNAGHAT, SOLAN (H.P.) - 173234
INDIA

DECEMBER 2014

SYNTHESIS, CHARACTERIZATION AND APPLICATIONS OF ZnO NANOSTRUCTURES

thesis submitted in the fulfillment for the requirements of the degree of

DOCTOR OF PHILOSOPHY

IN

Physics

BY

RICHA KHOKHRA

(Enrollment No. 116901)

DEPARTMENT OF PHYSICS AND MATERIALS SCIENCE

JAYPEE UNIVERSITY OF INFORMATION TECHNOLOGY
WAKNAGHAT, SOLAN (H.P.) - 173234
INDIA

DECEMBER 2014

JAYPEE UNIVERSITY OF INFORMATION TECHNOLOGY
(Established by H.P. State Legislative vide Act No. 14 of 2002)
Waknaghat, P.O. Dumehar Bani, Kandaghat, Distt. Solan – 173234 (H.P.) INDIA
Website : www.juit.ac.in
Phone No. (91) 07192-257999 (30 Lines)
Fax: (91) 01792 245362

CERTIFICATE

This is to certify that the thesis entitled, **"Synthesis, Characterization and Applications of ZnO Nanostructures"** which is being submitted by **Richa Khokhra** in fulfillment for the award of degree of **Doctor of Philosophy** in **Physics** by the **Jaypee University of Information Technology, Waknaghat, India,** is the record of candidate's own work carried out by her under my supervision. This work has not been submitted partially or wholly to any other University or Institute for the award of this or any degree or diploma.

Dr. Rajesh Kumar

Department of Physics and Materials Science
Jaypee University of Information Technology
Waknaghat, India
Email: rajesh.kumar@juit.ac.in
Phone: +919418965337

JAYPEE UNIVERSITY OF INFORMATION TECHNOLOGY
(Established by H.P. State Legislative vide Act No. 14 of 2002)
Waknaghat, P.O. Dumehar Bani, Kandaghat, Distt. Solan – 173234 (H.P.) INDIA
Website : www.juit.ac.in
Phone No. (91) 07192-257999 (30 Lines)
Fax: (91) 01792 245362

DECLARATION

Certified that the work presented in this thesis entitled "**Synthesis, Characterization and Applications of ZnO Nanostructures**" is based on the original research work done by me under the supervision and guidance of Dr. Rajesh Kumar, Assistant Professor, Department of Physics and Materials Science, Jaypee University of Information Technology, Waknaghat (H.P.) has not been included in any other thesis submitted previously for the award of any degree.

Richa Khokhra
Department of Physics and Materials Science
Jaypee University of Information Technology

To my loving parents & family…

ACKNOWLEDGEMENT

It has been a great privilege to be a PhD student in the Department of Physics and Materials Science, Jaypee University of Information Technology, Waknaghat. It provides many opportunities for me to learn from courses, books and persons around me. This thesis is a result of three years of work from many persons who have accompanied and supported me. Whereby, I would like to express my sincere gratitude and appreciation to them.

First of all, I would like to express my foremost gratitude to my supervisor, **Dr. Rajesh Kumar** for his guidance and support in the course of my PhD studies. His strict requirements to my study progress greatly improve the quality of my work. He has given me large freedom to do my research, and allowed me to make my own mistakes and learn from them. Without his continuous support and trust I could not complete my PhD work. In addition, his optimistic life attitude always inspirits me in all aspects. I will learn him forever.

I extend my sincere thanks to **Prof. (Dr.) P. B. Barman,** Head of the Department of Physics and Materials Science for allowing me to use the facilities. I greatly acknowledge the help and guidance of all the faculty members of the Department of Physics and Materials Science right from the beginning of my research work.

Special thanks should be sent to **Prof. Heong-No Lee** (Director of INFONET Laboratory at Gwangju Institute of Science and Technology, Republic of Korea), **Dr. Raj Kumar Singh** (Scientist, CSIR-Indian Institute of Petroleum, Dehradun (Uttarakhand), India), and **Dr. Manoj Kumar** (Centre for Nanotechnology, Bharat Heavy Electricals Ltd., Hyderabad (A.P.), India) for their stimulating suggestions and huge help throughout my whole research work. Their compelling creativity and persistent enthusiasm toward science will always be my great source of inspiration.

I would like to express my gratitude to **Prof. S. K. Kak** (Vice Chancellor) and **Brig. (Retd.) Balbir Singh** (Director (Administration & Students Welfare)/Registrar) of Jaypee University of Information Technology, Waknaghat for their interest, encouragement and help during the course of my research tenure. I would like to thank the authorities of University for providing the financial support during my research work.

With a sense of gratitude, I am thankful to all the office and library staff of the University and the technical staff of Department of Physics and Materials Science for all the help and co-operation.

I remember my friends Sonika Goyal, Swati Gupta, Sarita Kango, Mamta Chauhan, Richa Prabhakar, Akanksha, Neha Kondal and Bhoomika Maheshwari for their valuable friendship and some memorable moments during various stages of my life. I would like to express my sincere appreciation to my colleagues in the Nanotechnology and Microwave Antenna lab of Department of Physics and Materials Science for their sincere help and co-operation throughout this work.

Finally, I would like to express my deepest love, respect and admiration to my parents and all members in my family for their unconditional support, understanding, and dedication throughout the years. The help, support and encouragement from my husband is sincerely appreciated.

I thank almighty God for showering his blessings always to provide me enormous patience, inspiration, faith and strength to carry out this research work.

(*Richa Khokhra*)

ABSTRACT

Zinc oxide (ZnO) nanostructures show many interesting physical and chemical properties, and thus have been suggested for various applications in optical, electronic and photocatalytic devices. ZnO due to their wide range of nanostructures like rods, belts, wire, flower-like etc. has attracted much attention in nanoscience based applications such as memory devices, storage devices nanolasers, light emitting diodes, solar cells, gas sensors, photocatalysts, photodetectors etc.

Owing to the properties and applications, the facile synthesis of ZnO nanostructures with highly controlled structures, uniform morphologies and novel properties has been a field of significant interest. Innovative and effective techniques have been carried out to synthesize ZnO nanostructures such as sol-gel, hydrothermal process, chemical vapor deposition etc. But most of these techniques need complicated equipment; severe conditions or preparation procedures are complex or also have difficulty in controllability.

In the present work, a facile solution route is used for the synthesis of ZnO nanostructures viz. nanosheets, flower-like structures and nanoparticles at room temperature without using a directing agent or template in the precursor solution. By changing the synthesis parameters such as concentration of precursor and alkali solution, reaction time, solvent and addition of surfactant, the ZnO structures of different morphologies have been formed. The effect of synthesis parameter on the morphology of ZnO structures has been studied. The method adopted in this study is comparatively cost effective and low temperature for the synthesis of variety of ZnO nanostructures.

We know that the ZnO restricts its use only in UV region, by exhibiting no response to the visible light as about 3 to 5% spectrum of sunlight falls in UV region limiting its photocatalytic efficiency in the presence of sunlight. The oxygen vacancy defects are kind of self-doping without addition of external impurities, which enhances the visible photocatalytic activity by narrowing the band gap. In addition, concentration of oxygen vacancy defects on the surface, shape and size of nanostructures, existence of facets and surface area are also discovered as important factors to enhance the photocatalytic activity of undoped ZnO. In this work, faceted ZnO nanosheets and flower-like structures having large surface area and oxygen vacancies have been synthesized and were used for sunlight photocatalytic purification of organic pollutant methylene blue dye from water. A comparative study of the photocatalytic performance of as synthesized ZnO nanostructures

(nanosheets and flower-like structures) is studied. Since the as synthesized ZnO structures have surface defects, they have also used for opto-electronic application (photodetector). The effect of the morphology of ZnO structures on the response of visible photodetector has been discussed.

The synthesized ZnO structures have also been used for the enhancement of numerical aperture of a Nikon lens. Since for the better image resolution in optical microscopy using a turbid lens, not only the NA but also the transmittance of the turbid lens should be high. In the present study, we have demonstrated that the morphology of the ZnO structures is also an important factor when using this material in front of objective lens in order to enhance the NA of an objective lens. Also, in this analysis while using ZnO morphologies as a turbid lens, optical experiments were performed in order to estimate the transmittance of the ZnO turbid lens films.

LIST OF PUBLICATIONS

International Journals:

1. **Richa Khokhra**, Manoj Kumar, Partha Bir Barman, Nitin Rawat, Hwanchol Jang, Rajesh Kumar and Heung-No Lee "Enhancing the numerical aperture of lenses using ZnO nanostructure-based turbid media" *Journal of Optics* 15 (2013) 125714, 6pp.

2. **Richa Khokhra**, Raj Kumar Singh and Rajesh Kumar "Effect of synthesis medium on aggregation tendencies of ZnO nanosheets and their superior photocatalytic performance" *Journal of Materials Science* 50(2) (2015) 819-832.

3. **Richa Khokhra** and Rajesh Kumar "Multicolor photodetection by ZnO nanostructures", (*Manuscript submitted*).

Conferences (National/International):

1. **Richa Khokhra** and Rajesh Kumar "Effect of Fe doping concentration on photocatalytic activity of ZnO nanosheets under natural sunlight" published in *AIP Conference Proceedings* (vol. 1661, 080014(2015)) through *International Conference on Condensed Matter Physics (ICCMP-2014)*, Himachal Pradesh University, Shimla (H.P.), India during 4-6 November 2014.

2. **Richa Khokhra** and Rajesh Kumar "Sunlight photocatalytic activity of transition metal-doped ZnO interwoven nanosheets for degradation of methylene blue" published in book "Nanotechnology: Novel Perspectives and Prospects" by *Mc-Graw Hill Education, India* (ISBN: 978-93-392-2109-6) through *International Conference on Nanotechnology in the service of health, environment & society (NanoSciTech-2014)*, Panjab University, Chandigarh, India during 13-15 February 2014.

3. **Richa Khokhra** and Rajesh Kumar, "Magnetic properties of Fe doped ZnO nanosheets fabricated on glass wafer by chemical method" *International Union of Materials Research Society-International Conference in Asia (IUMRS-ICA 2013)*, Bangalore, India during16-20 December 2013.

4. **Richa Khokhra**, Partha Bir Barman and Rajesh Kumar, "Synthesis of ZnO nanostructures on silicon wafer by wet chemical method" *National Conference on Advanced Materials and Radiation Physics (AMRP-2013)*, SLIET, Longowal (Punjab) India during 22-23 November 2013.

5. **Richa Khokhra** and Rajesh Kumar" Effect of KOH concentration on morphology of ZnO nanostructures" published in *International Journal of Engineering Research and Technology* (*IJERT*) through *National Conference on Multifunctional Advanced Materials (MAM-2013) Conference Proceedings*, Shoolini University, Solan (H.P.) India during 2-4 May, 2013.

CONTENTS

LIST OF FIGURES

LIST OF TABLES

Chapter-1

Introduction

1.1. Introduction

The word "nano" means 10^{-9}, so a nanometer is one-billionth of a meter. One definition of nanoscience is the study of atoms, molecules and objects, the size of which is in the range of about one to 100 nanometers. The term "nanotechnology" was defined by Professor Norio Taniguchi [1] as "*Nano-technology mainly consists of the processing, separation, consolidation and deformation of materials by one atom or one molecule*". The real burst of nanotechnology didn't come until the early 1990s. Because in the past decades, sophisticated instruments for characterization and manipulation such as Scanning Electron Microscopy (SEM), Transmission Electron Microscopy (TEM) and Scanning Probe Microscopy (SPM) became more available for researchers to approach the nano world. Device miniaturization in semiconductor industry is also a significant factor for the development of nanotechnology.

The field of nanotechnology explores the materials and their properties [2-8], when at least one dimension of the nanostructure is in one hundred nanometer range; a regime is referred to as the nanoscale. Basically the materials in nanoscale have only few atoms or the clusters of atoms, and the properties of the materials have been found to be changed because of the quantum confinement effect. Nanomaterials have structural features in between to those of atoms and bulk materials. They exhibit a variety of properties that are different and often considerably improved in comparison with those of conventional materials because of the very fine grain sizes and consequent high density of interfaces. Some of the nanomaterials properties include increased strength, hardness, improved ductility, reduced elastic modulus, higher electrical resistivity and superior soft magnetic properties etc. Because of the change in the properties of the materials in nano range, nanomaterials have become important for the new research. According to literature, nanomaterials in different forms have gained interest because of their different applications such as nanosensors [9], nanomagnets [10], nanoparticles in drug delivery [11] etc.

Instead of variety of properties shown by nanomaterials still there is infancy, the fields of nanotechnology and the nanoscience are not fully developed; still we need to go deeper to understand the better ways of synthesis so as to use the nano products for device applications at an easy way. We need to fully understand and explore the basic phenomenon at the atomic level. In fact the research in this field aims to discover the unique structures properties and synthesis

mechanisms so that the nanostructures can be produced commercially. Even though the nanotechnology and the nanoscience have meaningful impact to the world of research at large, the fundamental characteristics and the rules governing the nanostructures still have to be uncovered. To understand the fundamental phenomenon in the nano range it is quite reasonable to know the synthesis processes as well as the structure of materials at the atomic level for the effective growth of nanostructures for commercial purpose. In the present work, we have synthesized zinc oxide (ZnO) nanostructures by facile solution route. The growth of synthesized nanostructures is investigated by varying the synthesis parameter. These synthesized ZnO nanostructures were used for environmental, optical and opto-electronics application.

The ZnO is an inorganic semiconductor material. In the old days, it was used as a salve for eyes and open wounds by humans around 500BC or before [12]. Naturally, it is a mineral found as zincite, however the ZnO is obtained by synthesis [13]. Normally, ZnO is white in color and it does not dissolve into the water. The ZnO has wide applications as an additive in rubbers, plastics, ceramics, cement, lubricants, paints, ointments, adhesives, pigments and first-aid tapes etc. As a history of the ZnO, in the period of twelfth to the sixtieth century, the Zn and ZnO were produced in India and in the seventieth century, Zn manufacture moved to China. In 1743, the first European Zn smelter was established in Bristol, United Kingdom (UK) and Antoine Lavoisier introduced Zn in the periodic table of elements in 1789 [14]. In earlier days; the main usage of ZnO was in paints and additive to ointments. Even up to 1834, ZnO did not mix well with oil, and was used as a watercolor. The problem of not mixing with oil was solved by finding optimized condition to synthesize ZnO, and in 1845 the first oil paint was produced by using ZnO in Paris. By 1850, Zn white was produced throughout Europe. The Zn white paint got success with respect to the traditional white lead because the Zn white is permanent in sunlight as it is not blackened, non-toxic and more economical. The Zn white being very clean was used for making tints with other colors and because of this it was used as a ground for oil paintings [15]. In electronics industry, the ZnO was started to use in 1920's. For making radio sets, a schottky barrier was created by contacting ZnO crystal with a copper wire, providing the rectification needed to convert the alternating current (AC) radio waves to direct current (DC) signals [16].

The semiconducting properties of ZnO were first studied in early ninetieth century [17]. After its semiconducting properties were found, the research was mainly on the growth of ZnO, characterizations and applications. Up to the end of the twentieth century, the ZnO was widely used in semiconductor industry for making the many elevated temperature devices [18] and ultrasonic transducers in high-frequency regions [19]. The ZnO was under the scientific spotlight after 1990s, because the scientists working in the field of ZnO wanted to develop high quality and closely lattice matched substrate materials for GaN. The GaN due to its promising wide band gap had been used for short wavelength photonic applications, such as UV and blue light emitting diode (LED) and lasers [20]. In the past decades, the ZnO is extensively studied and many interesting properties have been discussed. The very interesting aspect of ZnO is that it is relatively simple for ZnO to form various nanostructures including highly ordered nanowire arrays, tower-like structures, nanorods, nanobelts, nanosprings and nanorings [21] etc. Since the physical and chemical properties depends upon the type of nanostructures, the ZnO has been found to be promising in many applications, such as sensing [22-24], catalysis [25-27], photovoltaic [28] and nano-generators [29, 30] etc. Moreover, the ZnO has high refractive index, high thermal conductivity, binding, antibacterial and good UV-protection properties [31].

1.2. General properties of ZnO

The ZnO crystallizes in either of wurtzite, zinc blende or rock salt crystal structures. The crystal structures of ZnO are shown in Fig. 1.1. In these structures, each anion is surrounded by four cations in tetrahedral coordination, and vice-versa having sp^3 covalent bonding. These compounds also have ionic nature which tends to enhance the band gap beyond the limit of covalent bonding. However, the large difference of the electro negativity of the two constituents of ZnO (Oxygen = 3.44 and Zinc = 1.65) is responsible for the strong ionic bonding between them. The ZnO is a wide direct band gap semiconductor whose ionicity lies at the boundary of ionic and covalent semiconductors. The most thermodynamically stable phase of ZnO is wurtzite under atmospheric conditions. In case of zinc blende, it is metastable phase and is stable only in case of hetero-epitaxial growth on cubic substrates (GaN) [32]. The rock salt is stable at relatively high pressures. ZnO also shows phase transition from the wurtzite (thermodynamically

stable) to the rocksalt phase in the range of 10 GPa high pressure. During this phase transition, there is reduction in volume by 17% [33]. This causes attenuation of lattice dimensions which leads to the interionic coulomb interaction to favor the ionicity. The wurtzite structure has hexagonal unit cell arrangement in 3 dimension with two lattice parameters *a* and *c* in the ratio of $c/a = \sqrt{8/3} = 1.633$, with a density equal to 5.605 g cm^{-3} (for ideal wurtzite structure) [21]. The wurtzite structure deviates from the ideal arrangement in a real ZnO crystal by changing the c/a ratio. The lattice parameter ratio deviation from ideal one may be due to free charge, impurities, stress and temperature [34]. Since the c/a ratio also correlates with the difference of the electro-negativities of the two constituents, and also components with the greatest differences show largest departure from the ideal c/a ratio [35].

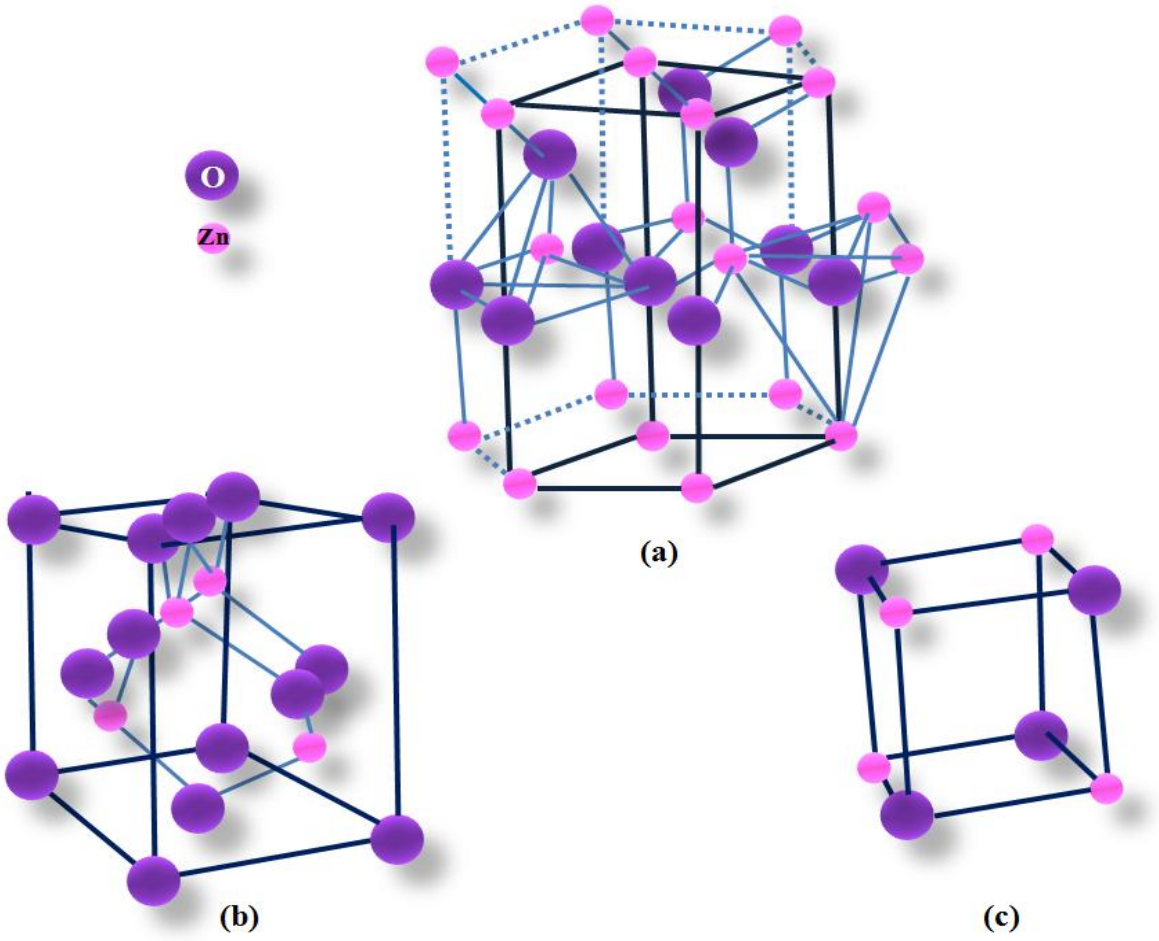

Figure 1.1: Crystal structure of ZnO (a) wurtzite (b) zinc blende and (c) rocksalt

The lattice constants for the wurtzite ZnO structure mostly range from 3.2475 to 3.2501Å for the a-parameter and from 5.2042 to 5.2075Å for the c-parameter and c/a ratio varies from 1.593 to 1.6035 [17, 36-43]. The lattice stability and ionicity changes cause deviation in value of lattice parameters from that of the ideal wurtzite crystal. It has been reported that lattice expands due to free charge, proportional to deformation potential of conduction band minimum and inversely proportional to the carrier density and bulk modulus. The point defects such as zinc antisites, oxygen vacancies, and extended defects, such as threading dislocations are also responsible for the increment in lattice constants. The investigated lattice constant for zinc blende phase varies from 4.37 to 4.47 Å depending upon various techniques. These values are extremely different from wurtzite phase, indicating the formation of zinc blende ZnO structure. High-pressure phase transition from the wurtzite to the rocksalt structure of ZnO lead to the attenuation of lattice constant down to the range of 4.271–4.294 Å [44].

In case of electronic band structure of ZnO as suggested [45-51], the band structure calculations using the Local Density Approximation (LDA) results accurately for the Zn 3*d* electrons as shown in Fig. 1.2 [51]. The band structure along high symmetry lines is represented in the hexagonal brillouin zone. Both the upper limit of valence band and the lower limit of conduction band occur at the Γ point k = 0 indicate that ZnO is a semiconductor with direct band gap. The bottom 10 bands which occurs around −9 eV correspond to Zn 3*d* levels and the next 6 bands from −5 eV to 0 eV correspond to O 2*p* bonding states. The first two conduction band states are strongly Zn localized and correspond to empty Zn 3*s* levels. From this calculation, direct band gap of ZnO has been determined as 3.77 eV [51] which correlates with the experimental value of 3.4 eV, and is much closer than the value obtained from the standard LDA calculation [21].

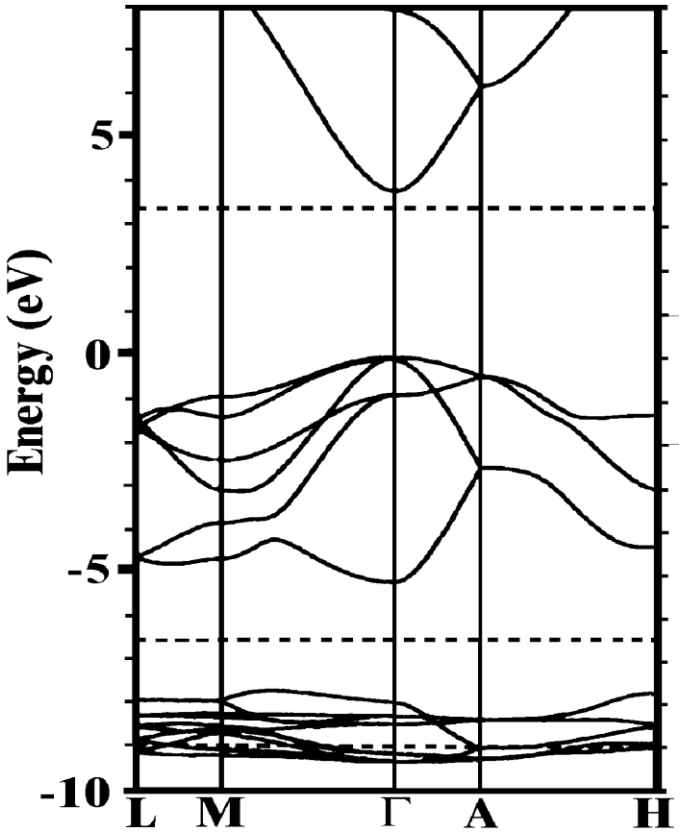

Figure 1.2: The LDA band structure of bulk wurtzite ZnO calculated using dominant atomic SIC-PP [51].

The ZnO crystal exhibits crystallographic polarity, which gives the direction of the bonds, growth and structural arrangement of the crystal. The close-packed (111) planes indicate zinc blende and rocksalt structures and corresponding (0001) basal planes in the wurtzite structure differ from ($\bar{1}\,\bar{1}\,\bar{1}$) and (000$\bar{1}$) planes, respectively. When the bonds along the c-direction are from Zn^{2+} to O^{2-} or vice-versa, the polarity is referred to as Zn and O polarity, respectively. Several physical and chemical properties of the material depend on its polarity, growth and defect generation. In addition to the primary polar plane (0001) and corresponding growth direction <0001> of wurtzite phase, which is the most commonly used surface and direction for growth, many other secondary planes and directions exist in the crystal structure. Similar to other nanostructures, the ZnO structure grows in such a way that it tends to minimize the surface energy which leads to formation of diverse nanostructures [52].

1.3. Some ZnO nanostructures

The nanostructures of ZnO have all three forms i.e. 1D, 2D and 3D such as nanorods, nanowires, nanobelts, nanosheets, nanoflowers, nanocages and nanoparticles etc. The ZnO is probably the richest family of nanostructures both in structures and properties among all materials. It is nontoxic, inexpensive and chemical stable substance [53]. During the past several years, ZnO nanostructures due to its novel luminescent, electrical, mechanical, chemical, magnetic, biological and optical properties has been used extensive in many technological applications such as transducers, nanosensors, nanocantilevers, field effect transistors, transparent electrode in the solar cells, flat panel displays etc. The ZnO nanostructures have been used in nanosized sensors for the detection of different gases, chemical and biological molecules, and dependent on surface-mediated phenomena [54-56]. It is a promising material for photonic and optoelectronic applications. Different ZnO morphologies have also potential application in purification of water from organic dyes and microorganisms which are referred as photo-catalytic and antibacterial activity, respectively. Surface area, surface defects, doping, porosity of ZnO nanostructures are the factors responsible for these applications [57-65].

The ZnO is a wide band gap semiconductor with high excitonic binding energy 60 meV possesses higher density of free carriers trapping centers. Although, there are many types of ZnO nanostructures reported in the literature but here we review only some of the specific nanostructures such as *flower-like structures, nanosheets* and *nanoparticles* considering their relatively different geometries and potential use in different applications. We start our discussion with the ZnO flower-like (nanoflowers) structures and their properties with applications.

1.3.1. Flower-like structures and their applications

The flower-like are the structures which have interwoven nanosheets in the form of a flower. In other words, the nanosheets are interwoven in a way to form a flower-like structure. As the application is concerned, the ZnO nanoflowers were suggested to have pro-angiogenic properties in biological applications. This property is observed by in-vitro and in-vivo angiogenesis assays which led to significant formation of new capillaries from pre-existing blood vessels. The mechanism for angiogenesis property of flowers is the formation of reactive oxygen species

(ROS). This strategy gave rise to ZnO nanostructures as emerging material for alternative therapeutic treatment strategies for cardiovascular and ischemic diseases [66]. Shi *et al.* [67] report a self-catalyzed growth of ZnO nanoflowers via the formation of ZnO nanowires (NWs) by vapor deposition kinetics of ZnO nanomaterials under controlled atmosphere. They stated that the synthesized structures resulted in strongly luminescent material which was successfully applied for optical imaging applications and in-vitro tumor cell imaging. The ZnO nanoflowers synthesized by hydrothermal method show effective osteoblast growth with higher DNA content, alkaline phosphatase (ALP) activity and adhesion strength than those on ZnO film. The approach for fabricating nanoflower structures on biomaterial surfaces shows a potential application in bone tissue engineering as well [68].

Vinod *et al.* [69] demonstrated that ZnO shows room temperature photoluminescence properties exhibiting emission at 392 nm (UV emission) without a visible emission. They synthesized ZnO nanoflowers by hydrothermal process at 200 ºC temperature and found defect free nanoflowers as observed by suppressed Raman bands at 541 and 583 cm^{-1}, leds to the application in UV light-emitting devices. Jun *et al.* [70] synthesized ZnO nanoflowers by low temperature solution-phase method, which was used as photoanodes on transparent conductive fluorine-doped tin oxide substrates by doctor-blade technique. They found that nanoflower structure enhances light harvesting and improves electron transport when used for fabrication photoanodes with a ZnO/TiO_2 composite of dye-sensitized solar cell. Similarly, Ahmad *et al.* [71] in their work showed that the well-crystalline flower-shaped ZnO structures exhibit good photocatalytic property for the degradation of rhodamine B (RhB) and good photo-anode material for dye-sensitized solar cell applications. Kim *et al.* [72] in their work grown ZnO nanoflowers on a conducting glass substrate using a chemical solution deposition method. When used as synthesized ZnO nanoflowers in LED devices application, they demonstrated strong light emission as the micropixels for display application.

Guo *et al.* [73] synthesized ZnO flower-like by combining laser direct writing and hydrothermal growth. They demonstrated that the flower-like morphology shows excellent wettability and photocatalytic activity in the degradation of RhB dye. Lei *et al.* [74] synthesized ZnO nanoflowers with dextran ($(C_6H_{10}O_5)_n$) assistance by a facile solution route. The flower-like

structure with dextran shows potential application for wastewater treatment by exhibits higher activity than ZnO fragments obtained without dextran. Umar *et al.* [75] investigated ZnO nanoflowers for their applications in an antimicrobial agent against escherichia coli (E.coli) and enzyme-free glucose sensor. They showed that ZnO nanoflowers are efficient as an antimicrobial agent and a highly sensitive non-enzymatic glucose sensor. ZnO nanoflowers as an efficient electron mediator also exhibit good sensitivity (~411 μA $M^{-1}cm^{-2}$) with detection limit of ~1.25 mM and response time of ~10 seconds (s) for non-enzymatic glucose sensor. Panwar *et al.* [76] used ZnO nanoflower structure for gas sensing purpose by growing them on glass substrates. They showed significant response (95%) for acetone gas at 325 ºC. They observed that structure exhibits a fast response and recovery due to its surface morphology.

ZnO nanoflowers composed of needle-like nanorods synthesized by using aqueous chemical growth method at low-temperature were used for piezoelectric energy harvesting source by Khan *et al.* [77]. They synthesized ZnO nanoflowers uniformly on conductive flexible textile fabric substrate. They observed a significant output potential and current more than 600 mV and ~650 nA, respectively and also good rectifying schottky behavior. Wang *et al.* [78] successfully synthesized ZnO nanoflowers by a simple low-temperature route and demonstrated that different ZnO morphology can be obtained simply by varying basicity in the solution and suggested ZnO nanoflowers growth mechanism in terms of the general theory of the crystal nucleation and crystal growth direction. The ZnO nanoflowers synthesized via surfactant free medium contains larger content of oxygen vacancy act as the active centers of the catalyst on the surface of 1D nanomaterials, responsible for good photocatalytic activity in degradation of 4-cholrophenol (4-CP) in aqueous solution under UV radiation.

1.3.2. ZnO nanosheets and their applications

The ZnO nanosheets is a two dimensional structure. The thickness of nanosheets is in tens of nanometer where as the width may be up to millimeters. Here we briefly discuss some important aspects of ZnO nanosheets.

Chen *et al.* [79] fabricated ZnO nanosheets by a physical vapor-transport technique and investigated by micro-photoluminescence spectroscopy. They observed that nanosheets resulted

in high-temperature (857 K) photon emission. The observed property could be used in high-temperature opto-electronic applications. Sesha *et al.* [80] synthesized nanosheets by wet-chemical method at low temperature (80°C) without substrate. ZnO nanosheets investigated by raman spectroscopy and photoluminescence measurements have shown intense green, blue and red emissions due to a variety of vacancy and interstitial defects, which attributed this material to act as blue-white fluorophore. The potential use of this blue-white fluorescent coating is in conjunction with ultraviolet emitting LEDs. Tan *et al.* [81] synthesized ZnO nanosheets on metallic Zn foils after hot-water treatment at 90 °C for 4, 8, 12 and 24 hours. They showed that the ZnO nanosheets exhibit near band edge UV and green emissions when observed by the photoluminescence spectra; indicating their good crystallinity with presence of oxygen related defects. Thus formed structure could be used for opto-electronic applications. Ahmad *et al.* [82] synthesized ZnO nanosheet networks on silicon substrate without any catalyst through thermal evaporation using $ZnCl_2$ and O_2 as source materials for zinc and oxygen, respectively. They observed that ZnO nanosheet networks showed a strong green band with a suppressed UV emission at room temperature. The UV emission at room temperature makes it applicable for opto-electronic and luminescence applications. The device made from two dimensional nanosheets and an anionic nanoclay layer heterojunction has potential to be the smallest size power package as observed by Kim *et al.* [83]. Further, this structure can be used to charge wireless nano/micro scale systems without the use of rectifier circuits to convert AC into DC to store the generated power. The combined effect of buckling behavior of the ZnO nanosheets, a self-formed anionic nanoclay layer, and coupled semiconducting and piezoelectric properties of ZnO nanosheets contributes an efficient DC power generation. The network of ZnO nanosheets proved a structurally stable system under huge external mechanical loads.

In wastewater treatment applications, the ZnO nanosheets show a good photocatalytic property for the degradation of methyl orange (MO), RhB and methylene blue (MB) dyes under UV light illumination and possess excellent super-hydrophilic ability. These properties demonstrate ZnO nansoheets as promising nanomaterials for wastewater treatment [84]. The electrical contact between the ZnO nanosheets and brass substrate demonstrated potential applications of ZnO nanosheets in gas sensing and photocatalytic degradation [85]. As the

properties of nanosheets depends upon fabrication method, ZnO nanosheets film was fabricated by dip-coating and inkjet printing on glass plates by Hynek *et al.* [86]. The film morphology is highly influenced by the deposition method as in dip coating method; the film morphology is very smooth and nonporous, while the inkjet-printed films were rough and porous. However, in the photocatalytic degradation of 4-CP these films show two-fold efficiency than ZnO films prepared by the sol–gel technique. The obtained higher efficiency is due to the side-by-side alignment of ZnO nanosheets on the substrate resulted in thin, transparent, oriented ZnO surfaces with the high-energy {001} facets exposed. Therefore, the surface arrangement of ZnO nanosheet films makes them applicable for the construction of optical devices and dye-sensitized solar cells.

Recently, Wang *et al.* [87] reported the effect of synthesis parameters on the biological applications of ZnO nanosheets. They synthesized hexagonal ZnO nanosheets at nearly neutral pH (i.e., 7.3) and low temperature (i.e., 80°C) using structure-directing agent, tris(hydroxymethyl)aminomethane (tris). The tris molecule acts as the hydroxide anion generator and surface modification agent. The obtained ZnO nanosheets show strong fluorescence at wavelength 590 nm, which attributed to the defects on the surface of ZnO nanosheets, which makes their use for cell imaging, suggesting their promising clinic and biomedical applications. The ZnO nanosheets are also used as a sensing material. Zhang *et al.* [88] used sonochemical process to synthesize sheet-like ZnO nanostructure without any catalyst, template or seed layer, followed by an etching treatment in an alkali environment at room temperature. The as-prepared nanosheets were used to fabricate micro gas sensor for testing different concentration of volatile organic compounds (VOCs) gases. They observed that the nanosheet structures, due to large specific area, accessible surface and less agglomerated configuration, are responsible for excellent sensitivity to acetaldehyde and formaldehyde with response time less than 10 s and detection limit of 50 ppb. Amini *et al.* [89] fabricated UV detectors by using Zhang *et al.* [88] method. They observed that ZnO nanosheet photosensor shows faster response time in the UV region as compared with conventional ZnO nanoparticles based photosensors. The higher sensitivity of nanosheets is attributed to the low density of defect states on nanosheets surfaces.

1.3.3. ZnO nanoparticles and their applications

The nanoparticle is zero dimensional structure while considering the allowed direction. In this section, we discuss some of the important aspects of ZnO nanoparticles.

As an optical property, ZnO nanoparticles show high luminescent properties. Daniele *et al.* [90] prepared ZnO nanoparticles by co-precipitation method with variable amounts of aminopropyltriethoxy silane (APTS). They generate LED devices based on the organo-modified ZnO nanoparticles with the photoemission and observed their higher luminescent properties. In another study, Liu *et al.* [91] reported a photodetector based on flexible nanoparticle-assembled ZnO cloth, which was synthesized *via* a carbon cloth templated hydrothermal method. Under UV irradiation, the conductance of the device increased more than 600 times having response and decay time to be around 3.2 s and 2.8 s, respectively.

In environmental applications, the ZnO nanoparticles were suggested by Bagabas *et al.* [92], as they follows room temperature wet chemical route based on cyclohexylamine for synthesizing ZnO nanoparticles in aqueous and enthanolic media, and also tested for the photodegradation of cyanide ions. They conclude that the morphology was crucial in enhancing the cyanide ion photocatalytic degradation efficiency. Also ZnO nanoparticles were synthesized by calcination of precursor by the precipitation method with grafting polystyrene onto the surface of ZnO nanoparticles to improve the dispersion of the particles. They showed that ZnO nanoparticles possess high photocatalytic activity [93].

The nanoparticles with luminescent and magnetic properties show applications both in vitro and in vivo as detection probes and drug carriers etc. These nanoparticles, due to their good biocompatibility [94] and low cost, have shown promising potential in bioimaging and drug delivery [95]. Recently, Matsuyama *et al.* [96] suggested biological application of ZnO nanoparticles by the use of silica-coated ZnO-nanoparticle quantum dots (QDs) with biotin as fluorescent probe in cell-labeling applications and have suggested for selective destruction of tumor cells applications [97]. Also, ZnO nanoparticles have been appeared as a promising candidate for the realization of dye sensitized solar cells [98] and are used for sunscreens lotion as UV blockers [99]. Sun *et al.* [100] suggested a flexible nanogenerator made of ZnO nanoparticles which may bring out some important and interesting applications in energy harvesting.

In the present work, we have synthesized three morphologies of ZnO viz. flower-like structure, nanosheets and nanoparticles by facile solution method and have applied them for optical, opto-electronic and environmental applications. The synthesized ZnO structures exhibit near band edge UV emission as well as emissions in visible regime also (violet, blue, blue-green and green) as observed by photoluminescence spectra. This indicates good crystallinity of as synthesized ZnO nanostructures and presence of oxygen related defects. These defects with surface free bonds make ZnO nanostructures as a potential structure for environmental and opto-electronic applications. We have performed experiments related to the photocatalytic activity of ZnO nanostructures for the degradation of MB in presence of the sunlight and photodetector for detecting visible light (white, violet and green). Synthesized ZnO nanostructures were also applied in turbid lens imaging application in enhancing numerical aperture (NA) of objective lens. A comparative study of their performance indicated that the nanosheets show better light bending as compared with other nanostructures. When used in visible-light photodetector for detecting visible light (white, violet and green) at room temperature, again the nanosheets showed better performance as compared to other morphologies. Better performance of nanosheets is attributed to their higher effect of surface area and oxygen vacancies.

1.4. Synthesis methods for ZnO nanostructures

The controlled synthesis of the ZnO nanostructures has been one of the motivations for the researchers because the properties of nanostructures can be controlled by controlling the shape and size of the structure [101-105]. In literature, various techniques have been suggested for the growth of ZnO nanostructures [106-108]. The synthesis methods can be categorized as solid, liquid and vapor phase methods. The synthesis methods are summarized in Fig. 1.3.

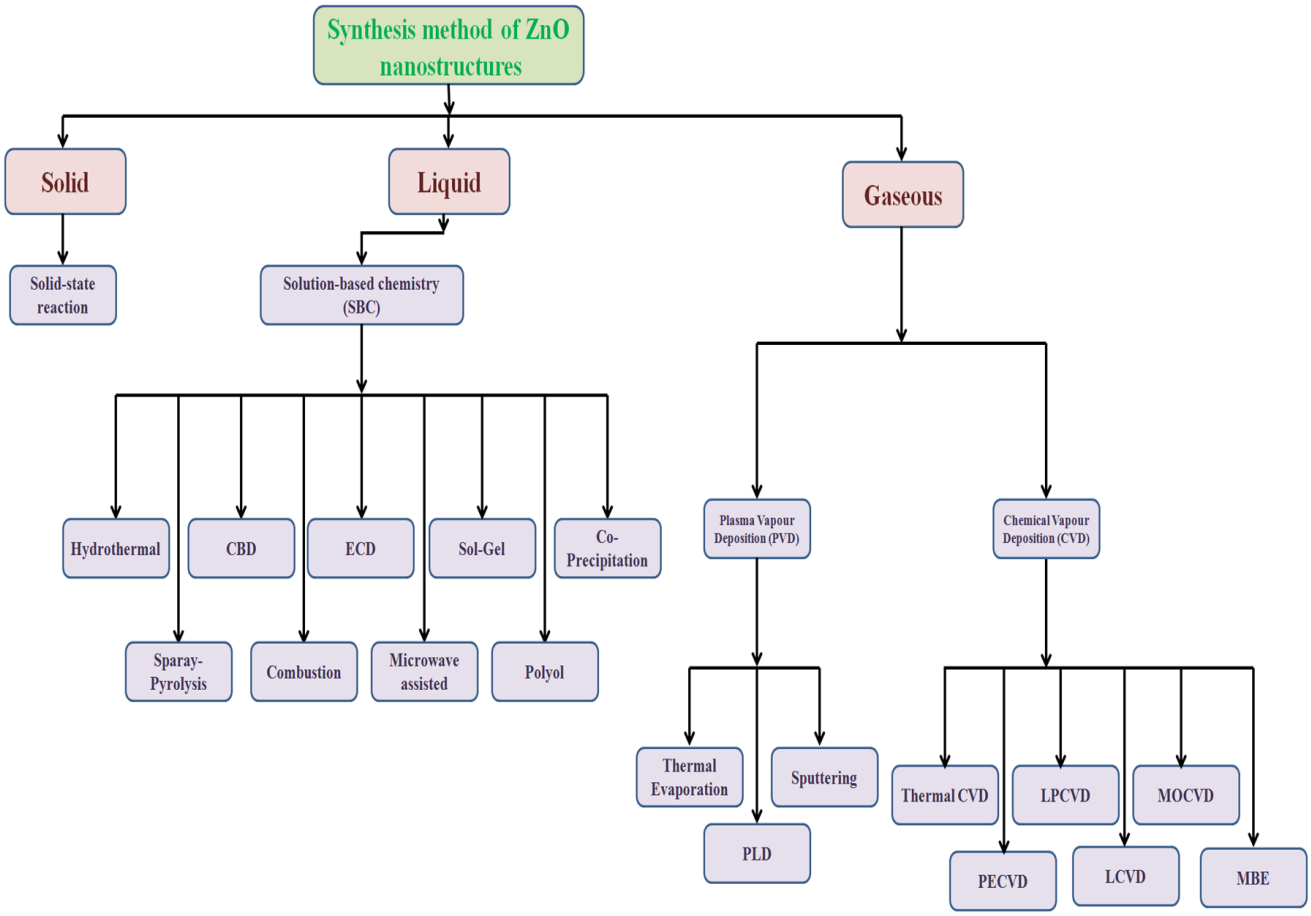

Figure 1.3: Summary of synthesis methods for ZnO nanostructures.

Mainly there are three methods namely solid phase, liquid phase and gas phase. First of all, the solid phase method is a solid-state technique [109-111] for the synthesis of ZnO nanostructures. It involves grinding, mixing and subsequent heat treatment at high temperatures of precursor materials (metal oxides or carbonates) to facilitate diffusion of atoms or ions in the host material by chemical reaction. In this method, it is difficult to control the particle properties. This method have many disadvantages such as inhomogeneity, bigger crystallite, poor stoichiometry, phase impurity [112, 113] etc. Gases or vapor phase method is categorized as physical vapour deposition (PVD) and chemical vapour deposition (CVD), they are further divided as thermal evaporation, sputtering, pulse laser deposition (PLD) for PVD and CVD: thermal CVD, low pressure CVD (LPCVD), plasma-enhanced CVD (PECVD), metal-organic CVD (MOCVD), laser CVD (LCVD), atomic layer deposition (ALD) and molecular beam epitaxy (MBE). These methods are differentiated from each other based upon their source of bombardment, catalyst, precursor etc. These techniques have been used for the synthesis of ZnO nanostructures like nanocombs, nanoparticles, nanorods, nanowires etc. In PVD processes, material in a vapor form is physically released from a source and is transferred to a substrate at high temperature. It generally involves bombardment of the substrate to be coated with energetic positively charged ions during the coating process to promote high density in vacuum at pressure 10^{-2} to 10^{-4} mbar. Various compound compositions have been created during metal deposition by the introduction of reactive gases such as nitrogen, acetylene or oxygen into the vacuum chamber. In this process, the solidification of a vapor from source directly onto a surface takes place without a chemical reaction. In CVD process, the reaction of vapor phase chemical reactants containing the material occurs to form a non-volatile solid film or structures on a substrate. Hot furnace as reaction chamber is used for this process in which the reactant gases (H_2, O_2, CH_4, argon etc.) are introduced to decompose and react with the substrate to form the film or structures at high temperature. Generally, the gas phase approaches are relatively easy to control for the production of a variety of high quality, single crystal ZnO nanostructures and doping. However, they have requirement of the high temperature, costly gases and vacuum level [114].

The liquid phase/solution-based methods are divided in hydrothermal, chemical bath deposition (CBD), electrochemical deposition (ECD), sol-gel, co-Precipitation, spray pyrolysis, combustion, microwave assisted and polyol synthesis routes. All these methods have some merits as well demerits. In case of solution-based methodologies, there is an advantage of low growth temperature, potential for easy scaling up, and simplicity for fabrication of ZnO nanostructures as compared to vapor phase methods. From the commercialization point of view, the chemical waste treatments will also require to deal with the environment issues in the future. However, a low-cost chemical synthesis with high yield certainly is appropriate for commercialized production of nanostructure materials. Among all solution based methods, the co-precipitation methods results in atomic scale mixing. The calcining temperature required for the formation of final product is low, which lead to lower particle size [115]. Since, each synthesis requires its own special conditions, precursor reactions etc. Therefore in the co-precipitation process, it is required to control the concentration of solution, pH, temperature and stirring speed of the mixture in order to obtain the final product with required properties [116, 117]. All other solution based methods which are commonly used have some disadvantages such as sol-gel method has disadvantages of their products would contain high carbon content when organic reagents are used in preparative steps and this would inhibit densification during sintering, hydrothermal slurries are potentially corrosive and also may cause accidental explosion of the high pressure vessel and in polyol method, requirement and selectivity of large amount of polyhydroxy alcohol for individual processes, and collecting and purifying the intermediate particles are complicated [118-120]. In the present work, we have used a facile solution method for the synthesis of ZnO nanostructures at room temperature. The advantages of this method are:

1. Particle size and morphology control
2. Without use of template, directing agent, high temperature and high pressure vessel.
3. Easy and cost-effective route.
4. No use of harmful and explosive gases.

1.5. Synthesized ZnO nanostructures were characterized using the following techniques

(i) Field Emission Scanning Electron Microscopy (FESEM) installed with Energy Dispersive X-rays (EDAX): Using FESEM, we have observed the surface morphology. From EDX the information corresponding to the different elements present in the nanostructures has been obtained.

(ii) Transmission Electron Microscopy (TEM) installed with Energy Dispersive X-rays (EDAX): TEMs provide structural, compositional and crystalline information. High resolution imaging mode gives information regarding crystal lattice of a materials. This allows observing planar and lining defects, grain boundaries, interfaces, etc. The bright field/dark field imaging modes of the microscope, which operate at intermediate magnification, combined with electron diffraction, are also invaluable for giving information about the morphology, crystal phases, and defects in a material.

(iii) X-ray Diffraction (XRD): X-ray diffraction provides a convenient and a practical means for the qualitative structural identification of compounds because of the uniqueness of the pattern for each compound.

(iv) Fourier Transform Infrared Spectroscopy (FTIR): Infrared spectroscopy is quite useful to predict each functional group present in molecule absorbs a certain frequency of radiation and show corresponding peak. Hence the position of peak gives the information regarding the presence of certain functional group and the shift due to environment effect can be easily observed in spectrum.

(v) UV-Vis Spectroscopy: UV-Vis spectroscopy is used to study the optical properties of compounds. It is routinely used in analytical chemistry for the quantitative determination of different analytes, such as transition metal ions, highly conjugated organic compounds, and biological macromolecules.

(vi) Photoluminescence Spectroscopy (PL): Photoluminescence spectroscopy is a contactless, nondestructive method of probing the electronic structure of materials. Radiative transitions in semiconductors involve localized defect levels. The photoluminescence energy associated with these levels can be used to identify specific defects, and the amount of photoluminescence can be used to determine their concentration.

(vii) Brunauer–Emmett–Teller (BET) surface area measurement: The BET method is widely used in surface science for the calculation of surface areas of solids. The specific surface area of a powder is determined by physical adsorption of a gas on the surface of the powder and by calculating the amount of adsorbate gas corresponding to a monomolecular layer on the surface. The determination is usually carried out at the temperature of liquid nitrogen. The amount of gas adsorbed can be measured by a volumetric or continuous flow procedure.

1.6. Thesis Outline

Chapter 1 begins with the basic introduction of the nanotechnology. Also the nanostructures on the bases of the dimensionality have been classified. A brief explanation of the different synthesis methods is explained. Used characterization methods for synthesized nanostructures have been briefly explained. The reason of selecting the present system has been discussed in the last of this chapter.

Chapter 2 explains the methodology, experimental procedure and morphology control used in this research work. In reference to the synthesis process the several processing parameters such as OH^-/Zn^{2+} ratio, reaction time, surfactant and solvent, which can be controlled and need to be selected properly before and/or during synthesis are also discussed. In the next section, the influence of synthesis conditions on the morphology of ZnO nanostructures is discussed. Then different characterizations for morphology, structural and optical properties of the grown nanostructures have been discussed.

Chapter 3 starts with a brief introduction of different types of nanostructures applied in environmental application and properties required for photocatalytic activity under sunlight. An experimental procedure for the photocatalytic activity is described in the second section of this chapter. In the next section, brief description of the mechanism of nanostructures formation and different aggregation tendencies of nanosheets is presented. Then photocatalytic performances of the grown nanostructures have been discussed. Further a brief description of the mechanism of photocatalytic activity of nanostructures is presented. Finally the chapter concludes with a brief summary.

Chapter 4 starts with an introduction of enhancing numerical aperture for turbid lens imaging is presented, and then the experimental process for enhancing numerical aperture and transmittance of turbid lens has been described. Characterizations of fabricated turbid film have been explained onwards in terms of their morphology and scattering. For a comparative study of the fabricated ZnO turbid film for enhancing numerical aperture and transmittance has been explained in brief. Next the principle behind this application is also given and in last a brief summary of the chapter is given.

Chapter 5 starts with an introduction of ZnO nanostructures based photodetectors. An experimental procedure for the formation of ZnO nanostructures film on glass substrate and fabrication of photodetector circuit has been described onwards. Next, for a comparative study of photodetector performance of the fabricated ZnO film has been explained in brief. Further the principle behind these performances is explained and in the end a brief summary is presented.

Chapter 6 includes summary conclusion and important suggestion towards the future work.

Chapter-2

Synthesis and characterizations

This chapter focuses on the synthesis and characterizations of nanostructures (nanosheets, flower-like structures and the nanoparticles) by facile solution method at room temperature. The goal of this chapter is to better understand the synthesis parameters used for the synthesis of ZnO nanostructures, and improve the precision and control. Many of the results attained in this research work may be indicative of the synthesis parameters. This chapter begins with a section that deals with the synthesis parameters related to the synthesis of ZnO nanosheets which is followed by their characterizations. Similarly, the two next sections discuss the synthesis and characterizations of ZnO flower-like structures and nanoparticles, respectively.

2.1. Synthesis of ZnO Nanosheets

Materials: Zinc acetate ($ZnAc_2$ or $Zn(CH_3COO)_2$) (purity 99.99%) and potassium hydroxide (KOH) (purity 98%) were procured from Sigma-Aldrich (USA) and Merck, respectively. The reagents were used as received without further purification. All reactions were carried out in glassware dried in an oven under ambient conditions.

Method: A zinc acetate ($ZnAc_2$) solution (0.5 M) and potassium hydroxide (KOH) solution (0.5M) were formed in ethanol (C_2H_5OH), separately. In KOH solution, $ZnAc_2$ solution was added drop wise under the vigorous stirring condition at room temperature. In order to monitor growth mechanism of ZnO nanostructures, small quantity of the samples was collected at 0.25, 1, 2 and 4 hours of time intervals from the reaction mixture. Collected precipitate was filtered, washed with deionized water and ethanol to remove undesirable ions such as CH_3COO^- and K^+, and dried for 1 hour.

2.1.1. Morphology Control

2.1.1.1. Effect of precursor and alkali concentration

The solubility of ZnO in an alkali solution increases with the concentration of alkali solution and temperature. Commonly, NaOH and KOH are used as alkali solutions. Since divalent metal ions do not hydrolyze in acidic environments therefore, an alkaline solution plays a crucial role for the formation of ZnO nanostructures [121-123]. The reactions involved in the formation of ZnO are [124, 125]:

$$Zn^{2+} + 2OH^- \longleftrightarrow Zn(OH)_2 \qquad (2.1)$$

$Zn(OH)_2 + 2OH^- \longleftrightarrow [Zn(OH)_4]^{2-}$ (2.2)

$[Zn(OH)_4]^{2-} \longleftrightarrow ZnO_2^{2-} + 2H_2O$ (2.3)

$ZnO_2^{2-} + H_2O \longleftrightarrow ZnO + 2OH^-$ (2.4)

$ZnO + OH^- \longleftrightarrow ZnOOH^-$ (2.5)

For the equation (2.2), the product could be different from $Zn(OH)_4^{2-}$, product may be in the form of $Zn(OH)^+$, $Zn(OH)_2$, or $Zn(OH)^{3-}$, depending on the parameters such as the concentration of Zn^{2+} and the pH value as shown in Fig. 2.1. Under different reactions conditions, all the intermediate forms are in equilibrium with the major forms being different [126]. According to the above reactions, the O^{2-} used in the formation of ZnO does not originate from the solvent H_2O or C_2H_5OH rather it comes from the base. Therefore, the formation of ZnO does not require water as the solvent [127], but it could be organic solvents, such as methanol [128], ethanol [129], and butanol [130], or even ionic liquids [131, 132]. The synthesis was done at room temperature by adjusting the ratio of Zn^{2+} and OH^-, and ZnO nanostructures under alkali conditions were formed [130]. The phase stability diagram for ZnO (s) and water at room temperature as a function of precursor concentration and pH of the solution is shown in the Fig. 2.1.

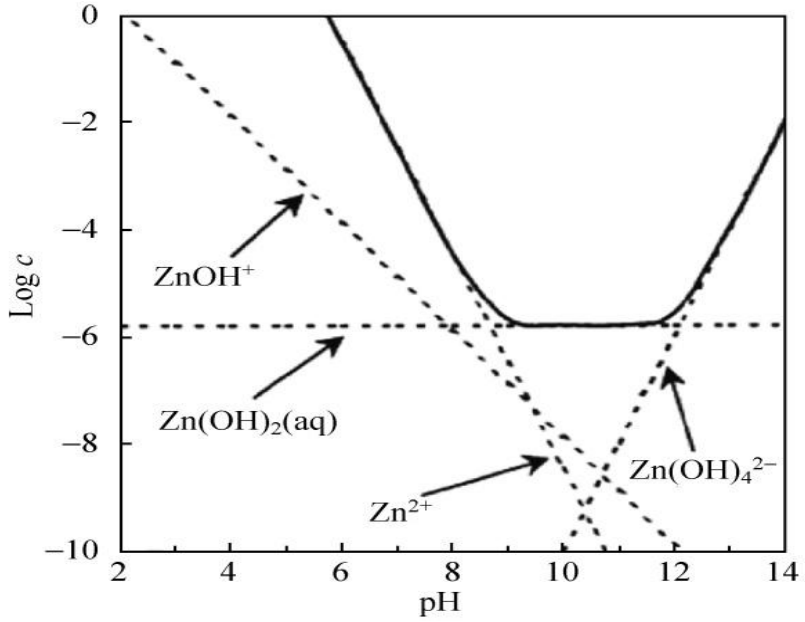

Figure 2.1: Phase stability diagrams for the ZnO(s) and H_2O system at room temperature (dashed lines denote the thermodynamic equilibrium between the Zn^{2+} soluble species and the corresponding solid phases) [126, 133].

In the present work, the results show that the concentration of KOH plays a crucial role for the formation of ZnO nanostructures. Figure 2.2 shows ZnO morphologies formed with different ratios of precursor ($ZnAc_2$) solution and alkali (KOH) solution when ethanol as solvent was used. In Fig. 2.2(a), when the molar ratio of OH^- : Zn^{2+} is 1: 4 (conc. of $ZnAc_2$ and KOH is 0.5 M and 0.125 M, respectively), the products are nanoparticles with size 25 nm. Increasing the KOH concentration (0.25 M) in 1: 2 ratios in the precursor solution, the nanoparticles aggregated in sheet-like structure as shown in Fig. 2.2(b). A further increase in the KOH concentration (0.5 M) such as 1: 1 resulted in the formation of nanosheets (Fig. 2.2(c)). As we know that ZnO is an amphoteric compound, which dissolves in acid or alkali solutions. Therefore, when the molar ratio reached 2: 1 (conc. of $ZnAc_2$ and KOH is 0.25 M and 0.5 M) and 4: 1 (conc. of $ZnAc_2$ and KOH is 0.125 M and 0.5 M), the ZnO started to dissolve which resulted in the formation of hierarchical structure associated with nanoparticles on their surface (Figs. 2.2(d) and 2.2(e)). In this study, we observed that molar ratio 1: 1 of $ZnAc_2$ and KOH is optimum for the formation of uniform ZnO nanosheets.

Along with the molar ratio of 1: 1 of OH^- to Zn^{2+}, the concentration of precursor and alkali solution also plays an important role in the formation of nanostructure. Initially, we used 0.1 M concentration for both of the solutions, the obtained structure was rough as shown in Fig. 2.3(a). For increased concentration to 0.2 M while keeping the molar ratio 1:1, a small change in the structure was obtained, some sheets-like structure appeared to form (Fig. 2.3(b)). With further increasing the concentration of $ZnAc_2$ and KOH solutions to 0.4 M, the sheets-like structures become clearer as shown in Figs. 2.3(c)-2.3(f), and at 0.5 M of both the solutions, uniform nanosheets appeared as shown inset of Fig. 2.3(g). The concentration 0.6 M of both the solutions gave rise to irregular structure with disappearance of the sheets in the product as shown in Fig. 2.3(h). All the experiments were performed in similar conditions merely the molarities of $ZnAc_2$ and KOH solutions were adjusted. In our study, we found that that in addition to the Zn^{2+} concentration a certain pH range (pH= 9 to 12) is suitable for the formation of ZnO nuclei in solution, which influences the crystal growth rate and the morphologies.

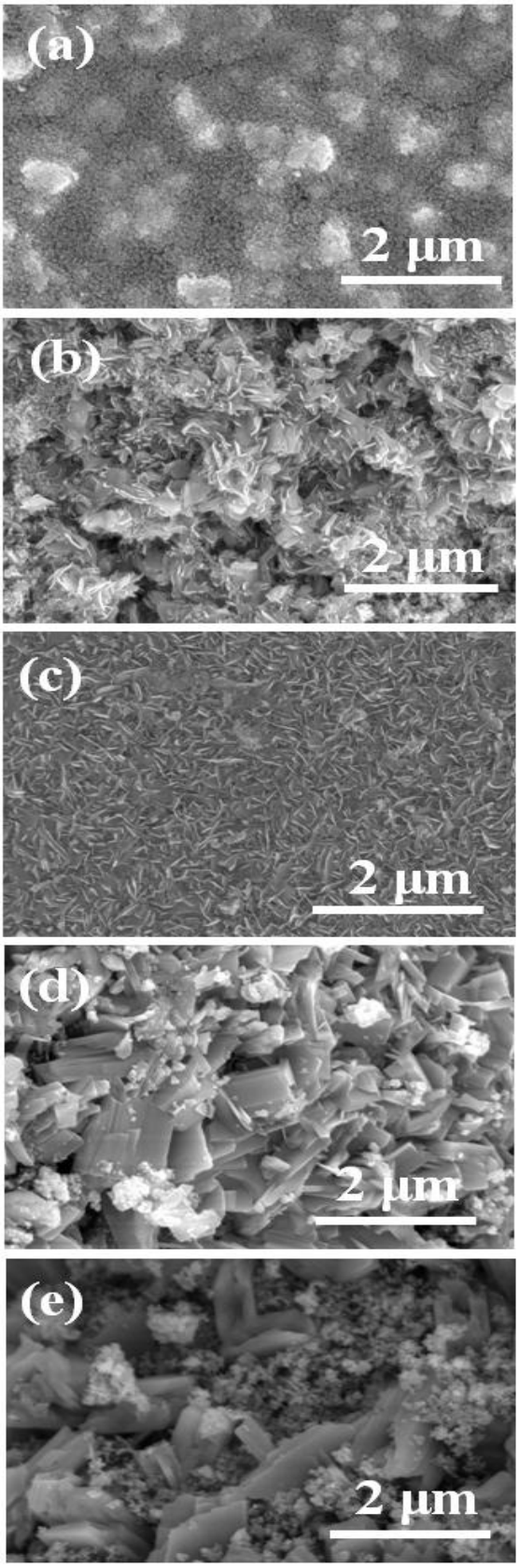

Figure 2.2: FESEM images show changes in morphology by variation of OH^- : Zn^{2+} ratio as (a) 1: 4, (b) 1: 2, (c) 1: 1, (d) 2: 1, and (e) 4: 1.

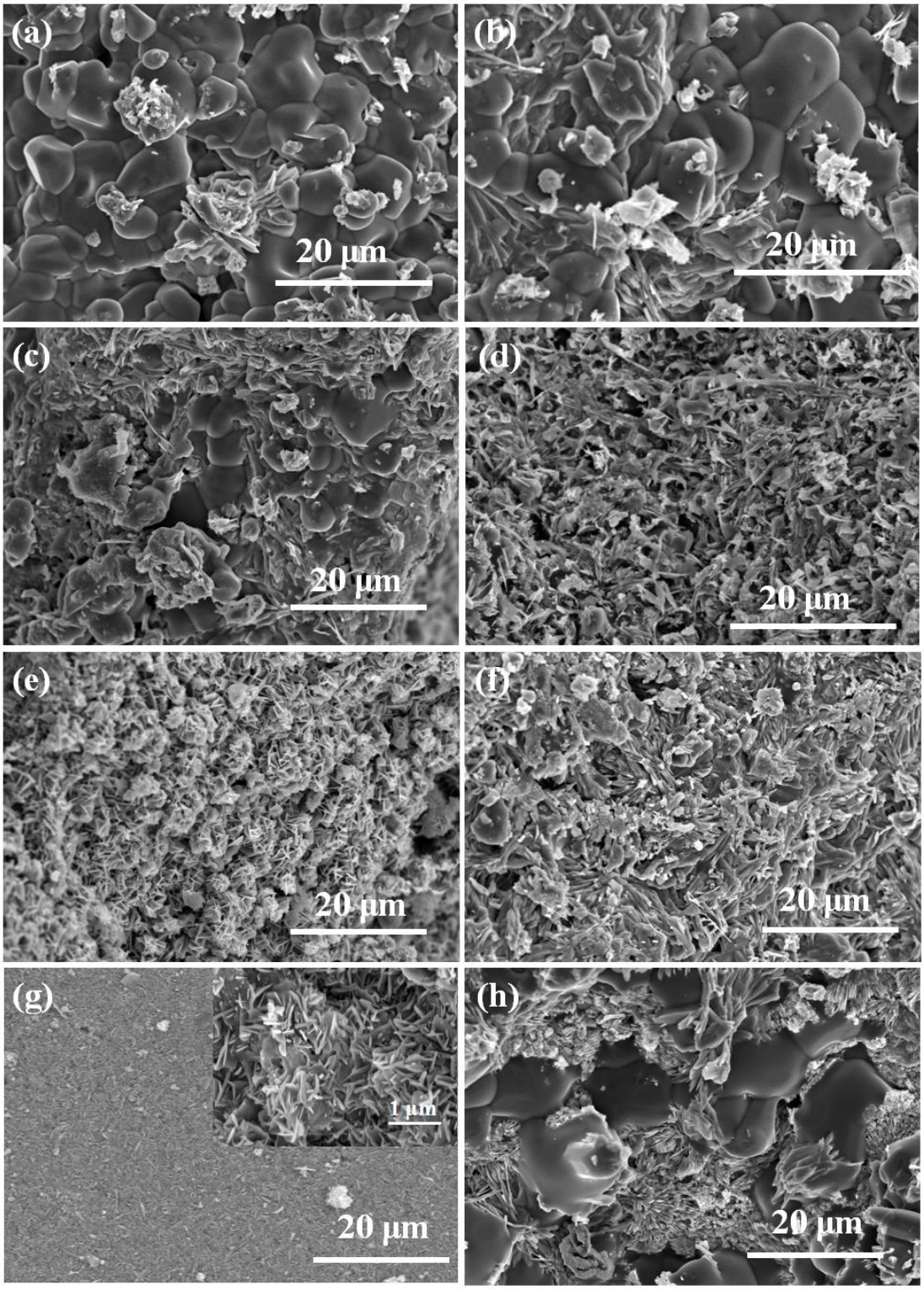

Figure 2.3: FESEM images show variation in morphology by varying precursor and alkali solution concentration as (a) 0.1 M, (b) 0.2 M, (c) 0.25 M, (d) 0.3 M, (e) 0.4 M, (f) 0.45 M, (g) 0.5 M, and (h) 0.6 M keeping OH^-: Zn^{2+} ratio = 1: 1.

2.1.1.2. Effect of reaction time

We used $ZnAc_2$ solution (0.5 M) and KOH solution (0.5 M) in ratio 1:1. To explain the effect of reaction time of ZnO nanosheets, the samples were collected at different time intervals (we selected 0.25, 1, 2 and 4 hours) from the reaction mixture. We took same molarity (0.5 M) of both solutions keeping OH^-: Zn^{2+} ratio = 1: 1. The samples collected at different time intervals are shown in FESEM images (Fig. 2.4). Fig. 2.4 also shows a schematic (left side) of the growth of nanosheets. A uniform reaction temperature 40 ^oC was maintained till the last sample (at 4 hours) was collected from the reaction chamber. All the samples collected from the reaction chamber were filtered, washed several times with deionised water, and finally dried at 100 ^oC for 1 hour.

From the FESEM images (Fig. 2.4) of the samples which were formed in C_2H_5OH medium at successive stages of reaction, it can be concluded that the ZnO nanosheets are resulted from the growth of ZnO nanoparticles. Initially, when the reaction proceeded for 0.25 hour, nanoparticles (around 25 nm in size) were formed as shown in Fig. 2.4(a). For 1 hour reaction time, the nanoparticles starts to aggregate in the sheet-like structure as shown in Fig. 2.4(b). From the Fig. 2.4(b), we can be seen that there are two different types of structures: nanoparticles with a diameter about 25 nm and nanosheets with a thickness about 25 nm. For 2 hours of reaction time, sheet-like structure becomes prominent as shown in Fig. 2.4(c). There sheet-like structure has thickness of 25 nm. Since both the nanoparticles and sheets-like structures have same thickness, it is inferred that initially the nanoparticles are formed which due course of time assemble in the form of sheet to reduce the surface energy. The growth of the nanosheet network continues until whole of the precursor is consumed, and for the prolonged reaction time of 4 hours, larger size nanosheets with a thickness of 25 nm are formed (Fig. 2.4(d)).

The whole process of formation of ZnO nanostructures i.e. nanosheets in brief may be described to proceed via the nucleation of ZnO nanocrystals, then subsequent directional growth to form nanosheet structures. The nucleation takes place in a condition when the concentration of precursors (i.e. nanocrystals or monomers) exceeds the critical super saturation level. In such a condition, smaller nanocrystals grow rapidly until their concentration falls below the critical level for nucleation [134]. According to Ostwald ripening process [126, 135], the large

nanocrystals grow at the cost of smaller nanocrystals. The growth of large nanocrystals proceeds by the capturing of Zn^{+} ion formed from the dissolution of smaller nanocrystals and brought near to the surface of larger nanocrystals by the process of diffusion. The whole mechanism for the formation of ZnO nanosheets is described in detail in chapter 3.

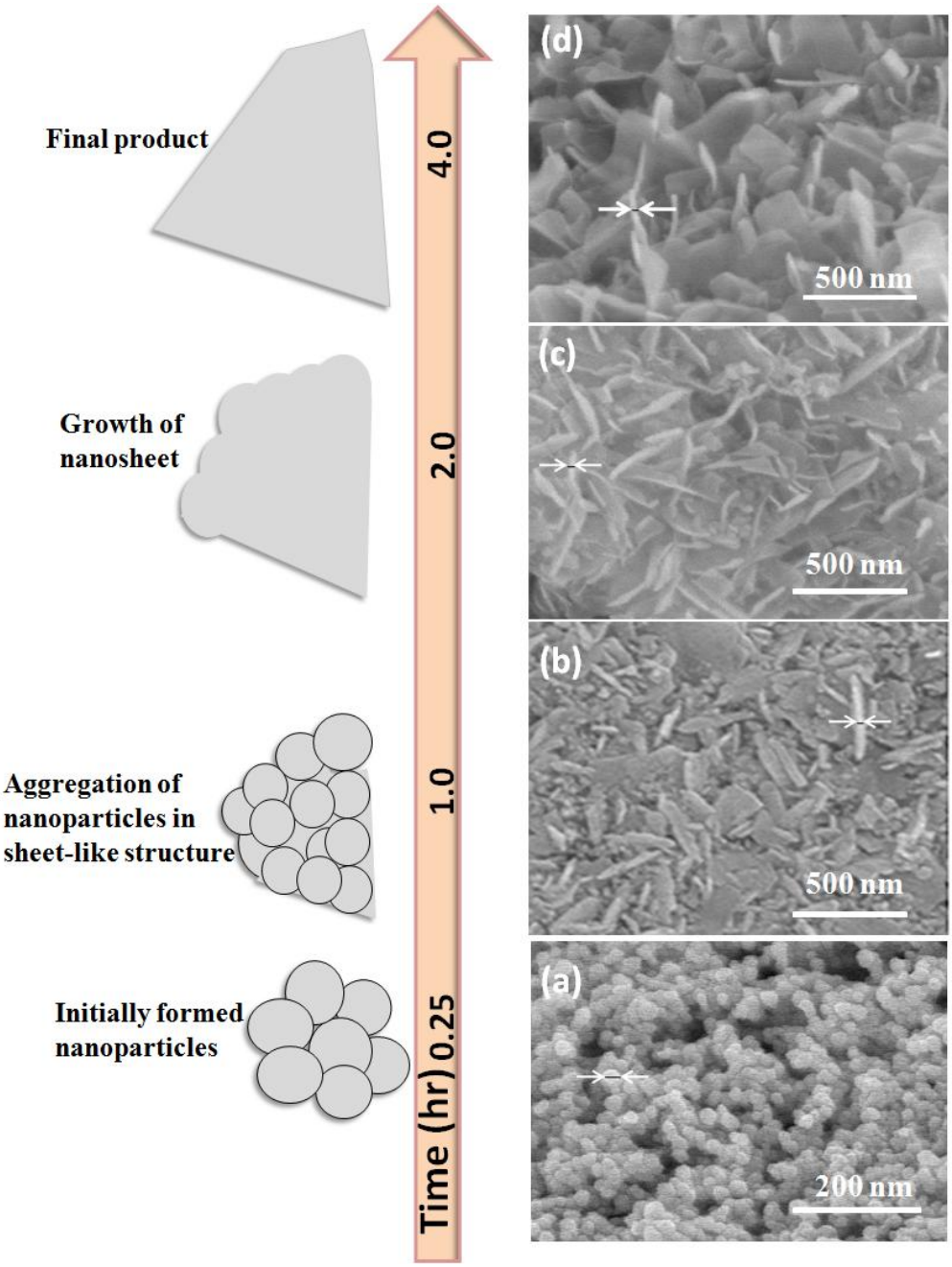

Figure 2.4: Morphological evolution of the ZnO products with respect to different reaction times: (a) 0.25 hour, (b) 1 hour, (c) 2 hours, and (d) 4 hours. The left of FESEM images corresponds to the schematic diagram of the proposed growth process of ZnO nanosheets.

2.1.1.3. Effect of surfactant

The growth mechanism of ZnO nanostructures is influenced by the existence of surfactant as cetyltrimethylammonium bromide (CTAB) in the solution. In the presence of surfactant, the surface tension of solution is decreased which minimizes the surface energy to form a ZnO nanocrystals. Being an ionic compound, the CTAB completely ionizes in water and forms a positively charged tetrahedron with a long hydrophobic tail, while the $Zn(OH)_4^{2-}$ is considered to be grown for ZnO crystal which has a negatively charged tetrahedron geometry.

The chemical reaction between the surface of ZnO nuclei and the ions produced by the ionization of capping material gives rise to the formation of different morphology. The ZnO nanoparticles with smaller size are obtained if the CTAB is present in the solution because the positively charged CTAB ions surround the surface of ZnO nuclei there by suppressing the growth of ZnO crystal [136]. In our case too, we obtained ZnO nanoparticles (Fig. 2.5(a)) in the presence of CTAB in precursor solution, while in absence of CTAB, ZnO nanosheets were obtained (Fig. 2.5(b)) for prolonged time.

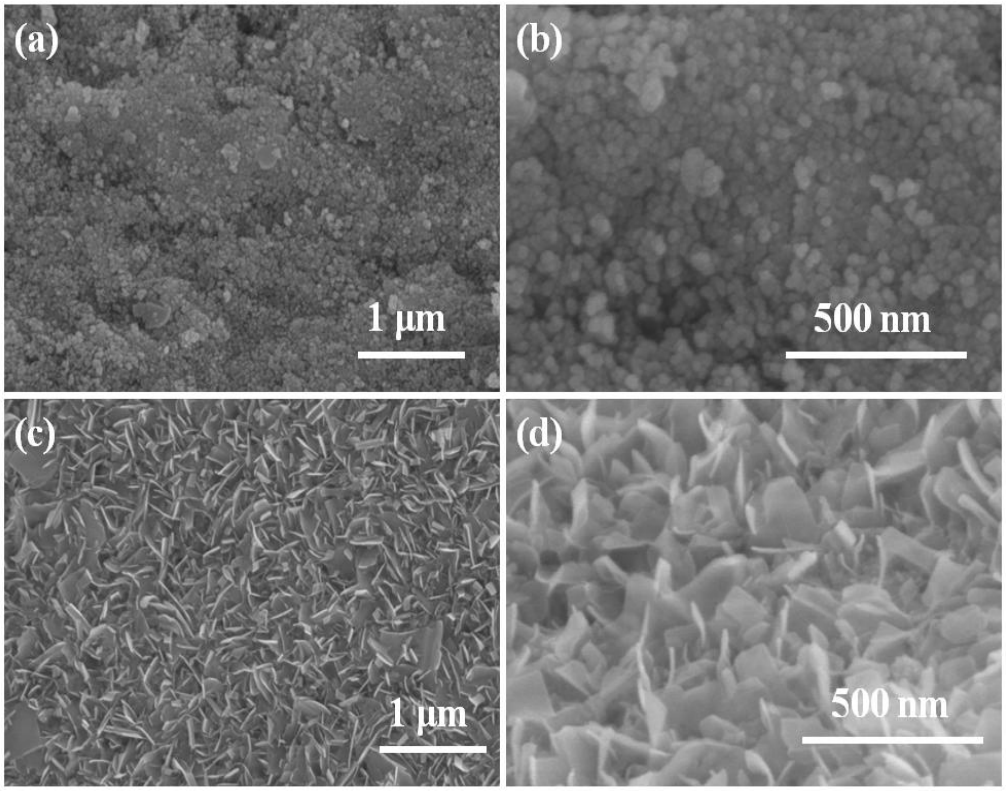

Figure 2.5: FESEM images show variation in morphology (a) & (b) when 0.005 M surfactant was used while synthesis and (c) & (d) shows surfactant free growth of nanosheets.

2.1.2. Characterizations

2.1.2.1. X-Ray Diffraction (XRD)

Figure 2.6 shows X-ray diffraction pattern of nanosheets synthesized in C_2H_5OH medium for 4 hours of reaction at 40 °C. The diffraction peaks at 2θ = 32.7º, 34.5º, and 36.42º in XRD pattern corresponds to (100), (002) and (101) planes of ZnO. The diffraction peaks match well with the single crystalline hexagonal structure of ZnO (JCPDS file no. 36−1451). The calculated lattice constants (a= 3.253Å and c= 5.211Å) also indicate the hexagonal structure of ZnO. The absence of impurity peaks in the XRD pattern indicates the formation of pure ZnO.

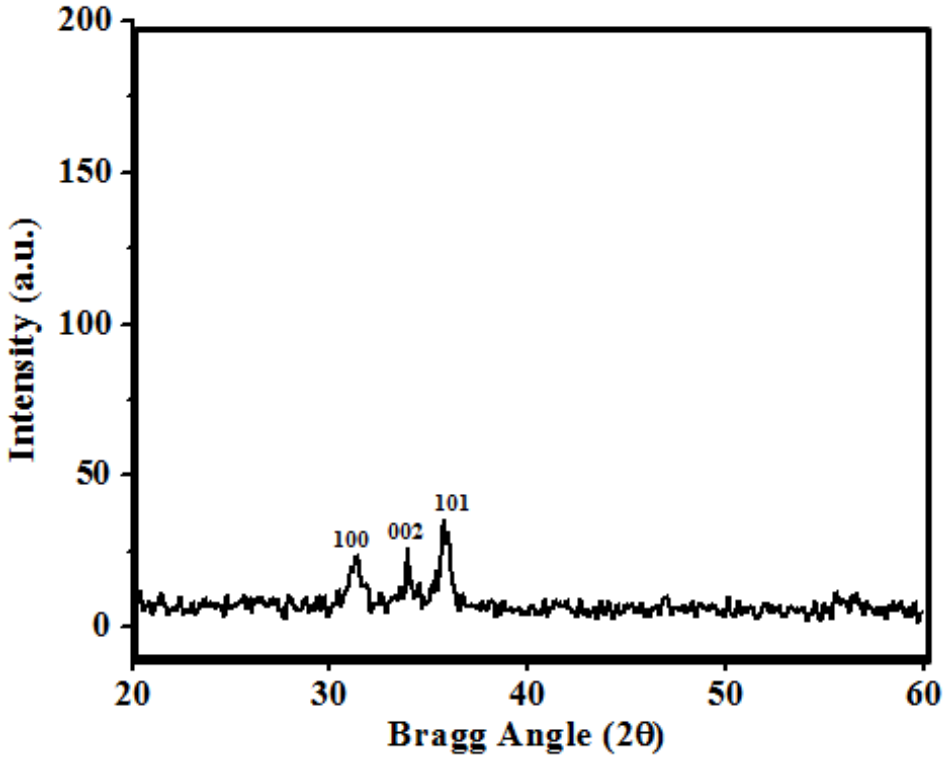

Figure 2.6: X-ray diffraction pattern of ZnO nanosheets synthesized at room temperature for 4 hours of reaction time.

2.1.2.2.Transmission Electron Microscope (TEM)

To explore the structure and elemental composition of nanosheets, we performed TEM and Energy Dispersive X-ray spectroscopy (EDAX) (installed in JEM-2100). The TEM study was carried out at an acceleration voltage of 200 Kilo-Volt and probe current of 1 Nano Ampere. For TEM sampling, powder of ZnO nanosheets was taken in small amount and dissolved in ethanol

which was dispersed by sonication. Then with the help of a syringe, a drop of ethanol dispersed nanosheets was placed on the carbon coated TEM grid.

Figure 2.7 shows TEM image of ZnO nanosheets. The TEM study was done in order to obtain growth of nanosheet. The TEM in Fig. 2.7(a) shows that nanosheets are interwoven to each other. Fig. 2.7(b) is HRTEM image, in this image the nanosheet has a lattice spacing of 0.26 nm. This lattice spacing is corresponding to the growth direction (002) of the wurtzite structure of ZnO. The elemental characterization was done by EDAX installed in TEM which is shown in Fig. 2.7(c). The EDAX shows that the sample contains only Zn and O elements forming ZnO.

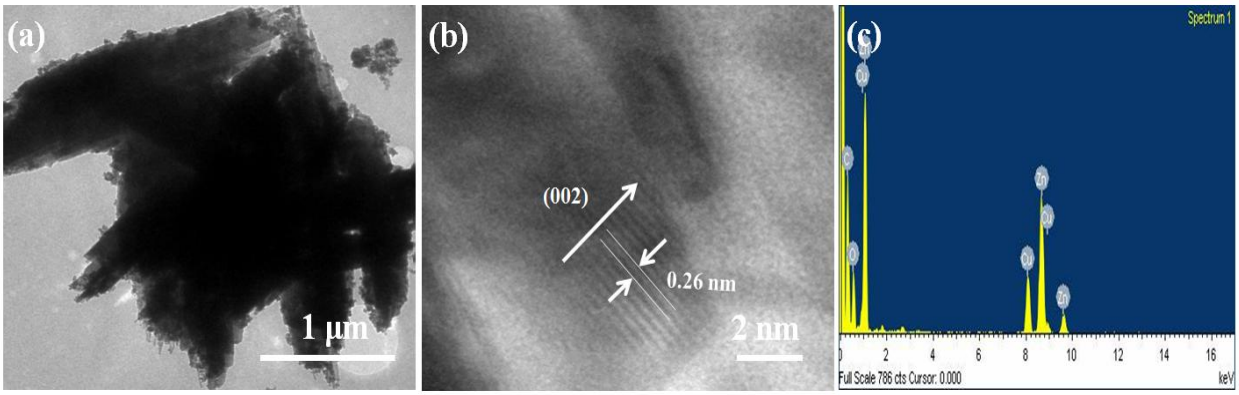

Figure 2.7: HRTEM images of ZnO nanosheets grown after 4 hours of reaction: (a) bunch of ZnO nanosheets, (b) high resolution lattice image of nanosheet shows perfect crystalline structure and (c) EDAX of nanosheets.

2.1.2.3. UV-Vis Spectroscopy

UV-visible absorption spectroscopy is widely being used technique to examine the optical properties of nanosized particles. The UV–Vis spectrum of the ZnO nanosheets is shown in Fig. 2.8. The absorption spectrum of ZnO nanosheets presents a sharp absorption peak around 355 nm which is the characteristic single peak of hexagonal ZnO nanosheets. The nature of the optical band gap can be determined using the fundamental absorption, which corresponds to electron excitation from valence band to conduction band. Direct absorption band gaps of the ZnO nanosheets can be obtained by confirming the absorption data to the following equation [137];

$$\alpha h\nu = B(h\nu - E_g)^n \qquad (2.6)$$

where α is the absorption coefficient, hν is the photon energy, E_g is the optical band gap of the material, B is the material constant and n is either 2 for direct transition or ½ for an indirect transition. Therefore, the optical band gaps of ZnO nanosheets for the absorption edge can be determined by extrapolating the straight portion of the curve $(\alpha h\nu)^2$ versus hν when α = 0. Another way to estimate band gap is by using following equation;

$$E_g = 1.24/\lambda\ (\mu m) \qquad (2.7)$$

where λ is absorption or cutoff wavelength in microns. We have used second approach to calculate approximate band gap. Here cutoff wavelength at 355 nm (Fig. 2.8) and calculated E_g value was approx. 3.49 eV for ZnO nanosheets.

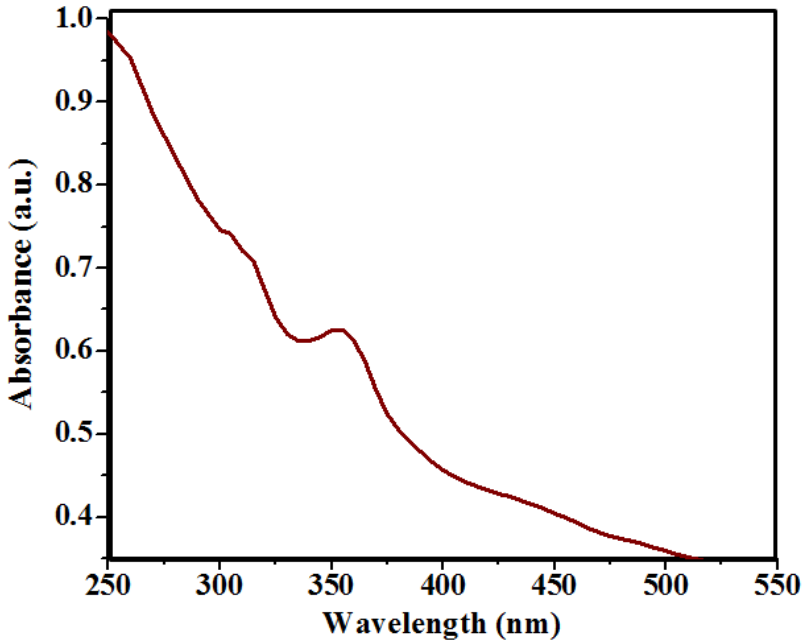

Figure 2.8: Optical absorption spectrum for ZnO nanosheets prepared by chemical route at room temperature for 4 hours of reaction time.

2.1.2.4. Fourier Transform Infrared Spectroscopy (FTIR)

The ZnO nanostructure sample was also investigated by FTIR. Figure 2.9 shows FTIR spectrum of ZnO nanosheets. The FTIR spectrum contains broad peaks at around 3392 and 1635 cm^{-1}. These peaks may be assigned to the stretching and bending modes, respectively, of hydroxyl groups (chemisorbed and/or physisorbed H_2O molecules) on the surface of ZnO nanocrystals. A

band at 1403 cm^{-1} related to the symmetrical/asymmetrical stretching modes of the carboxylate group of acetate coordinated to the surface of ZnO nanocrystals is also observed. Also, a high intensity broad band around 884 cm^{-1} due to the typical bending mode of hydroxyl group is observed in the spectra of the structure. Other unsigned peaks are attributed to remnant organic species in the samples.

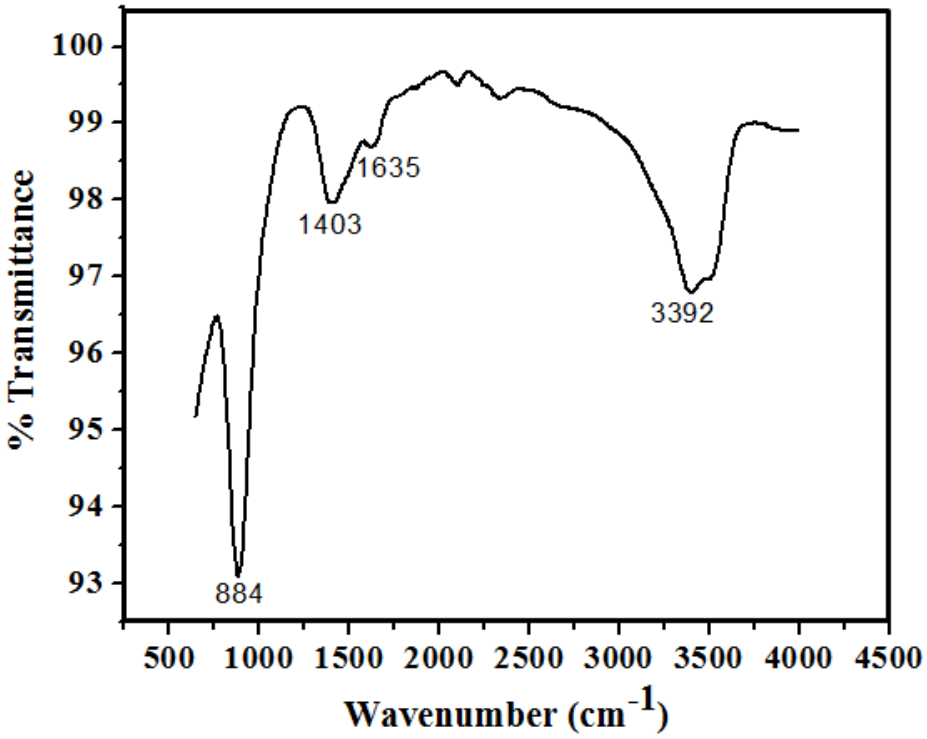

Figure 2.9: FTIR spectrum of ZnO nanosheets show IR absorption frequencies of organic functional groups.

2.1.2.5. Photoluminescence Spectroscopy (PL)

In order to investigate the defects in as synthesized ZnO nanosheets photoluminescence was performed. The PL spectrum of ZnO nanosheets investigated at an excitation wavelength 340 nm is shown in Fig. 2.10. The PL spectra is fitted with a five Gaussian function at the center wavelengths of 390 nm (UV), 420 nm (violet), 466 nm (blue), 485 nm (blue-green) and 520 nm (green) using origin software, which reproduces the PL spectrum more reasonably. The UV emission around 390 nm (3.17 eV) corresponds to near band edge (NBE) emission [138]. The band edge emission is mainly due to radiative recombination of excitons. The emission at 420

nm (2.95 eV) is attributed to the transition between shallow donors (oxygen vacancy) to the valence band VB [139-141]. The peak at 465 nm (2.66 eV) is related to zinc vacancy and interstitial defects [142]. The emission at 485 nm (2.55 eV) wavelength is assigned to recombination between the oxygen vacancy and interstitial oxygen, and lattice defects related to oxygen and zinc vacancies [140, 143]. A broad peak around 520 nm (2.38 eV) is due to radiative recombination of a photogenerated hole with an electron occupying the oxygen vacancy, which is attributed to the single ionized oxygen vacancy [144]. These transitions confirm the existence of the oxygen and zinc vacancies in nanosheets.

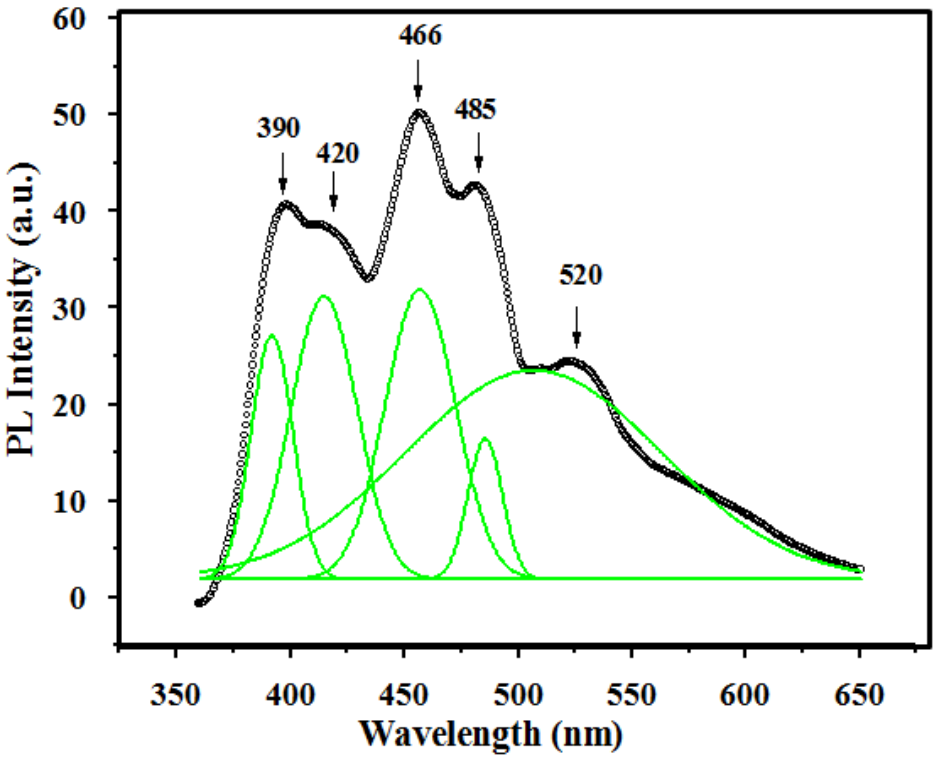

Figure 2.10: Visible PL spectrum of ZnO nanosheets grown in ethanol. The black solid curves are the experimental data and the green curves are individual peaks from the fittings. Spectrum was recorded at 340 nm excitation wavelength.

2.2. Synthesis of ZnO flower-like structures

To synthesize flower-like structure, solutions of 0.5 M $ZnAc_2$ (purity 99.99%, Sigma Aldrich) and 0.5 M KOH (purity 98%, Merck) were prepared in distilled (DI) water. Prepared $ZnAc_2$ solution was added dropwise to the KOH solution at 40 °C under continuous stirring for 4 hours,

and a white precipitate was obtained. After the reaction, the precipitate was filtered and washed several times with DI water and ethyl alcohol. To evaporate the water, the precipitate was dried for 1 hour at 100 °C in a horizontal tube furnace. After drying of the above precipitate, nanosheets were obtained in bunches (which we call flower-like structure).

2.2.1. Morphology Control

2.2.1.1. Effect of precursor and alkali concentration

The experiment showed that the existence of hydroxide ion played an important role in the formation of ZnO structures in water as solvent. It is found that the morphologies of the ZnO structures are sensitive to the amount of KOH. Figure 2.11 shows ZnO morphologies formed with different concentration of precursor solution ($ZnAc_2$) and alkali solution (KOH). Figures 2.11(a)-2.11(d) shows the change in the morphologies of the product with different concentrations of KOH. Figure 2.11(a) shows the FESEM image of the obtained ZnO structure formed for the molar ratio of OH^-: Zn^{2+} equal to 2: 1 (conc. of $ZnAc_2$ and KOH is 0.5 M and 1 M, respectively), the octahedral-like structure of micrometer range can be observed. This is inferred due to the more basic nature of the solution due to which recrystallization occurs which give rise to microstructure. The size of the particles goes on increasing with increasing pH of the solution [145]. The decrease in the KOH concentration (0.5 M) for molar ratio 1: 1 results in the formation of flower-like structures (Fig. 2.11(b)). Therefore, it is speculated that the amount of KOH in solution can adjust the ZnO crystal growth. Further, by decreasing the KOH concentration (0.25 M) in 1: 2 ratios in the solution resulted in the formation of nanoparticles as shown in Fig. 2.11(c). A further decrease in the KOH concentration (0.125 M) in ratio 1: 4 resulted in the layered small sheet-like structure network (Fig. 2.11(d)).

Similar to above, Figs 2.11(e)-2.11 (h) shows the morphological change of the product with varying concentration of precursor solution ($ZnAc_2$). In Fig. 2.11(e), when the molar ratio of OH^- : Zn^{2+} was chosen as 4: 1 (conc. of $ZnAc_2$ and KOH was set as 0.125 M and 0.5 M, respectively), the obtained products were microstructures having some sheets like structures. An increment in the precursor solution concentration (0.25 M) for 2: 1 ratio of OH^-: Zn^{2+} in the solution, a non-uniform aggregation of sheet-like structures was obtained as shown in Fig. 2.11(f). A further increase in the $ZnAc_2$ solution concentration (0.5 M) such as 1: 1 resulted in the formation of flower-like structures (aggregation of sheets) (Fig. 2.11(g)). Further, increase in

precursor solution concentration to 1 M (OH^-: Zn^{2+} = 1: 2) resulted in the coagulation of sheet-like structure (nest-like structure) (Fig. 2.11(h)). In this study, we observed that molar ratio 1: 1 of $ZnAc_2$ and KOH is optimum for the formation of uniform ZnO flower-like structures.

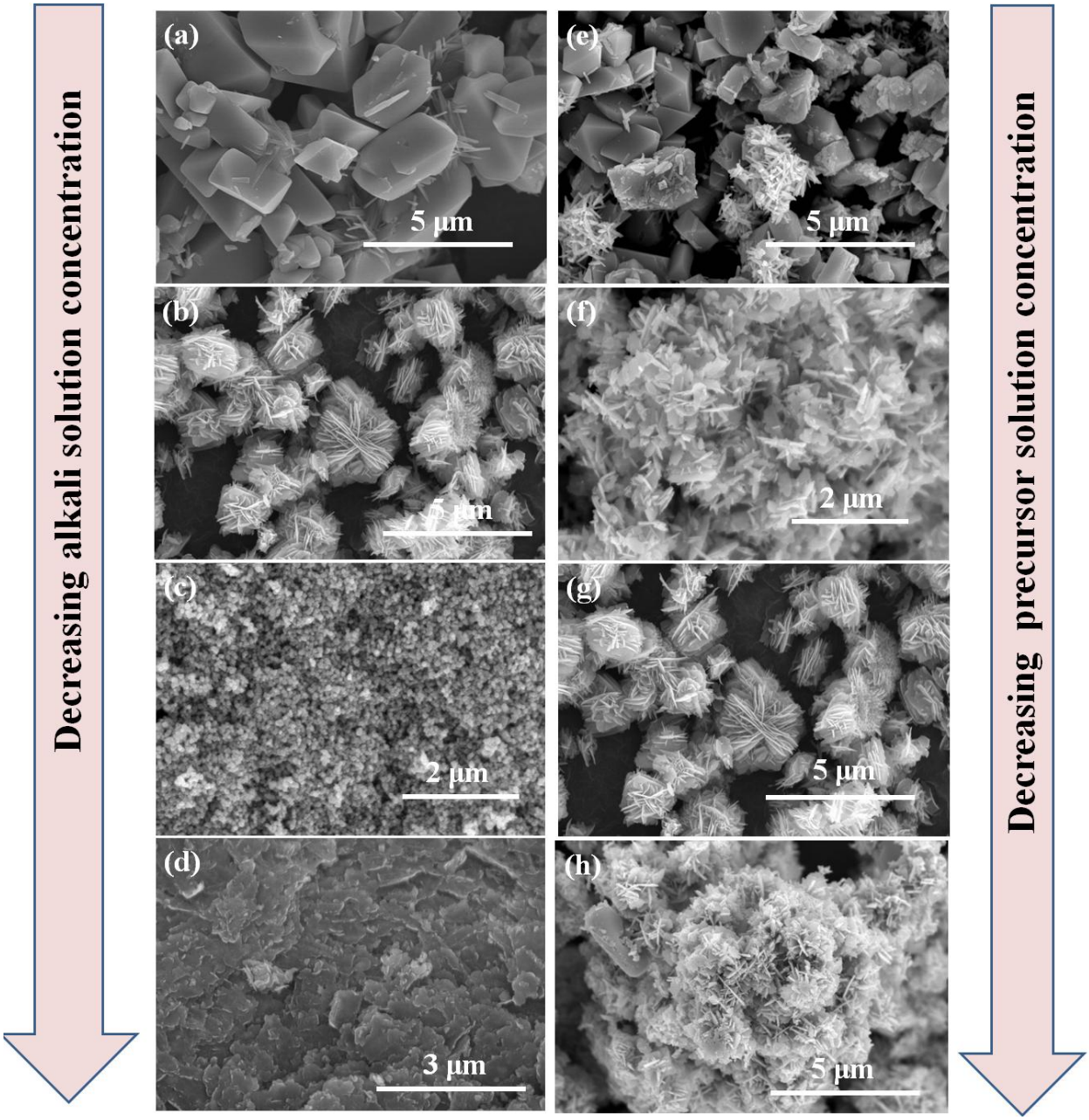

Figure 2.11: FESEM images show change in the morphology by varying alkali to precursor solution ratio (OH^-: Zn^{2+}) (varying concentration from 0.125 to 1 M) as (a) 2: 1, (b) 1: 1, (c) 1: 2, (d) 1: 4, and (e) 4: 1, (f) 2: 1 (g) 1: 1 (h) 1: 2, respectively, in H_2O medium.

In this case too, when water was used as solvent, along with the molar ratio of 1: 1 of OH^- to Zn^{2+}, the concentration of precursor and alkali solution also plays an important role in the formation of nanostructure. Initially, we used 0.1 M concentration for both of the solutions, the obtained structure was irregular structure as shown in Fig. 2.12(a). When we increased the concentration to 0.2 M while keeping the molar ratio of precursors as 1:1, a small change in the structure was obtained but still it was irregular microstructures as shown in Fig. 2.12(b). With a further increase in the concentration of $ZnAc_2$ and KOH solutions to 0.4 M, the flower-like structure in large amount as compared with microstructures was obtained as shown in Figs. 2.12(c)-2.12(f). And at 0.5 M of both the solutions, only flower-like structure appeared as shown in Fig. 2.12(g). The concentration 0.6 M of both the solutions gave rise to disappearance of flower-like structure with nanoparticles on their surface in the product as shown in Fig. 2.12(h). All the experiments were performed in similar conditions merely the molarities of $ZnAc_2$ and KOH solutions were adjusted. Similar to the ethanol as a solvent, from these observations we observed that in addition to the Zn^{2+} concentration only a certain pH range (pH= 9 to 12) is suitable for the formation of ZnO nuclei in solution in water as solvent, influencing the crystal growth rate and the resulting morphologies.

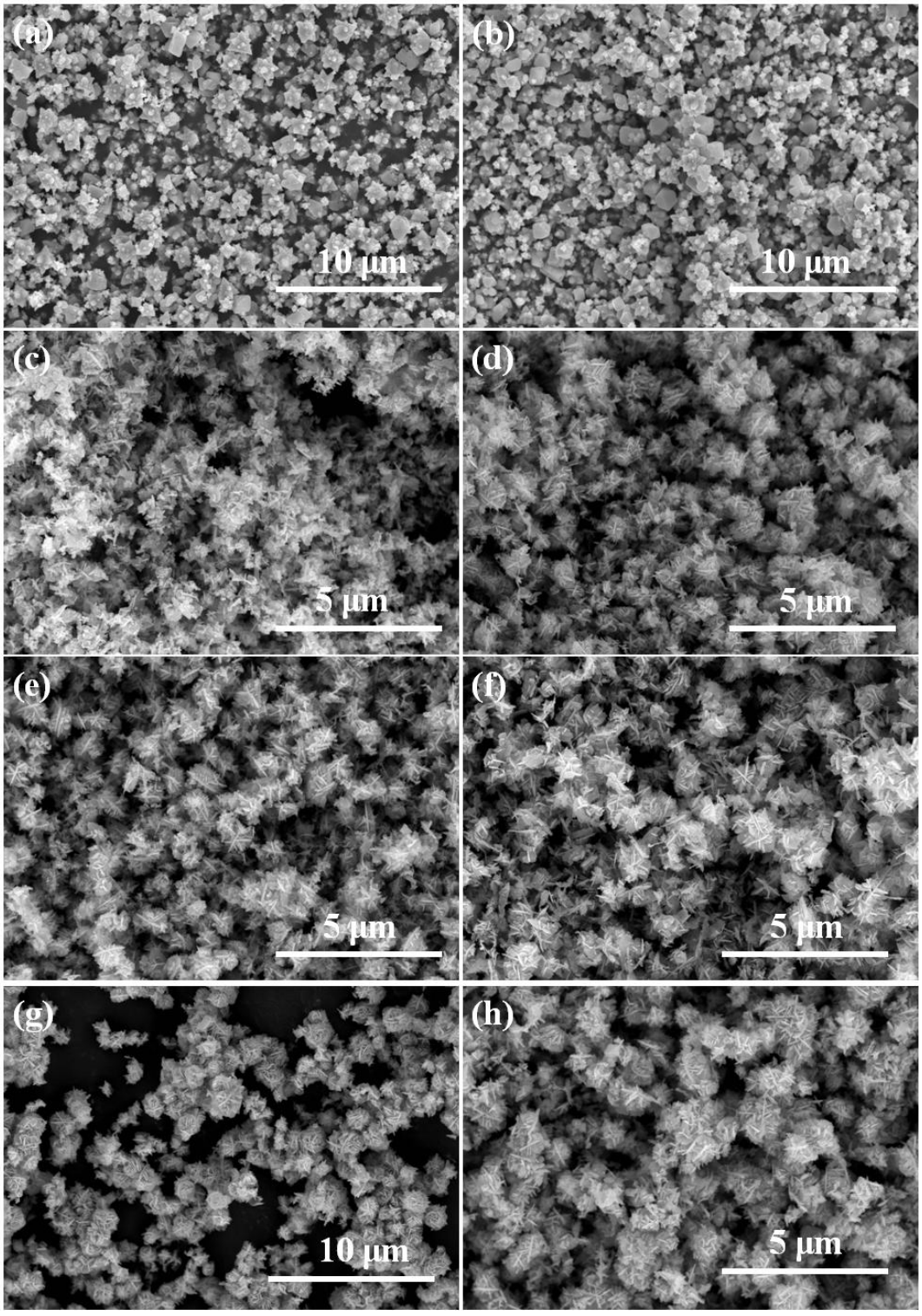

Figure 2.12: FESEM images show small change in morphology with variation of concentration of precursor and alkali solution concentration simultaneously as (a) 0.1 M, (b) 0.2 M, (c) 0.25 M, (d) 0.3 M, (e) 0.4 M, (f) 0.45 M, (g) 0.5 M, (h) 0.6 M, by keeping OH^-: Zn^{2+}=1: 1.

2.2.1.2. Effect of reaction time

In case of nanoflowers, two possibilities exist for the growth of the flower-like structures in aqueous medium. The first is the growth of monodispersed nanosheets in aqueous solution which aggregate together in the form of flower-like structure (almost spherical) to attain the minimum surface energy. The second is the formation of aggregates of nanoparticles in the solution which by consuming the precursor from the solution grows further and forms a flower-like structure with the passage of time. Each nanoparticle in an aggregate which grows with the passage of time in 2D (sheet like structure), consuming the precursor present in the solution along the (002) direction. A random orientation of the nanosheets (as in Fig. 2.13) may be attributed due to the random orientation of the growth direction in an aggregate. Since the nanoparticles in an aggregate arranged in a random manner their growth direction (002) is also oriented randomly, therefore the nanosheets are randomly oriented.

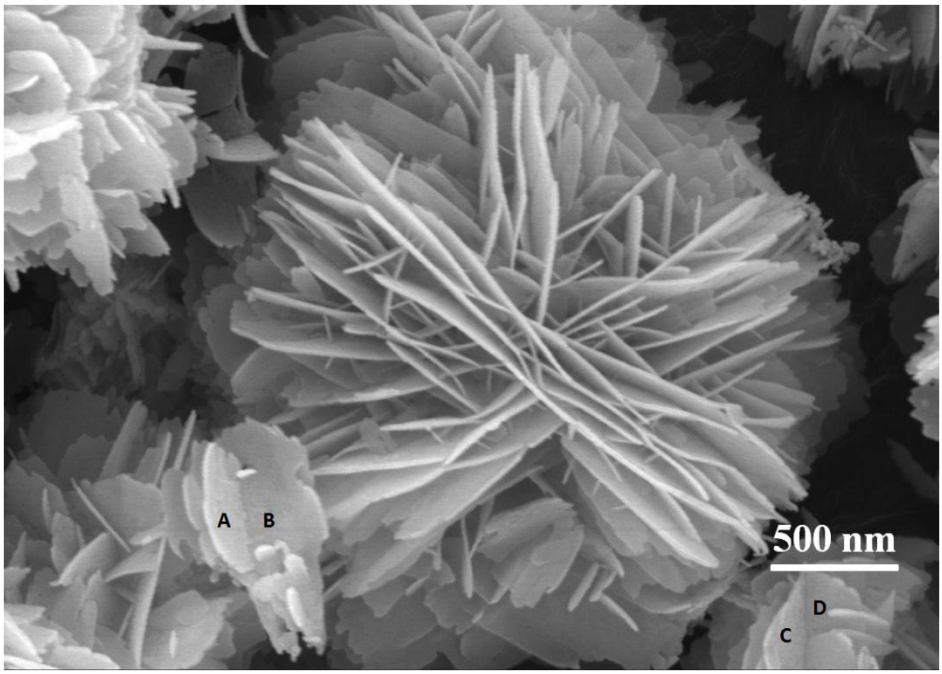

Figure 2.13: FESEM image of a single flower-like structure indicating random orientation of the nanosheets.

The first possible growth mechanism is unlikely for the reasons. If the nanosheets are grown initially inside the solution they cannot interwoven in a compact manner as indicated in Fig. 2.13. Also, in this image many of the nanosheets can be seen to be grown normally to each

other (nanosheets A is normal to B and C is normal to D in the FESEM image Fig. 2.13). Therefore, the second possibility is more plausible. In this case, flower-like structure is formed as the growth of the ZnO nanoparticles aggregate.

The FESEM images in Fig. 2.14 show the growth of flower-like structure at successive reaction time. A schematic in Fig. 2.14 (left of the FESEM images) represents the growth mechanism of a flower-like structure composed of nanosheets. In the aqueous medium, when the reaction elapsed for 0.25 hour, nanoparticles (size about 25 nm) aggregate in a bunch like structure (Figs. 2.14(a) and 2.14(b)). As the reaction proceeds further each nanoparticle aggregate grows to form a sheet-like structure as indicated in Figs. 2.14(c)-2.14(h). The growth mechanism of nanosheets composing the flower-like in aqueous medium is similar to the growth mechanism of nanosheets in alcohol medium. The mechanism can also be correlated to the adsorption phenomenon of the acetate and hydroxyl ions which is explained in detail in chapter 3. Initially in 0.25 hour time although there is an absence of the sufficient adsorbed ions over the ZnO centers (Fig. 3.3) but due to the strong hydrogen bonding network facilitated by the highly polar water molecules, the adhesion can be seen among ZnO nanoparticles. Further with time the adsorption of the ions increases and more interwoven structures appear and finally in the form of flower-like structures.

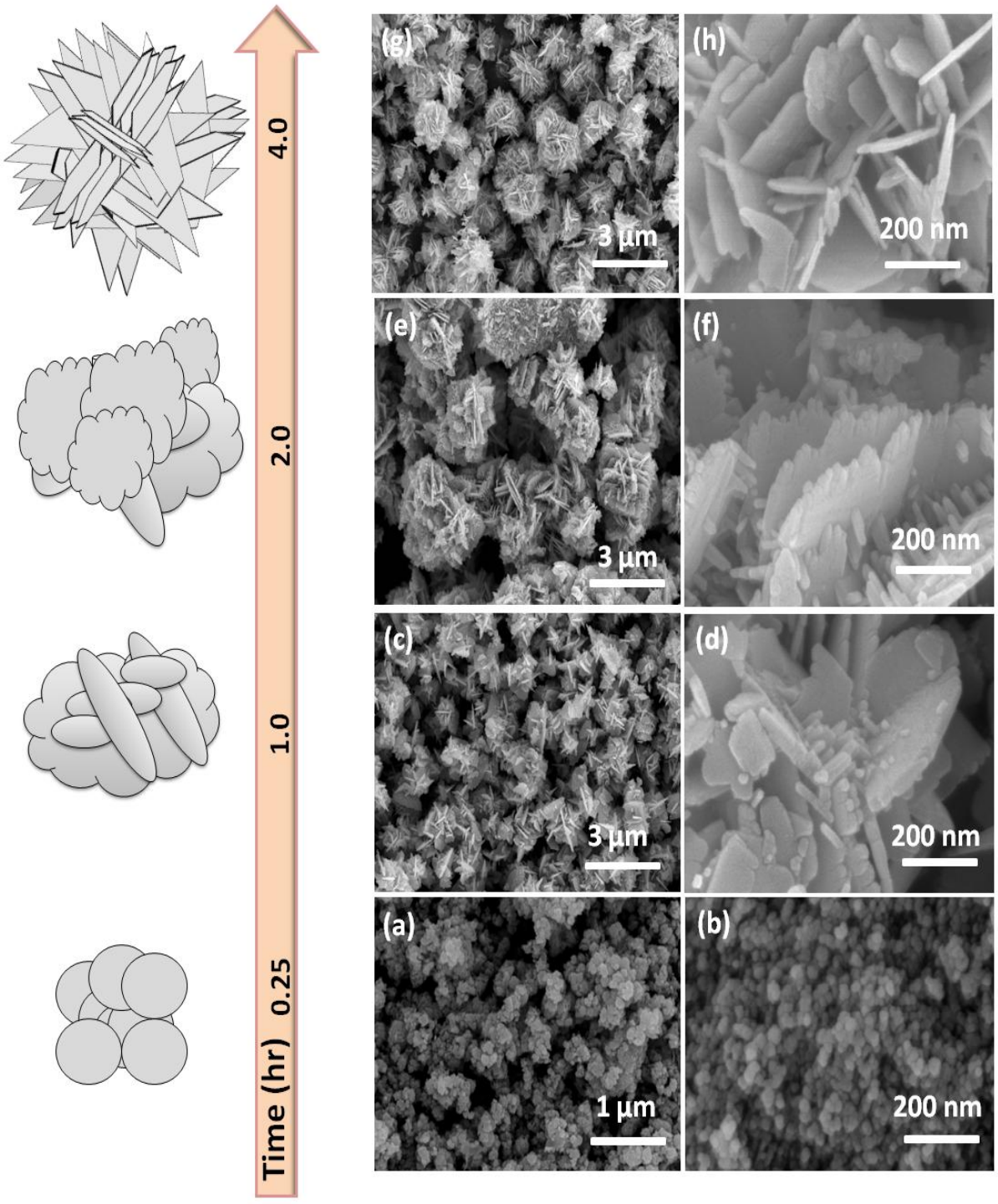

Figure 2.14: FESEM images of the products prepared in (a, b) 0.25 hour, (c, d) 1 hour, (e, f) 2 hours and (g, h) 4 hours at a 40 ºC reaction temperature. Schematic illustration of the formation stages of different shapes of the ZnO nanostructures (in the left of FESEM image).

2.2.1.3. Effect of surfactant

The growth mechanism of ZnO is different in the existence of surfactant i.e. CTAB in solution. Similar to the case of C_2H_5OH solvent in H_2O too, the capping material CTAB caps the surface of nanoparticles and hinders their further growth. Therefore, we got nanoparticles of ZnO as shown in Figs. 2.15(a) and 2.15(b) in the presence of CTAB in solution while in the absence of surfactant in solution results ZnO flower-like structure (Figs. 2.15(c) and 2.15(d)).

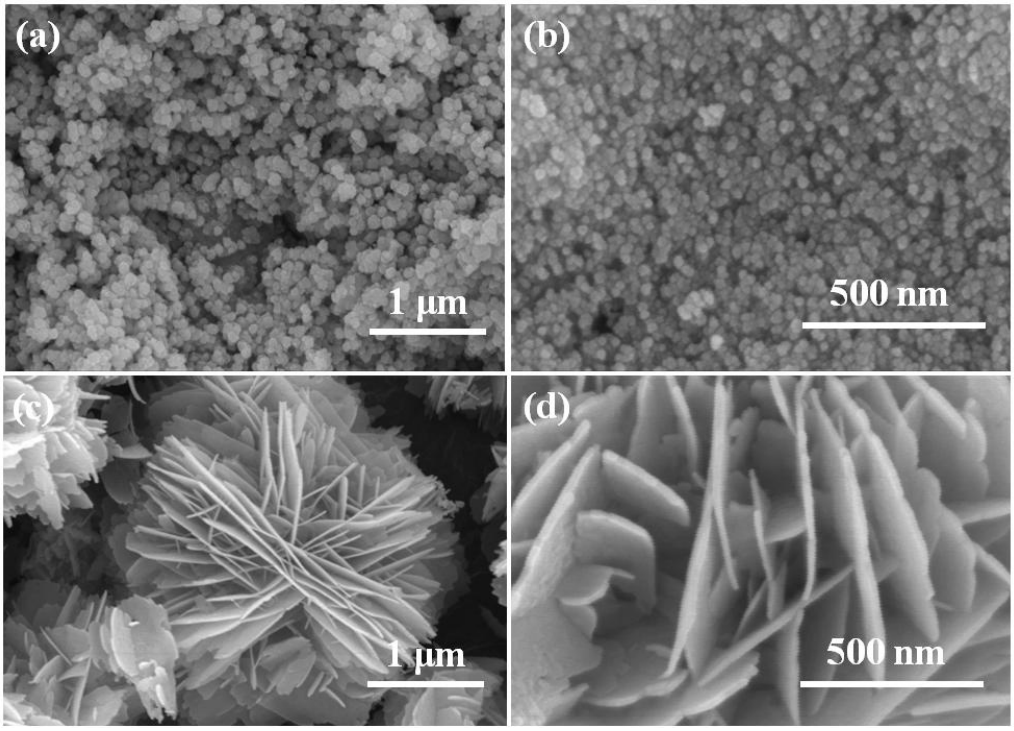

Figure 2.15: FESEM images show variation in morphology (a) & (b) when 0.005 M surfactant was used while synthesis and (c) & (d) shows surfactant free growth of flower-like structure.

2.2.2. Characterizations

2.2.2.1. X-Ray Diffraction (XRD)

Figure 2.16 shows the XRD patterns of flower-like. The sharp intense peaks of ZnO confirm good crystalline nature of the product. The peaks originated at (100), (002), (101), (102), and (110) reflections show formation of hexagonal ZnO similar to the case of nanosheets.

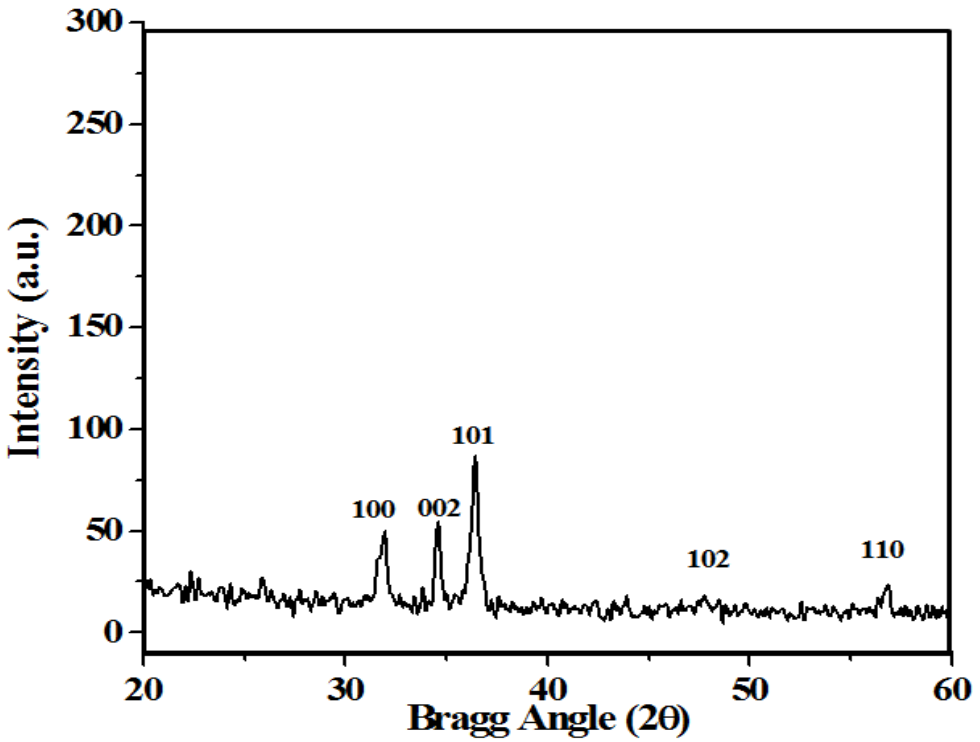

Figure 2.16: X-ray diffraction pattern (λ=1.54056 Å) of the flower-like structure grown at 40 ^{o}C for 4 hours of reaction time. The diffraction peaks for ZnO are indicated according to the JCPDS file (36-1451).

2.2.2.2. Transmission Electron Microscope (TEM)

To explore the structure and elemental composition of flower-like structures, we performed TEM and Energy Dispersive X-ray spectroscopy (EDAX) (installed in JEM-2100). For TEM sampling, powder of ZnO was taken in small amount and dissolved in ethanol which was dispersed by sonication. Then with the help of a syringe, a drop of ethanol dispersed powder was placed on the carbon-coated TEM grid.

Figure 2.17(a) represents TEM image of flower-like structures. Here each of the flowers is composed of very thin sheets-like structure. Figure 2.17(b) is HRTEM image, which indicates the lattice fringe spacing equal to 0.26 nm. From HRTEM image, ZnO nanostructures i.e. flower-like structure has the crystallographic orientation along (002) direction. The EDAX result obtained for the flower-like is shown in Fig. 2.17(c). The obtained 'O' (by 52.43 at. %) and 'Zn' (by 47.57 at. %) peaks in EDAX shows that the flower-like structure is composed of ZnO.

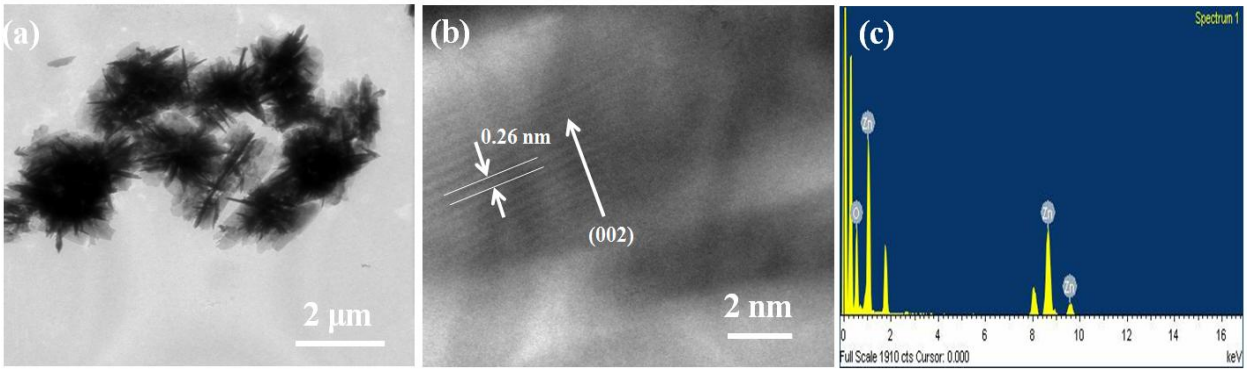

Figure 2.17: HRTEM images of ZnO flower-like structure grown after 4 hours of reaction: (a) bunch of ZnO nanoflowers, (b) high resolution lattice image of flower-like structure showing perfect crystalline structure with (c) corresponding EDAX spectrum shows the different elements component.

2.2.2.3. UV-Vis Spectroscopy

The absorption spectrum of ZnO flower-like structures sample is shown in Fig. 2.18. It exhibits a strong absorption peak at about 365 nm wavelength. The band gap calculated from the UV cut-off is 3.39 eV.

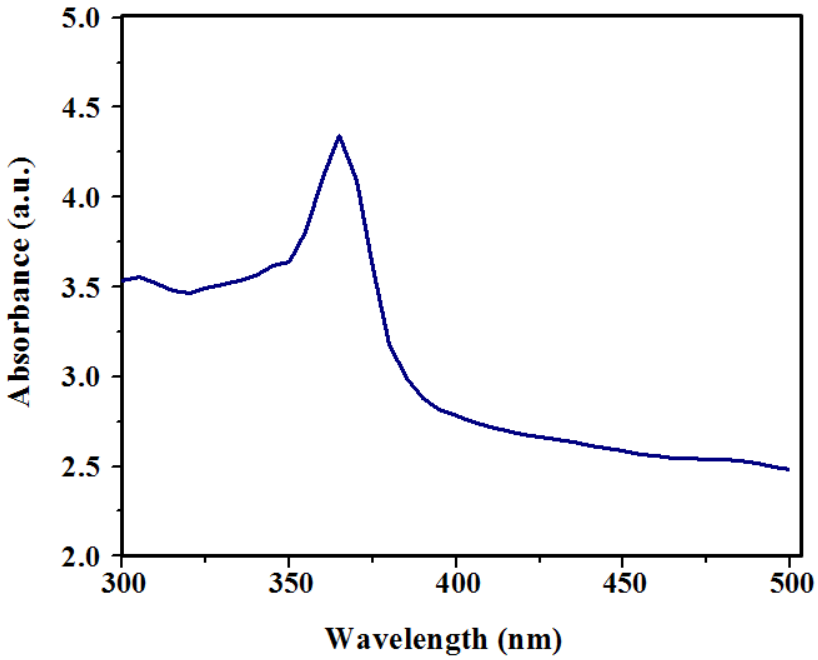

Figure 2.18: Optical absorption spectrum of ZnO flower-like structures shows absorbance peak of powder at 365nm wavelength.

2.2.2.4. Fourier Transform Infrared Spectroscopy (FTIR)

The FTIR analysis was carried out to investigate organic functional groups in ZnO flower-like structure. Figure 2.19 shows FTIR spectrum of ZnO flower-like structures. As seen in Fig. 2.19, the ZnO exhibits characteristic peaks around 3392 cm^{-1} which is attributed to O–H stretching mode. The bending mode of hydroxyl group occurs at 1635 cm^{-1}. The band at 1403 cm^{-1} is assigned to the symmetrical/asymmetrical stretching modes of the carboxylate group of acetate coordinated to the surface of ZnO nanocrystals. And the band at 884 cm^{-1} is due to the typical bending mode of hydroxyl group. Other unsigned peaks in FTIR spectrum are attributed to remnant organic species in the samples.

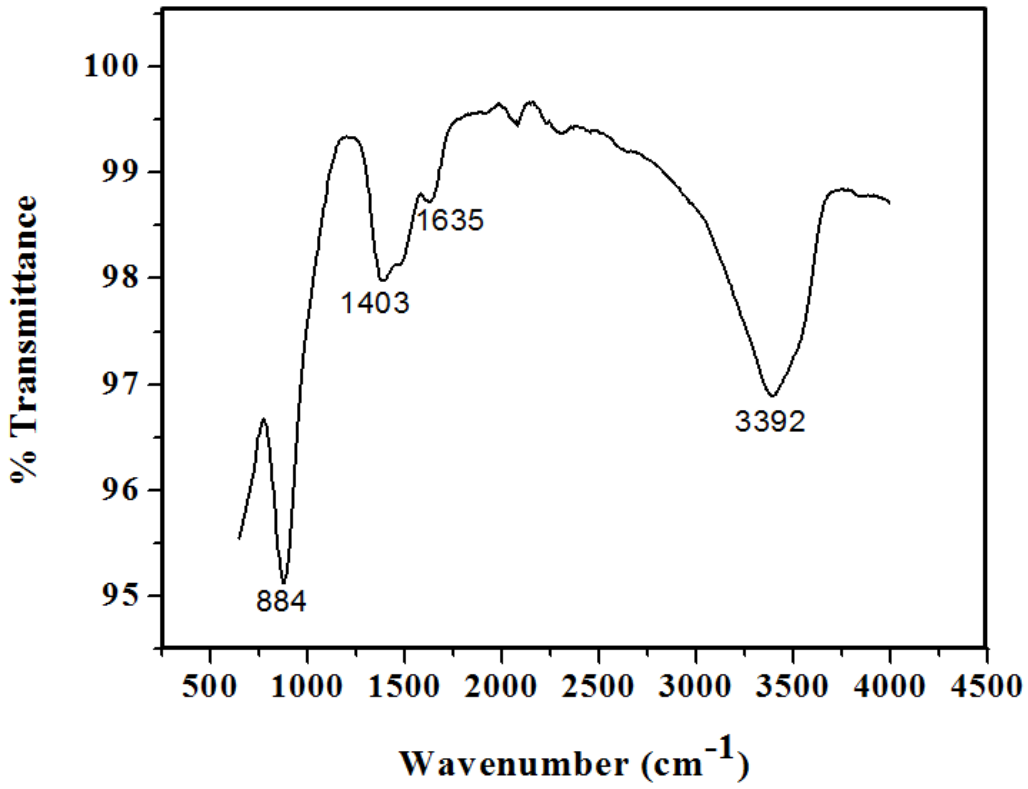

Figure 2.19: FTIR spectrum of ZnO flower-like structures show IR absorption frequencies of organic functional groups.

2.2.2.5. Photoluminescence Spectroscopy (PL)

The room temperature PL spectrum of ZnO flower-like structures is shown in Fig. 2.20. Bands are observed around 390 nm (UV), 420 nm (violet), 466 nm (blue), 485 nm (blue-green) and 520

nm (green). The UV emission corresponds to the near band edge emission of the wide band gap of ZnO, which is caused by annihilation of the excitons by recombination [146-148]. The observed violet emission is caused by electron transitions from the shallow donor levels of oxygen vacancies to the valence band [139-141]. The blue emission is due to the zinc vacancy and interstitial defects [142], and blue-green emission is related to recombination between the oxygen vacancy and interstitial oxygen, and lattice defects related to oxygen and zinc vacancies [140, 143]. The presence of these peaks indicates UV as well as visible emissions due to surface defects states present in synthesized ZnO structure. The broad green emissions results from the radiative recombination of photogenerated holes with singularly ionized oxygen vacancies [144]. The sharp, intense UV emission indicates that the ZnO structure is highly crystalline with excellent optical properties.

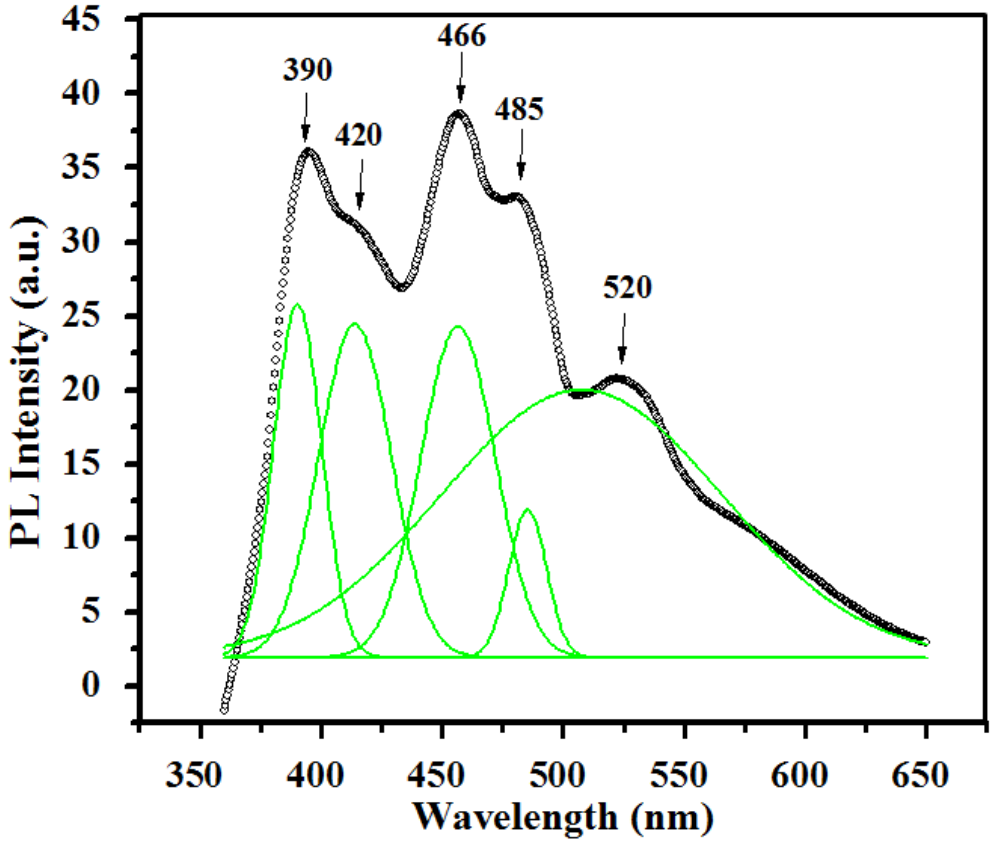

Figure 2.20: PL spectrum of ZnO flower-like structure grown in water as solvent. The black solid curves are the experimental data and the green curves are individual peaks from the fittings. Spectrum was recorded at 340 nm excitation wavelength.

2.3. Synthesis of ZnO Nanoparticles

Materials: Zinc acetate ($ZnAc_2$) (purity 99.99%, Sigma Aldrich), cetyltrimethylammonium bromide (CTAB) (purity 99%, Sigma Aldrich) and potassium hydroxide (KOH) (purity 85%, Merck) were used as the precursor and alkali solutions. Commercially available reagents were used as received without further purification. All reactions were carried out in glassware dried in an oven under ambient conditions.

Method: For the synthesis of ZnO nanoparticles, a 0.2 M solution of KOH was added dropwise to 0.1 M $ZnAc_2$ solution at vigorous stirring. A 0.05 M solution of CTAB was added abruptly to the solution. Thus obtained solution was stirred at 40 °C for 4 hours. After 4 hours, a precipitate was obtained which was filtered, washed with DI water and ethyl alcohol, and finally dried for 2 hours at 60 °C to obtain nanoparticles.

2.3.1. Field Emission Scanning Electron Microscope (FESEM)

Figures 2.21(a) and 2.21(b) are low and high magnification FESEM images of the nanoparticles, respectively. Figure 2.21(b) shows the formation of spherical nanoparticles with a size 20–30 nm. Since during the formation of the nanoparticles, a capping material CTAB, was used to control the growth, therefore small-sized nanoparticles have been obtained.

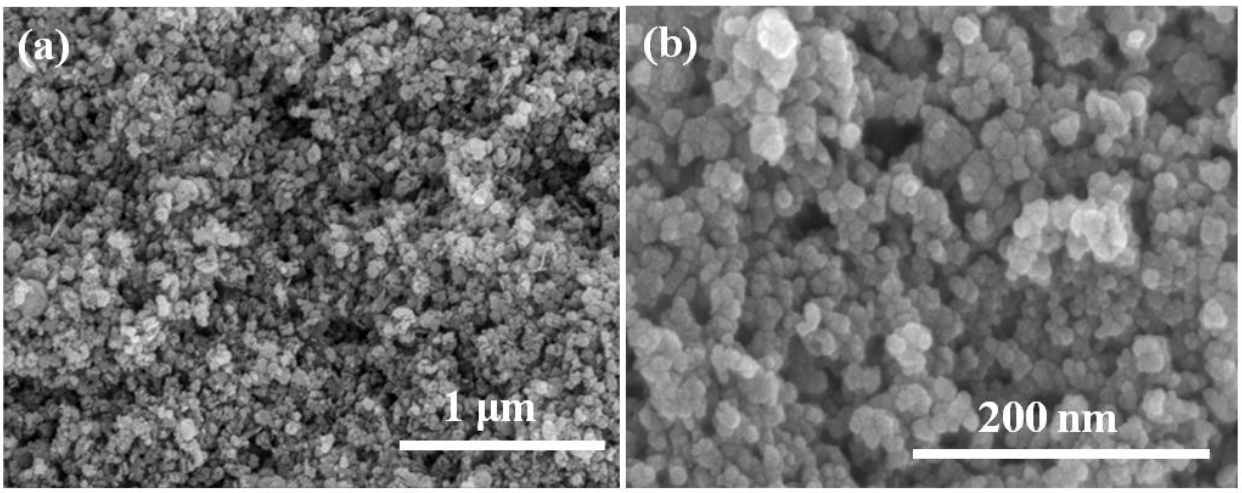

Figure 2.21: FESEM images of ZnO nanoparticles synthesized using CTAB as surfactant, which controls the size of the nanoparticles. (a & b) FESEM images at low magnification and high magnification, respectively. FESEM image in (b) shows the uniform size distribution of the nanoparticles.

2.3.2. X-Ray Diffraction (XRD)

The XRD pattern of nanoparticles is shown in Fig. 2.22. The diffraction peaks at 2θ = 32.7°, 34.5°, and 36.42° correspond to the (100), (002), and (101) planes of the ZnO structure. All the diffraction peaks in this pattern can be perfectly indexed as a wurtzite-structured ZnO with lattice constants a = 0.325 nm and c = 0.521 nm. In addition to these commonly observed orientations, the weak orientations at 47.44° and 56.58° corresponding to (102) and (110), respectively are also observed in the XRD pattern. The recorded XRD pattern well matched with the reference card JCPDS 89-1397 confirming the nanoparticles to be composed of ZnO. No characteristic peaks of impurities are detected in the XRD, which shows the high purity of the product. In addition, the strong and sharp diffraction peaks reveal that the as synthesized ZnO nanoparticles are well crystalline.

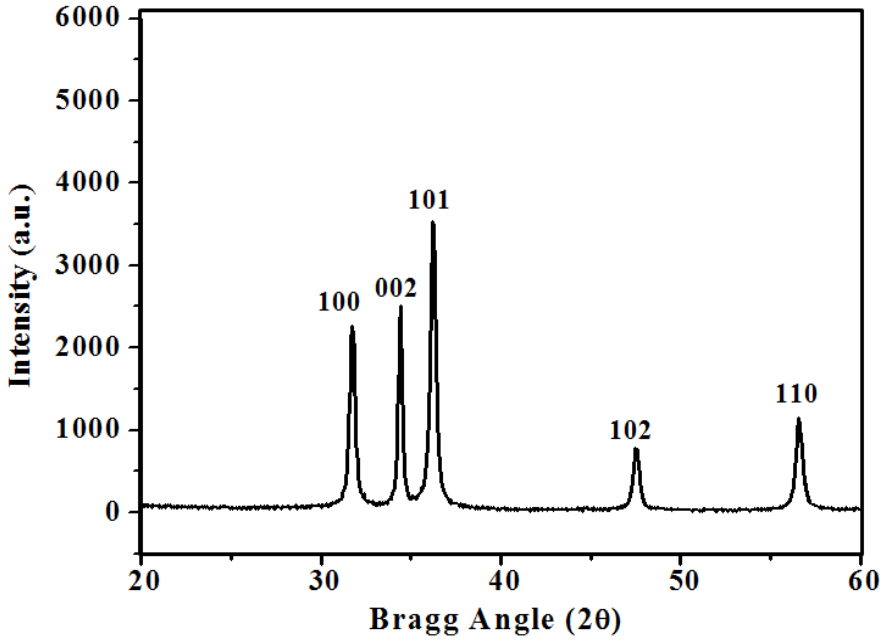

Figure 2.22: XRD pattern from ZnO nanoparticles prepared in the presence of surfactant after 4 hours of reaction time at room temperature.

The size of the particles is calculated by Debye Scherrer's formula:

$$D = k(\lambda/\beta\cos\theta) \qquad (2.8)$$

where k is a constant equal to 0.89, λ the X-ray wavelength (0.154095 nm), β the full wavelength at half maximum and θ the half diffraction angle. The crystal size of ZnO nanoparticles calculated from FWHM (Full Wave Half Width) is tabulated in Table 2.1.

Table 2.1: Particle size estimated from the diffraction spectrum by using half maximum widths.

Pos. [°2Th.]	(hkl)	FWHM Left [°2Th.]	d-spacing [Å]	Particle size (nm)
31.724	100	0.315	2.81827	25.94
34.387	002	0.213	2.60591	38.63
36.211	101	0.313	2.47872	26.42
47.488	102	0.36	1.91308	23.85
56.530	110	0.36	1.62665	24.79

2.3.3. UV-Vis Spectroscopy

Figure 2.23 shows optical absorption spectrum of CTAB capped ZnO nanoparticles. Excitonic absorption peaks are blue shifted with respect to the absorption edge which appears at 400 nm at room temperature [149, 150] in the case of bulk ZnO. The excitonic absorption feature for nanosized particles can be seen at about 315 nm which gives approx. 3.93 eV of band gap.

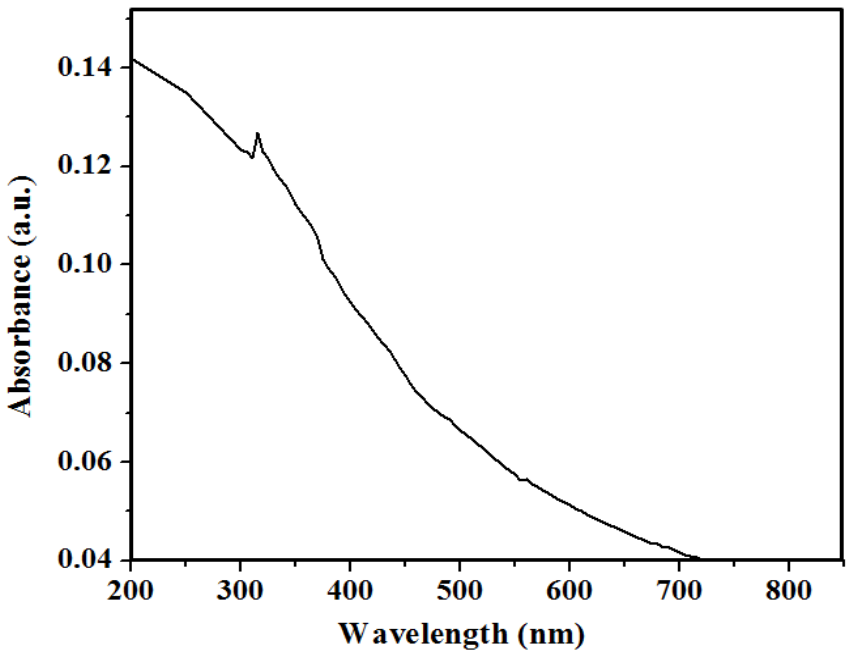

Figure 2.23: Optical absorption spectrum of ZnO nanoparticles showing absorption at 315 nm.

2.3.4. Photoluminescence Spectroscopy (PL)

The room temperature PL spectrum of nanoparticles is shown in Fig. 2.24. Characteristic peaks are observed at 390 nm (UV), 420 nm (violet), 466 nm (blue), 485 nm (blue-green) and 520 nm (green). The explaination of these peaks is similar to the nanosheets and flower-like structure. The sharp, intense UV emission indicates that the nanoparticles are highly crystalline with excellent optical properties. Similar to nanosheets and flower-like structure, the presence of these peaks indicates UV as well as visible emissions due to the surface defects states in nanoparticles also.

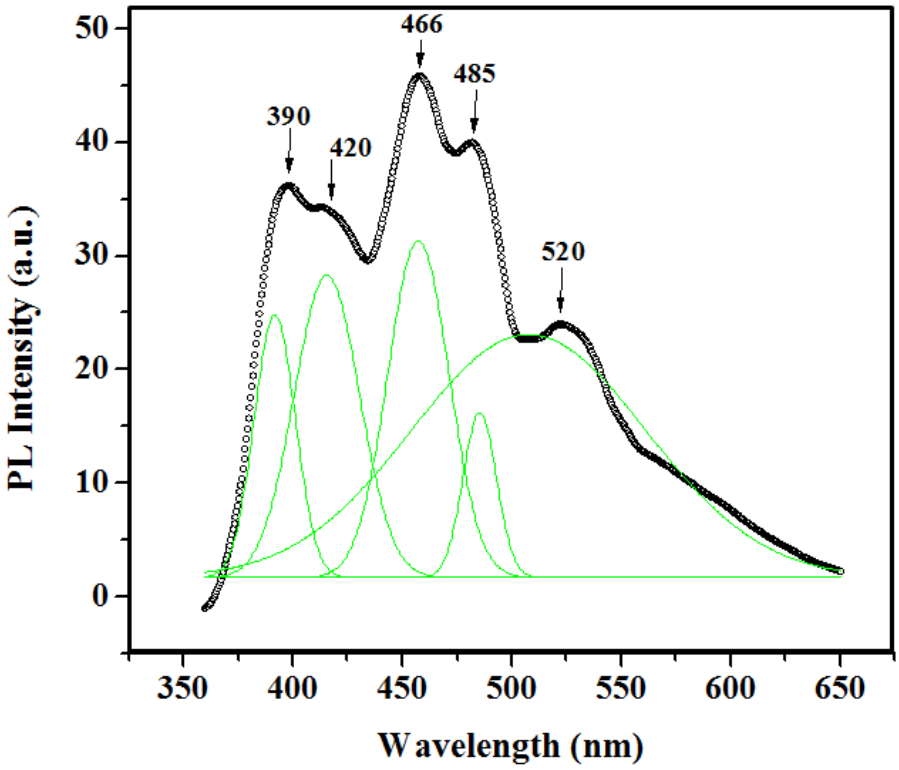

Figure 2.24: PL spectrum of ZnO nanoparticles prepared in presence of surfactant. The black solid curves are the experimental data and the green curves are individual peaks from the fittings. Spectrum was recorded at 340 nm excitation wavelength.

Chapter-3

ZnO nanocrystals and their photocatalytic activity

This chapter starts with a brief introduction of different types of nanostructures applied in environmental application and their properties required for photocatalytic activity under sunlight. An experimental procedure for the photocatalytic activity is described in the second section. In the next section, brief description of the mechanism of nanosheets formation and different aggregation tendencies of nanosheets is presented. Then photocatalytic performances of the grown nanosheets have been discussed. Further a brief description of the mechanism of photocatalytic activity of nanosheets is presented. And finally, the chapter concludes with a brief summary.

3.1. Introduction

The ZnO nanostructures show many interesting physical and chemical properties such as optical, electronic, catalyst, photocatalysts [151-159] etc. In recent years, especially for industrial wastewater treatment for environmental remediation, the ZnO has attracted great attention [160] owing to its high quantum efficiency, excellent thermal and chemical stability, non-toxicity, low cost and high photocatalytic efficiency for decomposing organic pollutants in water [161-163]. However, the wide band gap 3.2 eV (λ= 380 nm) of ZnO restricts its use only in UV region, exhibiting hardly no response to the visible light as about 3 to 5% spectrum of sunlight falls in UV region limiting its photocatalytic efficiency. Several efforts have been made to overcome this disadvantage and to expand visible light absorption such as by doping with Co, Mn, Ni, N etc. element, which narrows the band gap of ZnO, coupling of ZnO with other oxides like ZnO/ SnO_2, ZnO/ZnO_2 and deposition of Fe_2O_3, WO_3, CdS on ZnO substrate [80]. In addition, concentration of oxygen vacancy defects on the surface [164-166], shape and size of nanostructures [167], existence of facets [168-170] and surface area [171, 172] are also discovered as important factors to enhance the photocatalytic activity of undoped ZnO.

The oxygen vacancy defects are kind of self-doping without addition of external impurities, which enhances the visible photocatalytic activity by narrowing the band gap [173] while preserving the intrinsic crystal structure unlike to impurity doped ZnO. The oxygen vacancies induce visible spectrum absorption and enhance photocatalytic activity as reported by Li *et al.* [173-175] for TiO_2. The surface oxygen vacancies act as the photoinduced charge trap and adsorption sites to diminish the probability of recombination of photoinduced electron-hole pairs [176]. The photocatalytic activity is mainly a surface phenomenon; therefore,

nanostructures perform much better than their bulk counterpart. Besides that, the photocatalytic activity is not only dependent on surface oxygen vacancies but also influences to the shape of nanostructures. As reported earlier, the polar surfaces of ZnO demonstrate greater photocatalytic activity than its non polar surfaces [177, 178]. It is demonstrated that due to the surface positivity of (0001) polar surface, the OH^- ion gets adsorbed preferably on it, which then reacts with hole (h^+) and generates reactive $^{\cdot}OH$ radical, thereby enhancing the photocatalytic activity. Compared with spherical nanocrystals, the one dimensional (1D) nanostructures would have larger number of h^+ and e^-, determining the photocatalytic reaction rate, on the faceted surfaces/active sites, which results from the dimensional anisotropy [168, 169]. Conclusively, utilization of ZnO structures of large surface area, large number of oxygen vacancy defects and faceted surfaces would enhance photocatalytic activity.

Nanostructures shape with large surface area depends upon the synthesis methods. Although, there are several approaches to tune the shape and size of ZnO nanostructures but mainly they are synthesized by hydrolytic method explained elsewhere [179]. In hydrolytic method, the controlled ZnO nanostructures are obtained by using templates [170, 180-187], or properly selecting (structure directing) a hydrolyzing agent [188, 189] or reaction media [190, 191]. A template provides the shape/size to the nanostructures by confining the reaction in a restricted space [185]. Similarly, a hydrolyzing agents act as a soft template, which controls the shape/size of nanostructures e.g. the room temperature ionic liquids (RTIL) form different pre-organized solvent structures, which assist in the anisotropic growth of nanostructures [187, 192]. In case of reaction media, the reaction media controls the rate of hydrolysis thereby controlling the growth process and hence the shape/size of nanostructures [127, 188].

Now, so far the increase in the number of oxygen vacancies is concern; it is basically related with the disorders at higher temperature (post-annealing). Although, converting white color of ZnO nanostructures to yellow is an enhancement in oxygen vacancies however, in most of ZnO nanostructures except perfect single crystals [193] the oxygen vacancy defects always exist. There are various studies on the surface oxygen vacancies of the ZnO nanosheets [194-199] but it is rarely reported the formation of ZnO nanosheets without surfactant, directing agent and templates. Here, we have created surface oxygen vacancies in ZnO nanosheets while synthesis without post-annealing.

The ZnO nanostructure with large surface area, which remains stable against aggregation and possess faceted surface to enhance photocatalytic activity still remains a challenge. Herein, for the first time, we demonstrate different aggregation tendencies of ZnO nanoparticles, which lead to the formation of faceted ZnO un-aggregated interwoven nanosheets and group wise interwoven i.e. flower-like structures in different reaction mediums without utilizing template or directing agent at room temperature. Although, similar ZnO structures have been already synthesized in many cases using templates, directing agents and surfactants [194, 200-202] but in this work, we have prepared ZnO nanosheets without surfactant, directing agent and templates. In whole of the discussion, we would call un-aggregated interwoven nanosheets simply as '*nanosheets*' and group wise interwoven nanosheets as '*flower-like*' structures. In this work, the alcoholic (C_2H_5OH) medium leads to the formation of ZnO *nanosheets* whereas *flower-like* structures were obtained in aqueous medium. The obtained faceted ZnO *nanosheets* and *flower-like* structures having large surface area were used for sunlight photocatalytic purification of organic pollutant 'methylene blue (MB) dye' from water. A significantly high photocatalytic activity is achieved in this work, which is due to the oxygen vacancies, large surface area and faceted structure of as synthesized ZnO nanostructures.

3.2. Experimental Procedure

The photocatalytic activities were investigated for both of ZnO nanostructures, synthesized for 4 hours reaction time in C_2H_5OH and H_2O media, respectively. The MB dye was used as degraded material in quartz beakers. A 50 mg of each ZnO nanosheets was dispersed separately in 150 ml aqueous solutions of MB formed with initial concentration 20 mg/L. The mixtures after sonicating for 15 minutes and stirred for 15 minutes were exposed to sunlight. The experiment were performed from 9:00 am to 2:00 pm on a sunny day (6% clouds and 34% humidity) on 29 and 30 April, 2014 in Solan city, India (geographical location: 31.15 degree north latitude and 77.20 degree east longitude, environmental temperature: 25ºC). The small aliquots (5 ml) were drawn from the reaction mixture at fixed interval, subsequently centrifuged at a rate of 5000 rpm for 10 minutes and monitored for the absorbance at a wavelength of 660 nm. The degradation of MB was monitored using the UV-Vis spectroscopy.

The efficiency of the degradation processes was analyzed using UV-Vis spectroscopy by monitoring dye decolorization at the maximum absorption wavelength. Photocatalysts were then

separated from solutions via centrifugation, rinsed with ethanol to fully remove the residual organic species, and reused for the next run. The procedure was performed for three cycles to evaluate the stability of ZnO nanostructures for multiple uses in photodecomposition of common organic dye molecules.

3.3. Results and discussion

3.3.1. Growth mechanism of ZnO nanocrystal in C_2H_5OH and H_2O medium

In nut shell, the whole process of formation of ZnO nanostructures i.e. nanosheets and *flower-like* nanostructures may be described to proceed via the nucleation of ZnO nanocrystals, their different aggregation in respective mediums and then subsequent directional growth to form nanosheet structures. The nucleation takes place in a condition when the concentration of precursors (i.e. nanocrystals or monomers) exceeds the critical super saturation level. In such a condition, smaller nanocrystals grow rapidly until their concentration falls below the critical level for nucleation [134]. To understand the nucleation process, the chemical reaction must be understood. Initially, the Zn^{2+} from $ZnAc_2$ and O_2^{2-} ions from KOH in different mediums (H_2O or C_2H_5OH) coordinate with each other to form an aggregate of the type $[Zn_x(OH)_y]^{(2x-y)+}$ [203], which after dehydration forms a small ZnO nanocrystal. These nanocrystals that are oriented randomly in the beginning start aggregating with different tendencies depending upon the medium (H_2O or C_2H_5OH). Such a tendency of initially formed ZnO nanocrystals is higher in aqueous medium than that in alcoholic medium (Fig. 2.4 and Fig. 2.15). After aggregation of nanocrystals, the anisotropic growth, leading to the formation of nanosheets and *flower-like* nanostructures, may occur either by (*i*) collision (due to random Brownian motion) [204] and fusion between the particles, known as *oriented attachment* [205] of nanocrystals or by *(ii)* exchange (dissolution and diffusion) of molecules between various particles, known as *Ostwald ripening* [206].

Since a hexagonal ZnO nanocrystal has two polar planes (±002) and six non-polar planes [122], the polar planes having relatively higher surface energy can promote the anisotropic growth in the ±001 directions. The polar ZnO nanocrystals show oriented attachment to minimize the overall system energy by rotating/piling up and then fusing with the attached nanocrystals [207]. Therefore, in the oriented attachment process, initially the randomly oriented ZnO nanocrystals aggregate, as indicated by encircles in Fig. 3.1(a), and then with the passage of

reaction time they might have rotated to ensure their orientations parallel to (±002) direction as indicated by arrows in Fig. 3.1(a). Further, as the observed nanosheets are smooth (Fig. 3.2), the bottle neck between the adjacent nanocrystals may later when the precursor concentration is lowered, have filled up by the Ostwald ripening process and thus smoothening the surface of nanosheets [182].

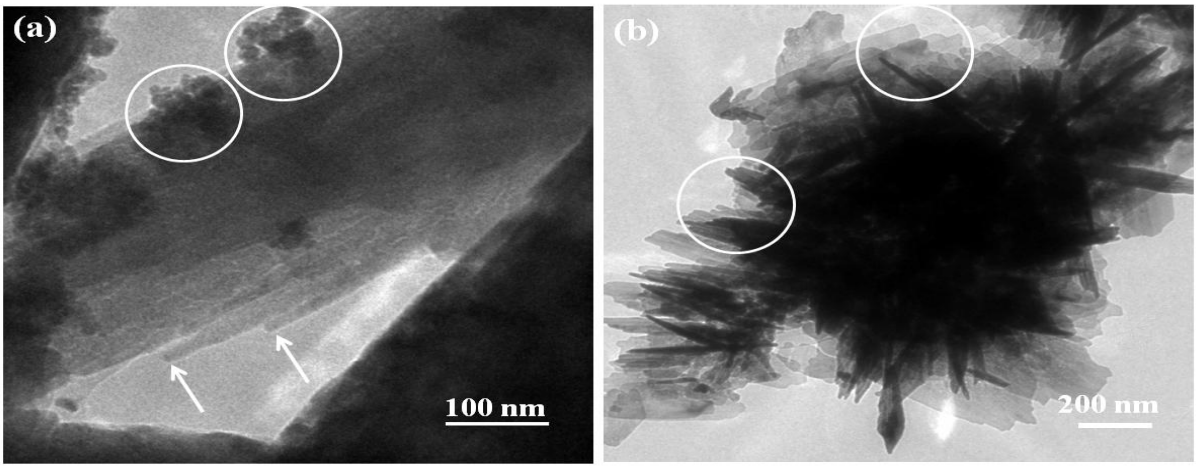

Figure 3.1: TEM images of ZnO nanosheets and flower-like structures (a) shows the nanosheets with facet edges indicated by arrows, and nanoparticles on the surface of nanosheet enclosed by circles, (b) the flower-like structures with facet edges as encircled.

In the other consideration, the anisotropic nanostructures may be supposed to be grown via directional Ostwald ripening process. In this process, similar to the above mechanism, initially the randomly oriented ZnO nanocrystals aggregate, and then with the passage of reaction time smaller nanocrystals dissolve into the solution and attach on the polar surfaces of larger nanocrystals in the aggregate, leading to the formation of oriented nanosheets in the aggregate. We know that when the precursor concentration falls below the nucleation concentration the nucleation stops. According to Ostwald ripening process [126, 135], the large nanocrystals grow at the cost of smaller nanocrystals. The growth of large nanocrystals proceeds by the capturing of Zn^{+} ion formed from the dissolution of smaller nanocrystals and brought near to the surface of larger nanocrystals by the process of diffusion. These surface Zn^{+} ions are terminated by OH^{-} ions available inside the solution. Thus, the growth continues further by capturing Zn^{+} ions, OH^{-} ions followed by dehydration [134]. Owing to the higher surface energy of polar surfaces of ZnO nanocrystals, the ions Zn^{+} and OH^{-} adsorb favorably on the polar surfaces. Such a process is

repeated over the time leading to the directional (±002) growth of nanosheets. Although, both of the growth mechanisms can be suggested for the obtained ZnO nanostructures but from TEM observations (Fig. 3.1) the oriented attachment of nanocrystals followed by Ostwald ripening process smoothening the surface is more plausible.

3.3.2. Investigation of different aggregation tendencies of ZnO nanocrystals in H_2O and C_2H_5OH mediums

We tried to investigate the reason behind the different aggregation tendencies of initially nucleated ZnO nanocrystals in H_2O and C_2H_5OH medium, which leads to the formation of *nanosheets* and *flower-like* structures with the reaction time (Fig. 3.2).

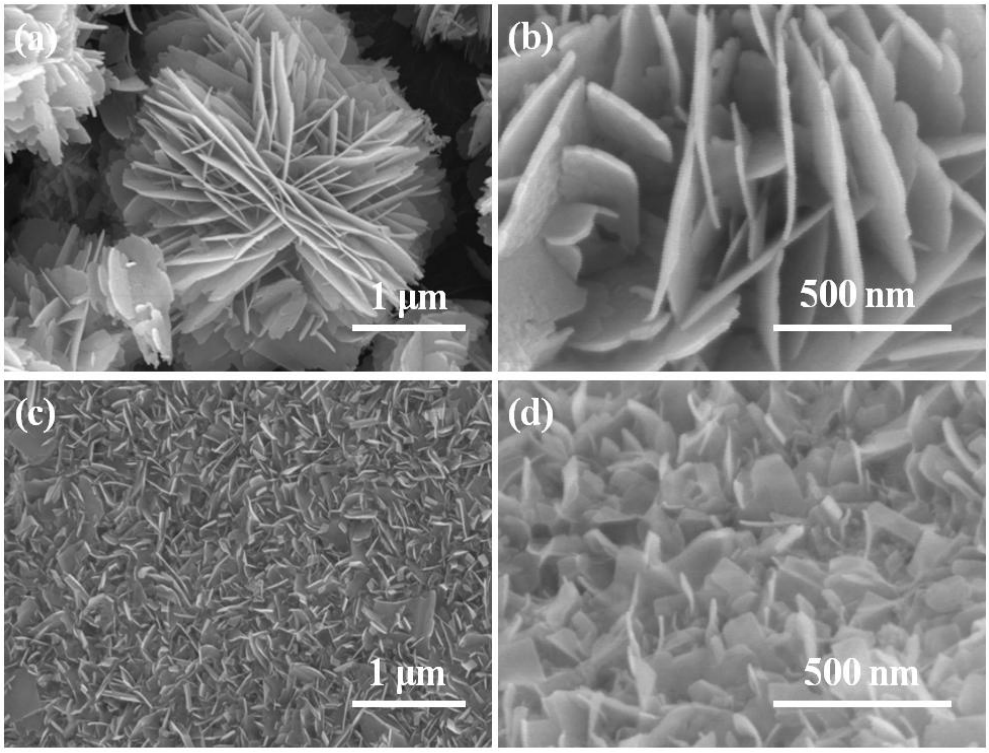

Figure 3.2: FESEM images show morphology by varying solvent medium (a, b) for water solvent and (c, d) for ethanol solvent at all similar conditions.

We presumed that difference in the aggregation tendencies is attributed to the extent of hydrogen bonding. The solvent facilitating the adhesion among the ZnO centres through hydrogen bonding will lead into the complex interwoven morphologies like nanoflowers. After formation of ZnO nanocrystals, the residual OH^- and CH_3COO^- ions remain adsorbed on the surface of ZnO nuclei. The CH_3COO^- ions adsorbed on ZnO nuclei as shown in Fig. 3.3(a) help

not only in hydrogen bonding but also in stabilizing such bonding in free form in crystal. In case of water as the reaction medium, water being a polar molecule because of the electro negativity difference of the O and H. The strong hydrogen bonding networking takes place between the adjacent ZnO nuclei as shown in the Fig. 3.3(b). The acetate adsorbed on the ZnO nuclei helps in hydrogen bonding and also in free form in crystal stabilizes the hydrogen bonding network (Fig. 3.3(c)). The alcohol medium also tries to do the same hydrogen bonding but the polarity is weaker than the water molecule due to the +I effect of the alkyl chain. More over the bulky ethyl group 'R' also interferes in the strong hydrogen bonding network formation. So the alcohol medium prevents nanoparticles from aggregation while water medium favors the aggregation.

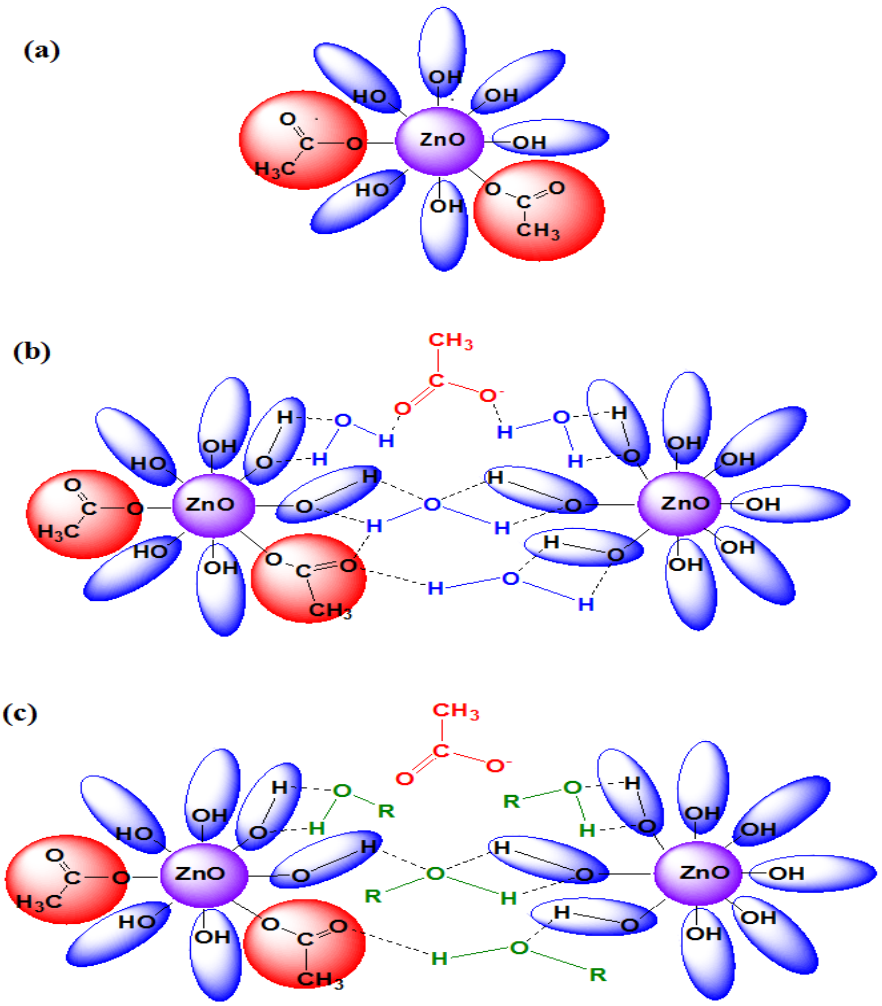

Figure 3.3: Aggregation mechanism of the ZnO nanoparticle (a) hydroxyl and acetate ion adsorbed on the ZnO (b) strong hydrogen bonding network in water solvent and (c) weak hydrogen bonding network in alcohol solvent.

To confirm the assumption related to hydrogen bonding, the ZnO nanostructure samples were investigated by FTIR. The FTIR spectra between 2750 cm^{-1} - 3750 cm^{-1} was plotted to determine symmetry distortion in the –OH stretching band for both the structures in respective mediums. In view of the possibility of occurrence of symmetry distortion in the –OH stretching band due to existence of hydrogen bonding, this distortion (i.e. Δ½) among corresponding peaks was compared by using a reported method [208] and calculated. The difference in the -OH stretching peak symmetry (between 2750 cm^{-1} - 3750 cm^{-1}) can be clearly seen in the spectra Fig. 3.4. First, a vertical line starting from the bottom of the peak was constructed parallel to y-axis. Similar straight lines were also drawn parallel to x-axis at various percent transmittances (%T). Then on each line, the distance from the vertical one to the left (a_1, b_1, c_1, d_1) and right (a_2, b_2, c_2, d_2) was measured. By taking the difference between two measurements (½ left – ½ right), symmetry distortion Δ½ was calculated as:

$$\Delta_{1/2} = (\partial a + \partial b + \partial c + \partial d)/4$$

Where $\partial a = a_1 \sim a_2, \partial b = b_1 \sim b_2, \ \partial c = c_1 \sim c_2, \ \partial d = d_1 \sim d_2$

Although, the difference is very small but the symmetry distortion is found to be higher in case of nanocrystals from H_2O medium revealing the strong inter hydrogen bonding among these ZnO nanocrystals as compared to the ZnO nanocrystals obtained from C_2H_5OH medium (Fig. 3.4). The possible distortion of -OH band can be influenced by many factors among others amount of OAc anions on the surface or different morphology. But in present work, -OH band distortion due to the OAc anions amount on the surface could be ruled out as the $ZnAc_2$ concentration is same in both the medium. As far as the different morphology is concerned, there is no report having evidence of IR band symmetry dependence on the morphology so far. Stretching peak symmetry distortion is an exclusive phenomenon of hydrogen bonding.

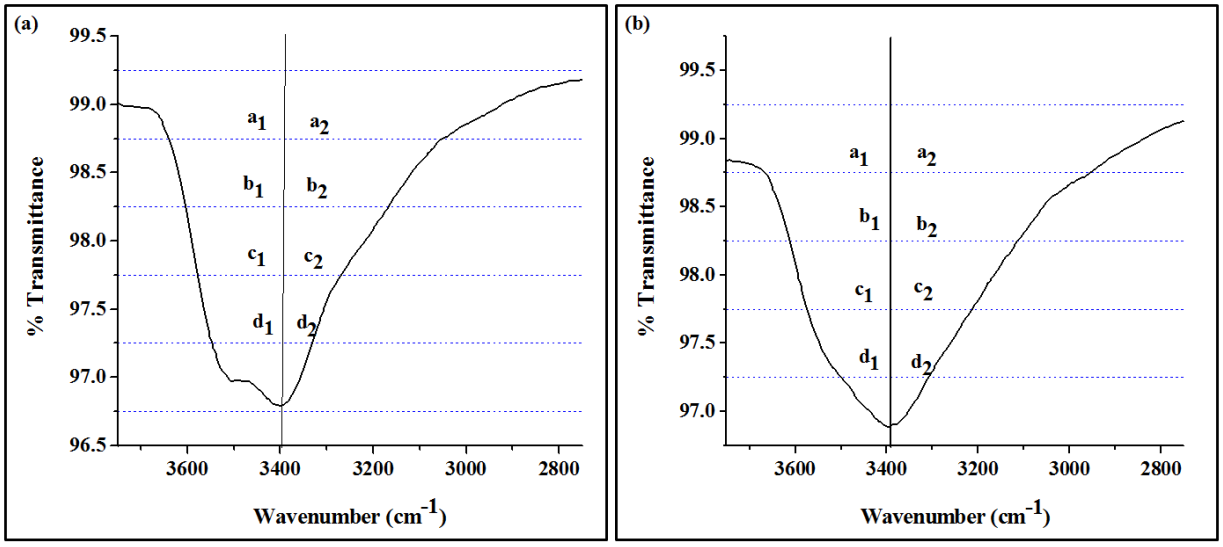

Figure 3.4: FTIR spectra of (a) nanosheets and, (b) flower-like structures for determining symmetry distortion between 2750 cm^{-1} - 3750 cm^{-1}.

3.3.3. Photocatalytic activity

3.3.3.1. Background of photocatalytic activity

We know that the dominant causes of surface water and ground water pollution are industrial wastes, municipal wastes, and agricultural runoff effluents which are highly variable in composition with relatively low biochemical oxygen demand and high chemical oxygen demand contents. Wastewater from various industries, factories, laboratories, etc. is a problem of non-aesthetic pollution in the environment and creates disinfection byproducts through oxidation, hydrolysis, or other chemical reactions [209-212]. Conventional wastewater treatment usually utilizes various physical, chemical, and biological technologies. Many industries establish wastewater treatment plants (WWTPs) for water treatment which combine multiple processes such as coagulation-flocculation-sedimentation, biological degradation, filtration, chlorination and ozonation [213-217], requiring high operating/maintenance costs. Many environmental remediation techniques employ simple physical processes such as adsorption to remove non-biodegradable, environmentally hazardous byproducts. Biological treatments are an inexpensive process but unable to degrade many toxic organic compounds such as pharmaceuticals or dyes. Some studies have been done on the treatment of commercial dyes solution with emphasis on azo dyes since these are widely used in dyeing processes in textile, printing, and paper

manufacturing industries. These azo dye molecules are chemically stable and hardly biodegradable aerobically. Oxidation process for the oxidative degradation of azo dyes has paid more attention [218, 219]. Photocatalysis using various metal oxide nanostructures offers an advanced technology for the elimination of toxic organic compounds from water [220-223]. Simple and economical water treatment techniques to remove persistent organic compounds and microorganisms in water including condensation, ultra filtration, membrane separation, and adsorption have been suggested [224, 225]. Among of them, advanced oxidation processes (AOPs) have the potential for the generation of highly short-lived transitory species, to efficiently degraded or mineralize organic compounds to eco-friendly or inorganic byproducts as CO_2 and H_2O, also have a great potential as a low-cost and high efficiency water treatment technology [226].

Among all nanomaterials, metal oxide such as bismuth tungstate [227], Ag-loaded Bi_2WO_6 [228], TiO_2 [229, 230], Ag_2O [231], TiO_2-rGO [232], and ZnO [233] show a great potential in advanced oxidation processes. In recent years, the development of visible light photocatalysts has become newly topics in photocatalysis research. Although metal oxide nanostructures has been widely used for the photocatalytic degradation of bio-recalcitrant organic compounds, such as pharmaceuticals or dyes in water under ultraviolet (UV) light irradiation (4% of the solar light). But these were inefficient under solar light irradiation due to its wide intrinsic band gap [234]. ZnO has emerged as a more efficient photocatalyst than others due to its high surface reactivity owing to its large number of active surface defect states. It also shows fast reaction and mineralization rates [235] because of its more efficient hydroxyl ion generation [236]. ZnO can be structurally modified for visible light absorption paving the way for visible-light photocatalytic activity [237]. Many studies have been cited showing that doping of a metal or transition element can cause a hyper-chromic red shift in the optical absorption of semiconductor metal oxide [238-240]. Usually doping has been carried out on the direction of utilizing narrower band gap semiconducting materials. The doping undergoes intrinsic photoexcitation, charge separation, and subsequently promote photoreactions using near ultraviolet and visible light [240, 241]. Also, it increases the surface area which is a beneficial aspect for significant increase in photocatalytic activity under sunlight irradiation.

3.3.3.2. Photocatalytic performance of ZnO nanosheets and flower-like structures: organic pollutant removal

The photocatalytic activity of *nanosheets* and *flower-like* structures as catalyst for the degradation of MB was investigated under sunlight irradiation. The degradation of MB by both of the ZnO nanostructures was carried out in the similar conditions. For this purpose, 0.34 g/L of ZnO nanosheets was added into 6.25×10^{-5} M of MB solutions (i.e., 3 g of MB in 150 ml aqueous solution). The change in optical absorption spectras with the degradation of MB dye by *nanosheets* and *flower-like* structures for different time intervals under sunlight irradiation is shown in Fig. 3.5. The observed decrease in the absorption band intensities of MB indicates that MB gets degraded by both ZnO nanostructures. In case of nanosheets, the disappearance of the characteristic band of MB dye at 660 nm after 2 hours of sunlight irradiation (Fig. 3.5(a)) indicates that MB has been degraded completely by nanosheets. For the similar conditions in case of flower-like structures there exists the characteristic peak of the MB dyes solution indicating the presence of MB molecules in the solution as shown in Fig. 3.5(b). The progress of photo-degradation of MB dye by both ZnO nanostructures under sunlight irradiation can simply be realized by the color change of solution as shown in the inset of Fig. 3.5.

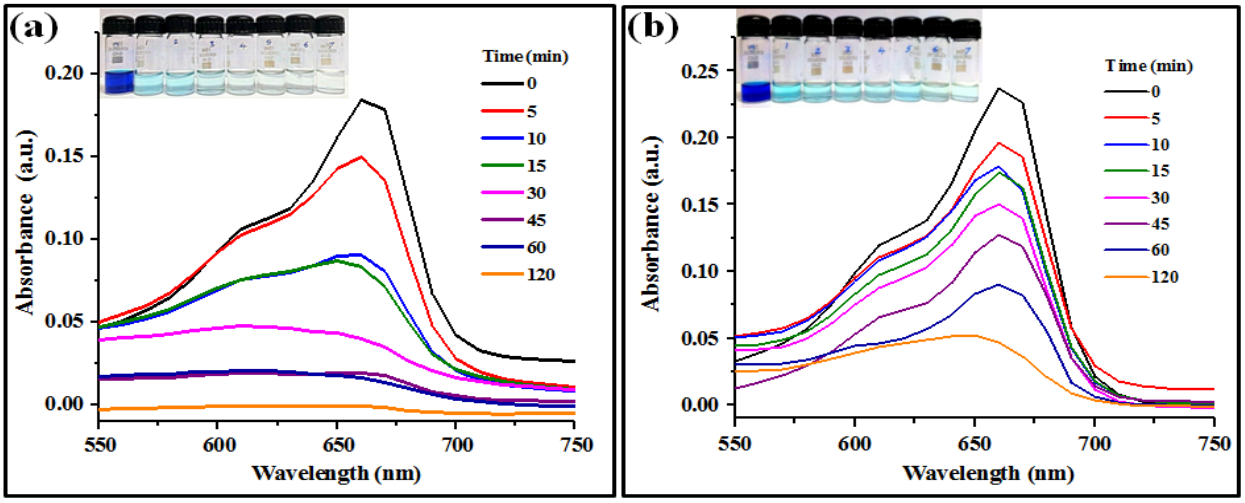

Figure 3.5: Time-dependant absorption spectra of MB dye solution under sunlight irradiation with catalyst (a) ZnO nanosheets and, (b) ZnO flower-like structures.

Figure 3.6 shows the relative concentration C/C_0 of MB dye with irradiation time, where C_0 is MB dye's initial concentration after the equilibrium adsorption of ZnO

nanostructures and C is concentration of MB at time *t*. Figure 3.6 shows that under sunlight irradiation, the self-degradation of MB without introducing ZnO nanostructures is negligible, whereas its concentration decreases rapidly in the presence of ZnO nanostructures. The photocatalytic efficiency was calculated using the expression $\eta = (1 - C/C_0) \times 100$, where C_0 is the concentration of MB before illumination and C is the concentration after irradiation time. Figure 3.6 shows photocatalytic efficiency, the MB dye is removed around 100% while using nanosheets, whereas the flower-like structures remove around 80% when irradiated for 120 minutes in sunlight.

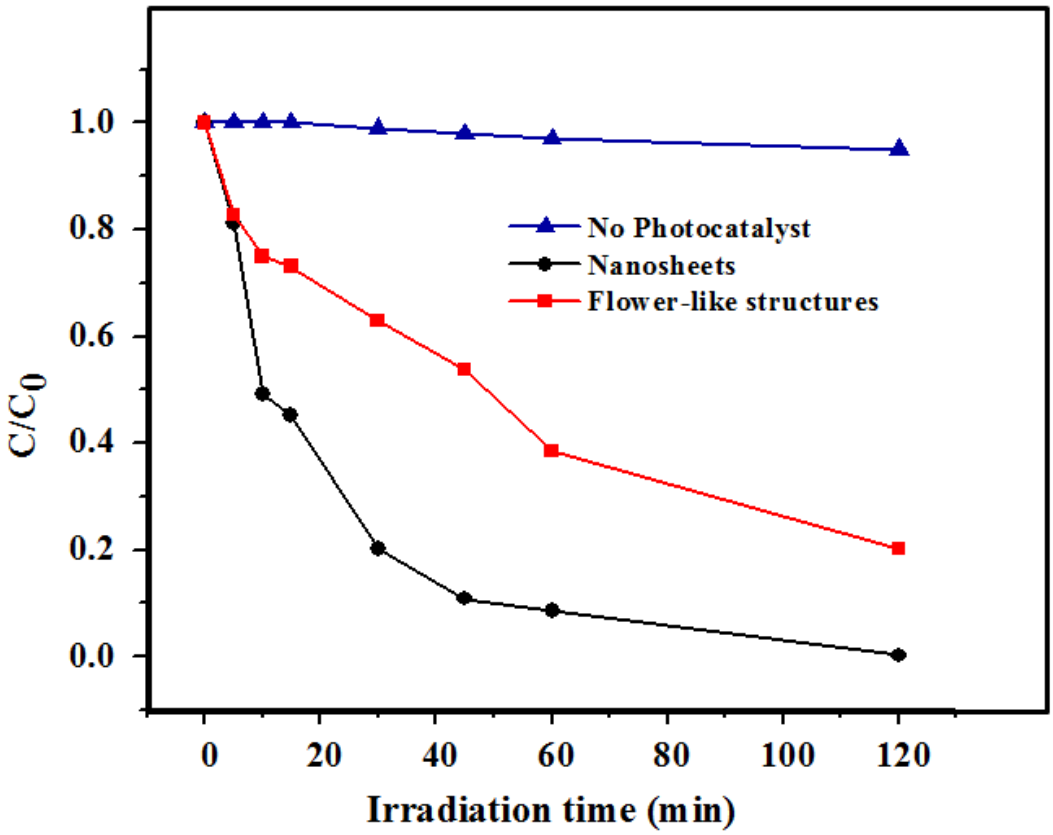

Figure 3.6: Plot represents photocatalytic activity of nanosheets and flower-like structures as catalysts under sunlight irradiation.

Figure 3.7 shows the plots between $\ln(C_0/C)$ and irradiation time. A linear relationship between $\ln(C_0/C)$ and irradiation time indicates that the photodegradation of MB dye, by *nanosheets* and *flower-like* ZnO structures, proceeds via a pseudo first order kinetic reaction i.e.,

$\ln(C_0/C) = kt$, where k is the photo-degradation rate constant. The corresponding parameters of degradation and pseudo first order model for ZnO nanostructures are summarizes in Table 3.1.

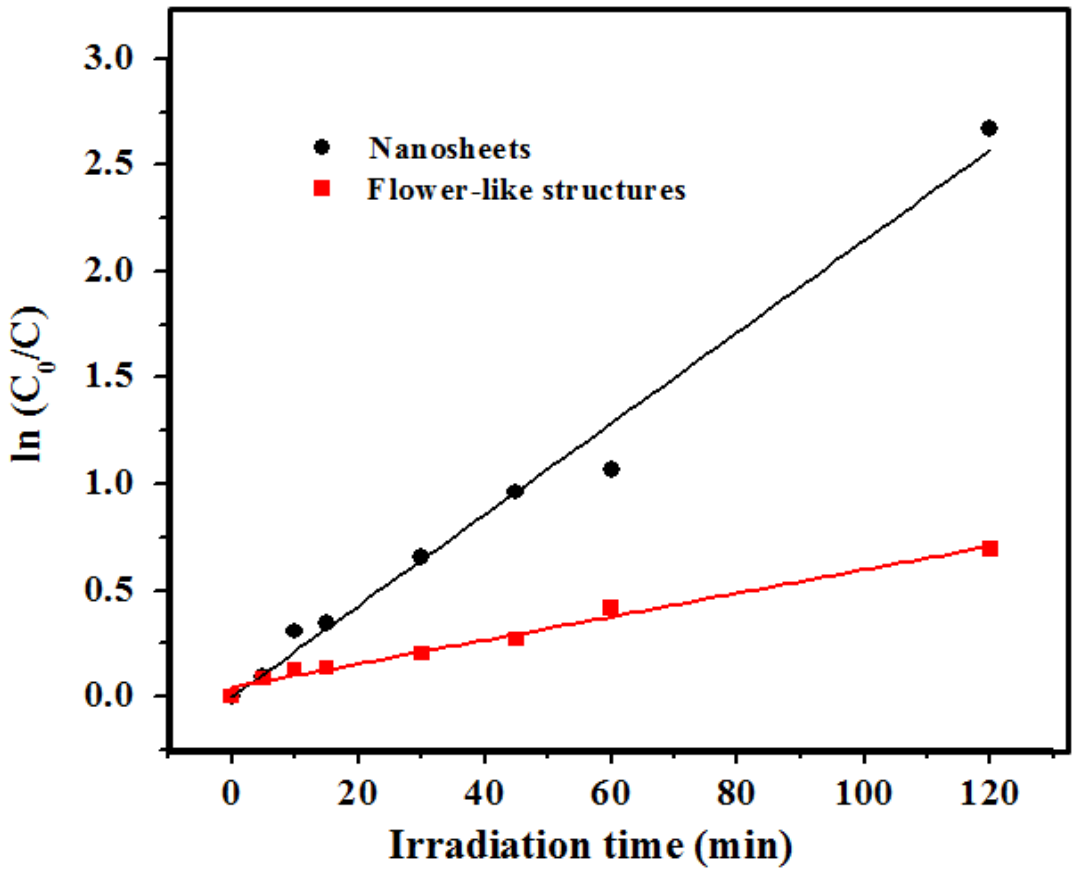

Figure 3.7: Plots for photocatalytic kinetics analysis for the degradation of MB with both types of ZnO nanostructures (initial concentration of MB =10^{-5}M).

Table 3.1: ZnO as photocatalysts follow the pseudo first order kinetics (initial concentration of MB was 10^{-5}M)

Nanostructure	% degradation (in 120 min)	k(min^{-1})	Standard error
Nanosheets	99.94%	0.0494	0.0023
Flower-like	79.76%	0.0127	6.38904e-4

We also investigated the degradation in photocatalytic performance of ZnO nanostructures. For this reason ZnO *nanosheets* and *flower-like* structures were used for three

photocatalytic cycles. In each cyclic run the photocatalytic experiment was performed as mention earlier using the concentration 0.34 g/L of ZnO nanostructures and 6.25×10^{-5} M of MB dye. The degradation of MB dye was investigated by UV–Vis spectroscopy. After each run the ZnO nanostructures were separated from the solution by centrifugation, which was reused after drying at 100^{o}C. Figure 3.8 shows the degradation of MB dye under sunlight irradiation for three cycles. Form Fig. 3.8, it is observed that after three catalytic cycles, there appeared a very negligible degradation in the photocatalytic performance of both types of ZnO nanostructures.

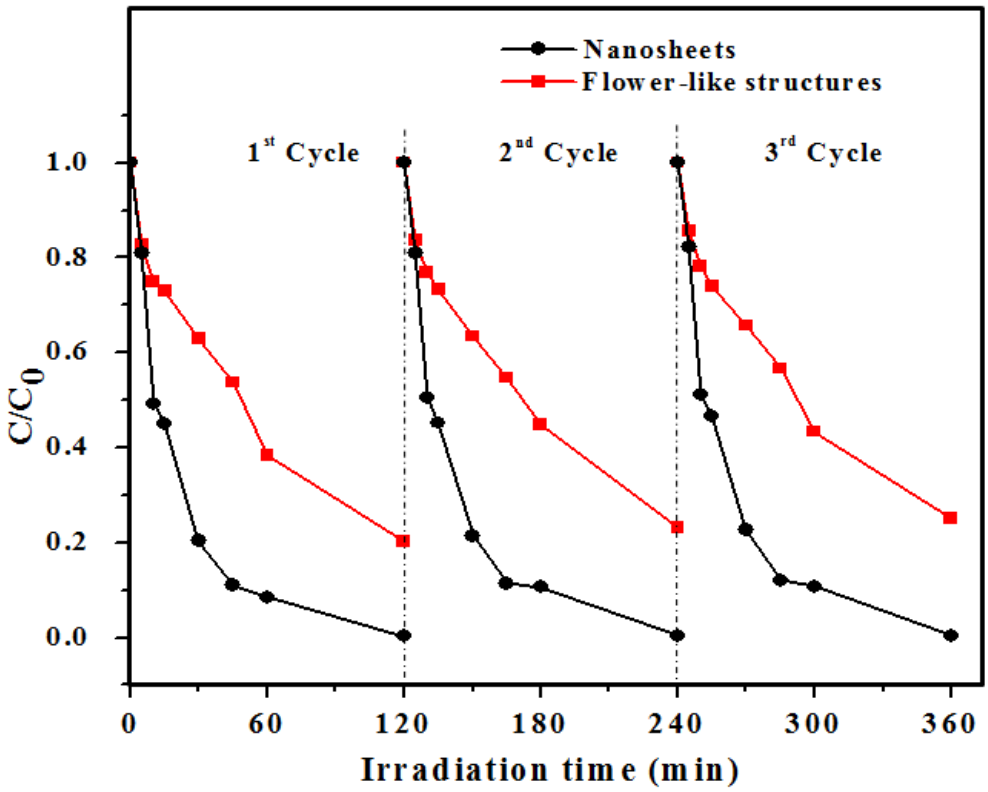

Figure 3.8: Effect of number of runs on the degradation of MB dye in the presence of ZnO nanostructures as catalyst under sunlight irradiation (catalyst concentration: 0.34 g/L; initial concentration of dye: 6.25×10^{-5} M).

3.3.3.3. Photocatalytic mechanism

Since photocatalytic activity is a surface phenomenon, therefore, a nanoscale ZnO material is believed to perform much better than its bulk counterpart [242]. The basic mechanism of photocatalysis of ZnO is well established [243-246]. Initially, when the solution was kept in dark for 30 minutes, the adsorption-desorption of MB on the surface of ZnO nanostructures

occurred. As a photocatalytic phenomenon, when the solution was irradiated with sunlight, electron–hole pairs would have generated in ZnO nanostructures. However, as the band gap of ZnO is 3.3 eV, only UV light can excite the ZnO nanostructures to generate electron–hole pairs. The created holes initiate reaction either with electron-rich surface hydroxyl groups or adsorb water molecules to yield hydroxyl $OH^{\bullet -}$. On the other hand, the electrons react with the dissolved oxygen molecules to produce superoxide radical anions $O_2^{\bullet -}$. Thereafter, the superoxide radical anions $O_2^{\bullet -}$ could yield hydroperoxyl radicals $HO_2^{\bullet}$ and $OH^{\bullet}$ by the subsequent hydration processes. These resultant radicals ($OH^{\bullet}$ and $O_2^{\bullet -}$) are responsible for decomposition or mineralization of MB [247]. In sunlight, there is only 3–5% of UV photons are present which cannot show higher photocatalytic efficiency [248] but since we observed significantly higher photocatalytic efficiency. Therefore, we might consider other factors such as self-photosensitization of MB, ZnO surface oxygen vacancies and presence of facets on ZnO nanostructures, which enhance photocatalytic activity of ZnO.

The MB itself helps in enhancing the photocatalytic activity because it acts as a self-photosensitizer under sunlight irradiation [249]. It absorbs visible light and transfers the absorbed energy to other molecules [250-252]. The transfer of energy may occur via two different processes: electrons transfer process; forming exciplex (excited state complex) and the energy transfer process; exciting the molecule to higher energy state. In the energy transfer process, when MB is exposed to both oxygen (O_2) and sunlight, the excited state MB transfers energy to ground state O_2 (triplet) and converts it into the excited state O_2 (singlet) for photo-oxygenation [251]. The transfer process of electron from the dye to semiconductor, especially for ZnO, has also been reported previously as well [248]. But in our case, in the absence of photocatalyst (Fig. 3.6(a)), a negligible amount of MB was degraded through 120 minutes of irradiation under sunlight. It indicates that the self-photosensitization process of MB can be neglected in our case.

Besides UV photon excitation of ZnO and self-sensitization of MB, the oxygen vacancies on the surface of ZnO nanostructures plays very important role for enhancing the photocatalytic activity of ZnO. The oxygen vacancies not only form the active centers or trap centers for photoinduced charge [166, 253 and 254] but they narrow the band gap of ZnO. The narrowing of the energy band gap is induced by the surface oxygen vacancies by the broadening of valance band, which results for the generation of visible-light photoactivity in ZnO and hence the

increase of the photocatalytic activity under sunlight irradiation. In our case, surface oxygen vacancies are considered as one of the factor enhancing the photocatalytic activities of both *nanosheets* and *flower-like* structures. We used PL measurements to confirm the existence and properties of surface oxygen vacancies in ZnO *nanosheets* and *flower-like* structures trusting that PL is a direct method to observe various behaviors of defects such as oxygen vacancies and zinc interstitials [166, 255]. The PL spectra contain the existence of emissions at 390 nm (UV), 420 nm (violet), 466 nm (blue), 485 nm (blue-green) and 520 nm (green). Therefore, the enhanced photocatalytic activity may be attributed to the presence of both UV and visible emission in both of the ZnO nanostructures as indicated in PL spectra (Fig. 2.10 and Fig. 2.20).

The absorption of UV and visible spectrum from sunlight by ZnO nanosheets excite to create electron-hole pairs [247], which react further according to the following reactions equations:

$$ZnO + h\nu \rightarrow h^+ + e^- \quad (3.1)$$

$$h^+ + H_2O \rightarrow OH^{\cdot} + H^+ \quad (3.2)$$

$$h^+ + OH^- \rightarrow OH^{\cdot} \quad (3.3)$$

$$e^- + O_2 \rightarrow O_2^{\cdot -} \quad (3.4)$$

$$O_2^{\cdot -} + H_2O \rightarrow HO_2^{\cdot} + OH^{\cdot} \quad (3.5)$$

$$HO_2^{\cdot} + H_2O \rightarrow H_2O_2 + OH^{\cdot} \quad (3.6)$$

$$H_2O_2 \rightarrow 2OH^{\cdot} \quad (3.7)$$

$$\left.\begin{array}{l} MB + OH^{\cdot} \\ MB + O_2^{\cdot -} \end{array}\right\} \longrightarrow CO_2 + H_2O + \text{Degraded products} \quad (3.8)$$

The schematic of photocatalytic mechanism, occurring in dye-photocatalyst solution under the sunlight irradiation, is shown in Fig.3.9.

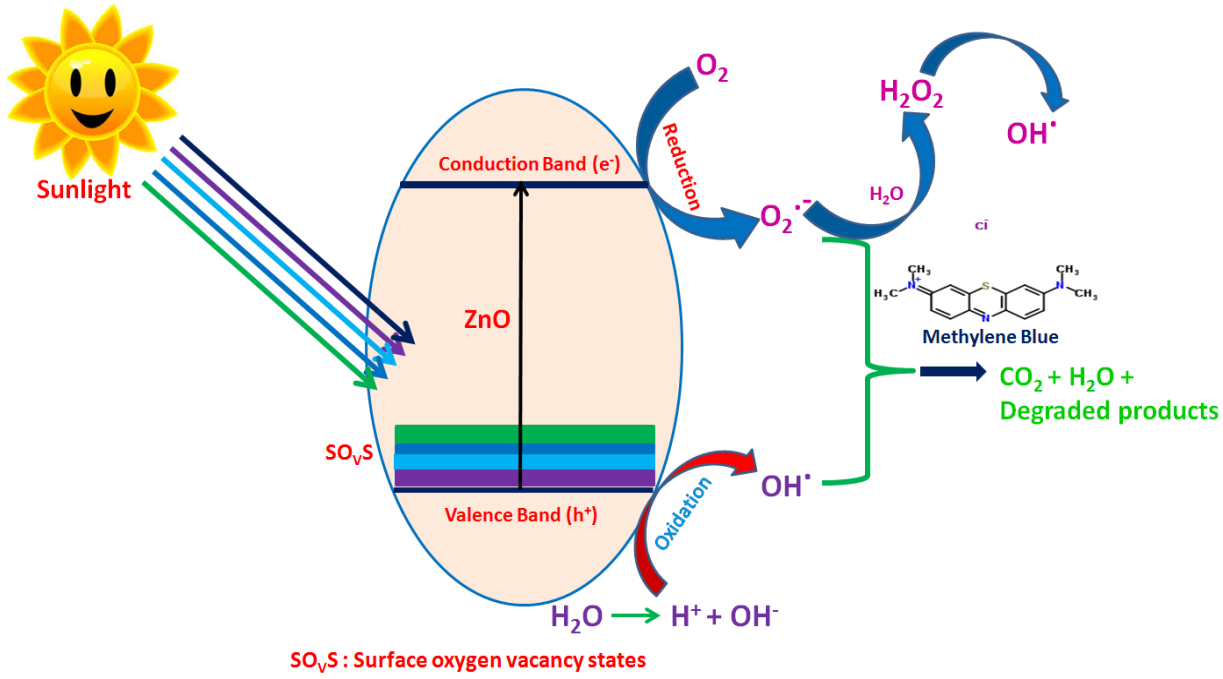

Figure 3.9: Schematic representation of photocatalytic mechanism for the degradation of MB dyes in presence of ZnO nanostructures under sunlight irradiation.

As compared with previous studies, a significant enhancement in photodegradation efficiencies, *nanosheets* 94% and *flower-like* structures 79.76% while irradiated for 120 minutes cannot be attributed only to the surface oxygen vacancies but also the faceted geometry and large surface area of ZnO nanostructures. As observed from the SEM and TEM characterizations, the nanostructures have more surface defects generated. As reported earlier [256, 257], in our case too the nanostructures with unique surface orientation exhibit high density of atomic steps and ledges, which serve as active sites for breaking chemical bonds, enhancing the photocatalytic activity. The observed difference between the degradation efficiencies of *nanosheets* and *flower-like* structures indicates that the morphology of ZnO influences the production of $OH^{\cdot}$ and $O_2^{\cdot -}$. So far the surface area effect is considered; the samples were characterized using BET measurement. Here, the *nanosheets* shows higher surface area (11.765 m^2/g) as compared with *flower-like* structures (10.247 m^2/g). The difference in the surface area of nanostructures would affect the production of free radicals responsible for photocatalytic activity. Further, in case of *flower-like* structure, the sheets being in aggregated form perform less efficiently as compared to *nanosheets* structure. When *nanosheets* are used as photocatalyst in the solution, each of the nanostructures get dispersed availing its whole surfaces for photocatalytic reaction and hence a

higher photocatalytic efficiency. The *flower-like* structures due to aggregation tendencies do not completely expose their surface for sunlight irradiation, resulting in less production of $OH^{\cdot}$ and $O_2^{\cdot-}$ radicals. Conclusively, in our case the photocatalytic activity is clearly dependent on the morphology, oxygen vacancies and textures of ZnO nanostructures formed [257-259].

3.4. Summary

The existence of hydrogen bonding among ZnO nanocrystals is less prominent when the C_2H_5OH medium is used due to the presence of ethyl group and hence lesser aggregation of ZnO nanocrystals, which results in the formation of *nanosheets* with the passage of reaction. Presence of surface oxygen vacancies, faceted structure and large surface area resulted in enhanced photocatalytic efficiency of both ZnO nanostructures. The *flower-like* structures due to aggregation tendencies do not completely expose their surfaces when irradiated in sunlight irradiation, resulting in less production of $OH^{\cdot}$ and $O_2^{\cdot-}$ radicals and hence a lower degradation efficiency of MB dye as compared with the *nanosheets*. Therefore, *nanosheets* can be used as an efficient material for water purification in photocatalytic mechanism under sunlight irradiation.

Chapter-4

Enhancing the numerical aperture of lenses using ZnO nanostructures-based turbid media

This chapter starts with the introduction of enhancing numerical aperture for turbid lens imaging, and then the experimental process for fabrication of turbid film has been described. In the next section, principle of enhancement of numerical aperture of fabricated turbid film has been explained. Then enhancement of numerical aperture of objective lens based on morphology and the transmitted of different morphologies is presented and in last a brief summary of the chapter is given.

4.1. Introduction

There are several studies on the propagation of light through scattering media to achieve better imaging/improved resolution [260-266]. The light passing through scattering media induces wavefront distortions that degrade the image quality of optical systems [267, 268]. However, on the other hand, distortions induced by scattering media can be used to manipulate the wavefront in order to focus the light for better imaging [269, 270]. Recently, an enhancement of resolution by calyx-4-hydroquinone spherical nanolenses abbreviated as n-SIL (nanoscale lenses in an Solid Immersion Lens type implementation) for near field focusing and high resolution optical imaging beyond diffraction has also been reported [271, 272].

Solid-immersion lenses, objective lenses, numerical-aperture increasing lenses etc., have been used to enhance the NA (i.e., the resolution) of optical microscopy [273-276]. Recently, scattering media was used by Choi *et al.* [158] to overcome the diffraction limit in wide-field imaging. A numerical method based on holographic imaging was used. This method converts a severely distorted image (an output from a turbid media) into a high-resolution image. The authors called this method "turbid lens imaging" (TLI) and demonstrated that a turbid lens applied in wide-area imaging may realize an improved spatial resolution and an enlarged field of view.

Normally, when a light ray passes through a turbid media it bends due to scattering. This bending of light has been used to increase the NA of an objective lens. However, owing to turbidity, the image is scrambled. By applying mathematical projection operations, it was shown that the image of an object can be extracted from holographically scrambled images [158]. Thus, the turbid medium itself acts as a lens and enhances the NA of an objective lens. In the literature, gallium arsenide (GaAs) [277], titanium dioxide (TiO_2) [278], ZnO [279], and porous structures of gallium phosphide (GaP) [280], have likewise been used as light-scattering materials. However, to the best of our knowledge, mainly ZnO films have been

used as random media for the focusing of light [281, 282] and as turbid lenses [158, 283] in optical imaging applications due to their negligible absorption in the visible regime [126]. The physical reason behind using ZnO is its band gap with a value of 3.27 eV. Therefore, it does not absorb visible light and causes only bending of light rays.

For better image resolution in optical microscopy using a turbid lens, not only the NA but also the transmittance of the turbid lens should be high [158]. The greater the transmittance and bending of a turbid medium, the higher the resolution achieved in optical microscopy. A previous study by Choi *et al.* [158] reported that the transmittance and the NA of a turbid lens depend on the thickness of the turbid film. In their study, only nanoparticles of ZnO were used to form turbid films and a high-resolution image was obtained by applying such a turbid film with a thickness of 25 μm having transmission of 6%.

In the present chapter, we aim to demonstrate that the morphology of the ZnO structures is also an important factor when using this material in front of objective lens in order to enhance the NA of an objective lens. Three ZnO structures, namely nanoflowers (composed of nanosheets), nanoparticles, and microstructures were synthesized via a facile solution method as explained in chapter 2. These synthesized ZnO structures were used to fabricate turbid films by the spray-coating method. Optical experiments were performed on thus-formed turbid films, and the corresponding transmissions of turbid films were measured. Further, these turbid films were used to enhance the NA of a commercial (Nikon) objective lens. It is observed that the transmittance of the ZnO turbid films and the enhanced NA of a Nikon objective lens are dependent on the morphology of the ZnO structures.

4.2. Experimental Details

4.2.1. Fabrication of ZnO structures: flower-like, nanoparticles and microstructure based turbid film

The ZnO structures: flower-like, nanoparticles and microstructures were dispersed in C_2H_5OH solution and sonicated for 30 min to achieve good dispersion of ZnO structures inside of the solution in order to achieve uniformity in the deposited films. Spray coating was used for the deposition of ZnO turbid films of varying thickness on glass slides. During spraying, the substrate temperature was kept at 150°C and the heater with substrate was kept inside a fume hood to remove vapors of the solvent. The carrier gas N_2 and the ZnO solution were fed into the spray nozzle at a constant spray rate of 1 ml /min. The carrier gas flow rate was maintained at 2×10^4 kg/cm^2. The thickness of each film was controlled by the number

of spraying cycles. Using FESEM, the thickness of the films was measured. Finally, using thus obtained ZnO turbid films, experiments were performed to estimate light transmission and enhancement of the NA of a Nikon objective lens with a He–Ne laser (λ = 632.8 nm) of 2 mW power as light source.

4.2.2. Experimental setup details

To determine the NA of these ZnO turbid films, an experiment was performed using a He-Ne laser (λ = 632.8 nm) as a light source. A schematic of the detailed experimental set-up is shown in Fig. 4.1. The intensity distribution after passing through each turbid film was observed on a screen placed behind the turbid film, as shown in Fig. 4.1.

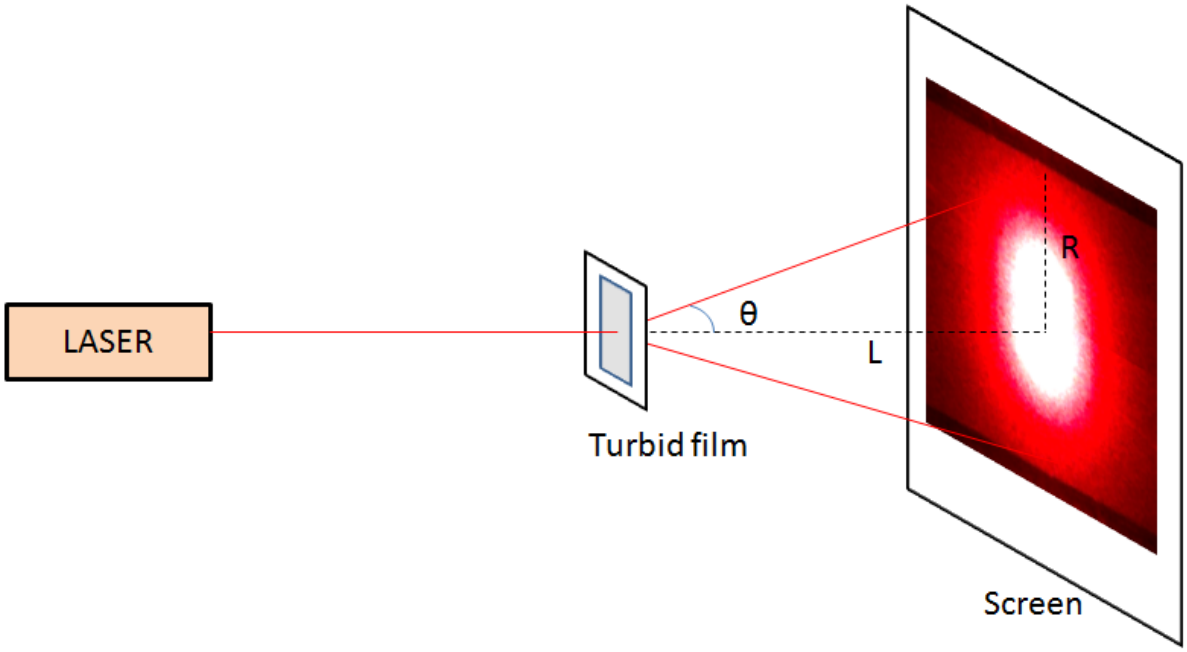

Figure 4.1: A schematic of the detailed experimental set-up for measuring NA and transmittance.

This intensity distribution as a function of distance from the light axis was measured by a lux meter. The observed intensity distribution plotted against the distance L from the initial laser axis formed a Gaussian curve as shown in Fig. 4.2. From this Gaussian curve, the NA was calculated using the displacement *R* from the centre point to the point at which the intensity falls to 13.6% ($1/e^2$ in percentage) of its peak at the centre. Namely, NA is $\sin\theta$ (in air medium), where the half angle θ is obtained from the right triangle shown in Fig. 4.1.

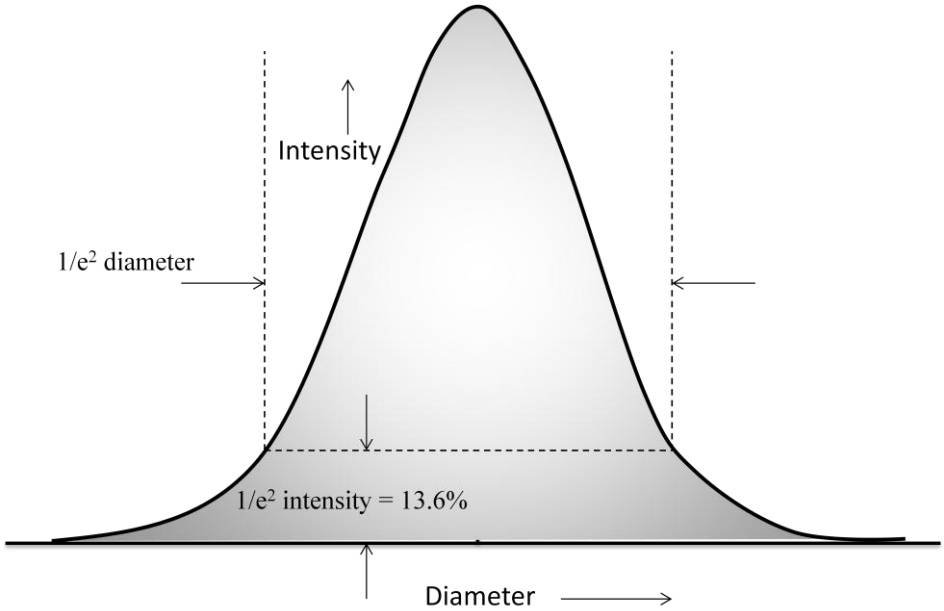

Figure 4.2: Gaussian shaped distribution of light intensity measured at the screen locations after scattering from the turbid film (ZnO structures).

4.3. Results and discussion

4.3.1. Measurement of NA and transmission

We attempted to enhance the NA of a Nikon objective lens using the synthesized ZnO nanosheets, nanoparticles, and microstructures turbid films. A schematic layout of the experimental set-up is shown in Figs. 4.3(a) and 4.3(b). Figure 4.3(a) shows a schematic of experimental set-up without using turbid film. The dotted lines are corresponding to the direction of incident laser beam at an angle (θ') greater than the acceptance angle (θ), these rays do not enter the lens aperture. But when a turbid film is placed in front of lens (Fig. 4.3(b)) the incident laser rays at an angle θ' (greater than θ) are also bended towards the lens aperture. Therefore by using the turbid film the acceptance angle can be increased and hence the NA of the lens. The NA was calculated using the formula NA = η (sin θ), where n is the refractive index of the medium, we have taken η = 2.008 for ZnO. The transmittance of the ZnO turbid films shows an increasing trend going from nanosheets to nanoparticles and further to microstructures (Fig. 4.3(c)). The NA of a turbid lens depends on how much light is scattered upon passing through the medium. We focused on investigating the impact of different geometries of the turbid films on the NA of a Nikon objective lens. An increased acceptance angle 79° of the objective lens is observed for a 44-μm-thick turbid film of nanosheets. The acceptance angle is 68° for a 46-μm-thick film of microstructures and 75° for 44-μm-thick film of nanoparticles, while in air, the objective lens has an acceptance angle

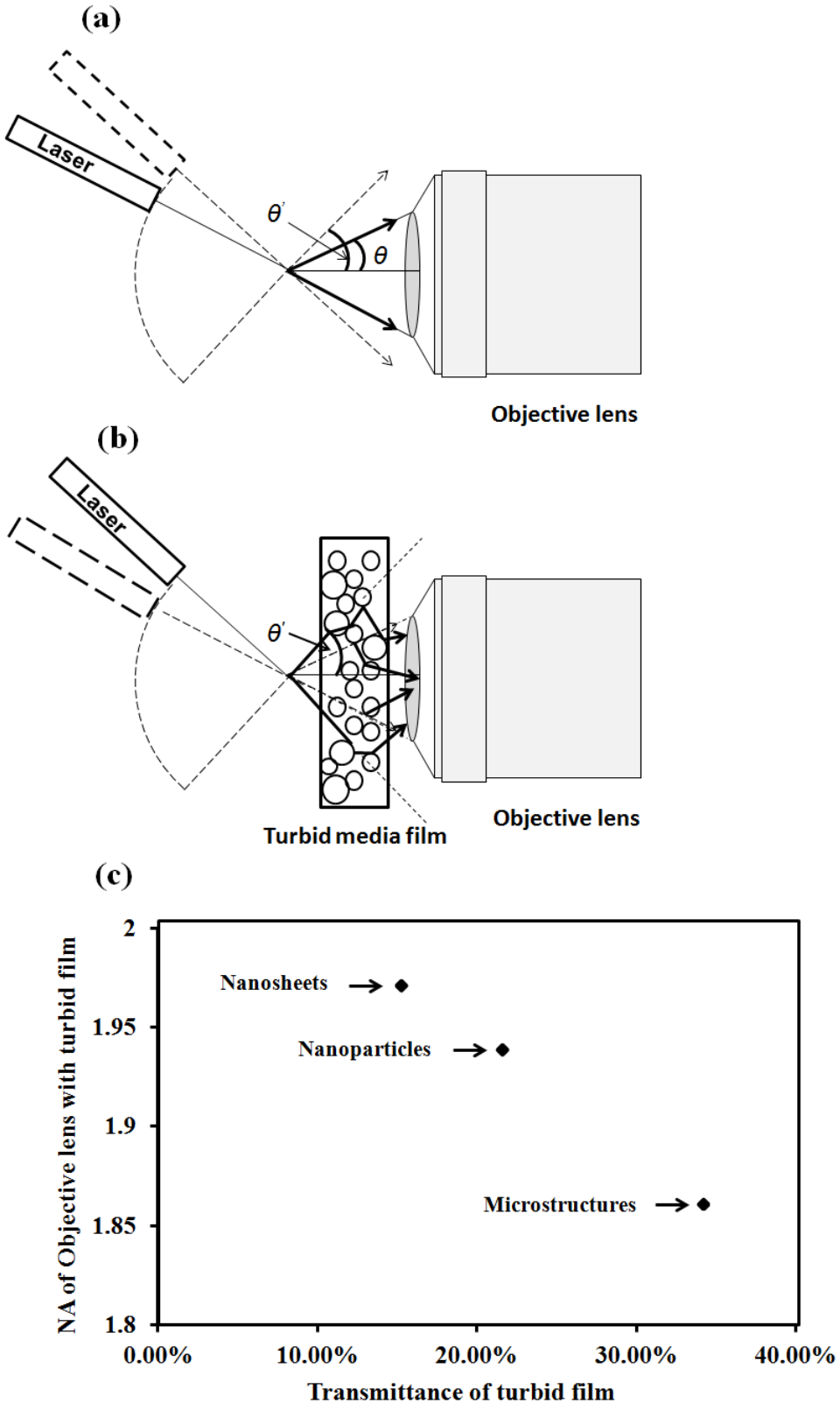

Figure 4.3: (a) Schematic layout of the experimental set-up without using turbid film and (b) with using turbid film in front of the lens, (c) the NA of an objective lens with turbid film versus transmittance of the turbid film, plotted for all three different ZnO turbid films.

only 65° which corresponds to the NA = 0.906(from the relation NA = η sinθ, η = 1). The acceptance angle for bare glass slide was 66°, which corresponds to NA=1.37. In our case, the turbid film of nanosheets has the maximum acceptance angle 79° which gives the NA equal to 1.971 (taking η = 2.008 for ZnO). This value of NA is obtained with a transmission of 15.23% for a 44-μm-thick turbid film of nanosheets. Similarly, NA equal to 1.939 and 1.861 are observed with transmissions of 21.51% and 34.14% for 44-μm- and 46-μm-thick turbid films of nanoparticles and microstructures, respectively, as shown in Fig. 4.3(c). The obtained results for the transmission and corresponding NA are better than that of reported in literature [158].

4.3.2. Principle of enhancement of NA

We know that the scattering of light depends upon the size of the particle as well as the wavelength of the incident light. In our case, since we used fixed wavelength (λ = 632.8 nm) therefore; in this case the scattering mainly depends upon the diameter (D) of the particles. It is well known that based upon the size parameter '$x = \pi D/\lambda$' the scatterings may be explained by rayleigh scattering ($x << 1$), mie scattering ($x \sim 1$) and geometrical optics ($x >> 1$). Since mie scattering is applied for spherical particles [284] of size range comparable to the wavelength of incident radiation, therefore it cannot be applied for used ZnO structures as these structures do not follow constraints of mie scattering. In our case, the scattering by the films of different ZnO structure (nanoparticles, nanosheets and microstructures) can be explained by using rayleigh scattering and geometrical optics.

The variation in scattering with respect to turbid films is shown in Fig. 4.4. The strength of scattering (SC) of the turbid films composed of three different ZnO nanostructures is in the following order: $SC_{nanosheets} > SC_{nanoparticles} > SC_{microstructures}$.

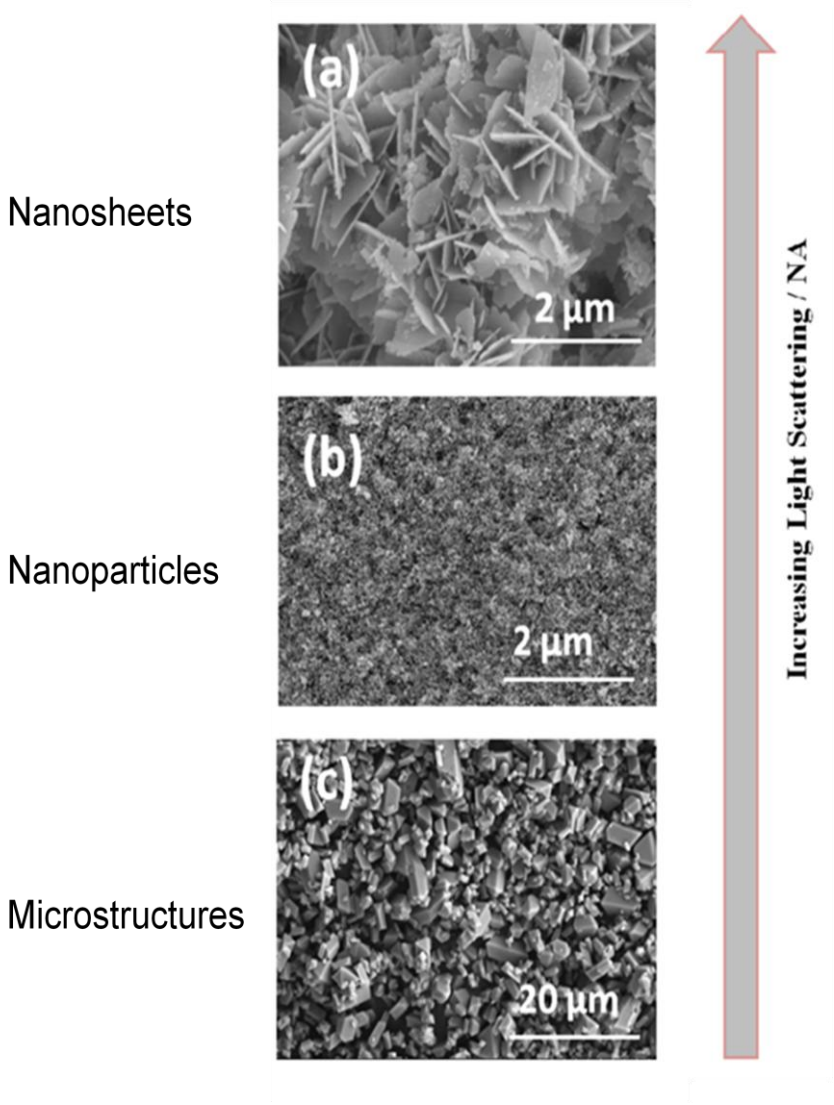

Figure 4.4: Light scattering originating from ZnO structures coated on a thin glass cover slip. FESEM images for (a) a turbid film of nanosheets, (b) a turbid film of nanoparticles, and (c) a turbid film of microstructures.

We start our discussion with ZnO nanoparticles. The ZnO nanoparticles being much smaller than the wavelength of incident radiation (satisfying the criterion of rayleigh scattering, i.e. $x << 1$) can be considered as rayleigh scatterers. When the laser radiation is incident on the film of nanoparticles, each of the nanoparticles in the path of radiation would scatter the radiation. In the transmission experiment, the light has to pass through the film of particles and since the film thickness (44µm) is much larger than the size of constituent nanoparticles, there would be multiple scattering of the radiation when it passing through the film. Therefore, the overall scattering by the film can be seen as the superposition of multiple scattering of incident radiation by nanoparticles in the film. Further, although the modeling of scattered radiation by the film of nanoparticles is complex, but we can visualize the scattered

radiation as composed of contribution of many waves from oscillating dipoles [285]. Under the condition of nanoparticle being much smaller than the incident wavelength, the nanoparticle will be in a uniform electric field and as a whole it can be considered as oscillating dipole [286, 287]. As the separation between the dipoles (ZnO nanoparticles) is much smaller than the incident wavelength, the phase differences are small and the collective scattering from all the dipoles occurs at larger angles in forward direction [288]. For clarification, we consider the scattering of two dipoles. Neglecting the dipole-dipole interaction, the scattered intensity in the direction θ is given by;

$$I = \text{constant}\,[E_1^2 + E_2^2 + 2E_1E_2\cos(\Delta\Phi)] \qquad (4.1)$$

where $\Delta\Phi = 2\pi r/\lambda\ (1-\cos\theta)$ is the phase difference and E_1 and E_2 are electric field from two respective dipoles. The phase difference ($\Delta\Phi$) in a particular direction θ depends upon size parameter ($2\pi r/\lambda$), where r is size of a particle. For $2\pi r/\lambda << 1$ (as in case of nanoparticles), the $\Delta\Phi$ would be negligible even for larger values of θ. So the scattering in case of nanoparticles occurs at larger angles. But in case of $2\pi r/\lambda \sim 1$ or $2\pi r/\lambda >> 1$, then $\Delta\Phi$ would be negligible only at smaller values of θ and hence the scattering occurs at smaller angles [288].

In case of nanosheets, although the size of the nanosheets is large (around 2μm wide) as compared to incident wavelength but due to their planer geometry, Mie scattering cannot be applied (since mie theory is applicable to spherical particles). Similarly, the fraunhofer scattering can be neglected as it occurs for the particles at least 5 to 6 times larger than the incident wavelength [289]. Nanosheets being larger than the incident wavelength, the scattering by a nanosheet can be considered as composed of contributions of many waves generated by oscillating dipoles that make up the nanosheet. As we know, larger is the particle more radiation is scattered in the forward [280]. But in our experiment, we observe that scattering angle for nanosheets film more as compared to the nanoparticles film; it may be due to the contribution of specular reflections from the surface of nanosheets. Due to the smooth surface of the nanosheets (as can be seen in SEM image Fig. 4.4(a)) the possibility of specular reflections cannot be neglected. Therefore, the emerging waves from the film of nanosheets can have specular reflections at the output side of the film, contributing to the scattering angle.

An another reason for increased scattering angle in the case of nanosheets may be their morphological structure in which many nanosheets, which are often aligned in parallel direction, are grouped in bunches. From the SEM image in Fig. 4.4(a), it is clear that there are

bunches of sheets, and most of the sheets have the same parallel arrangement. Light entering a particular area of a turbid film propagates through multiple reflections between the sheets until it faces a barrier or a normally oriented sheet within a bunch along its path. These normally oriented nanosheets in the path of light will scatter the light at higher angles.

The microstructures are larger (~5 μm) than the wavelength of the light, therefore geometrical scattering can be applied. In geometrical scattering the light is prominently scattered near to the forward direction [290] and hence the scattering angle in this case is smaller as compared to nanoparticles and nanosheets.

The contribution of diffused scattering can also be concluded in our samples from the measurement of intensity of transmitted radiation. Since the films are not smooth, the incident radiation will be scattered back due to the diffused reflections. The transmittance of ZnO films is observed in the order of nanosheets < nanoparticles < microstructures. The observed smaller transmittance in case of nanosheets is obvious, since the nanosheets would scatter back the radiation due to the diffused reflections as well as the specular reflections. In case of microstructures, due to their larger size the porosity of the film is smaller as compared to the films of nanoparticles and nanosheets, the transmittance (34.14% in case of microstructure film) will dominate in this case [291].

Table 4.1 shows the transmittance and enhanced NA of an objective lens coated by turbid films of different morphology. While comparing the results with the previous reported results [158] in which they have increased NA from 0.15 to 0.85 for nanoparticles, we observed better enhancement in NA (from 0.906 to 1.971) for nanosheets. As we know that for better image resolution in optical microscopy using a turbid lens, not only the NA but also the transmittance of the turbid lens should be high. In our case, we have obtained comparatively higher NA as well as the comparatively higher transmittance for nanosheets turbid film.

Table 4.1: Transmittance and enhanced NA of objective lens corresponding to different morphologies of turbid films.

Structures	**Thickness (μm)**	**Transmittance of turbid film**	**Enhanced NA of nikon objective lens using turbid films**
Nanosheets	44	15.23%	1.971
Nanoparticles	44	21.51%	1.939
Microstructures	46	34.14%	1.861

4.4. Summary

In summary, we have shown that the NA of an objective lens can be increased for better optical imaging/improved resolution depending upon ZnO nanostructure morphologies composing turbid films. By applying ZnO turbid films, the NA of an objective lens with an initial value 0.906 has been increased to 1.861, 1.939 and 1.971 using the films composed of microstructures, nanoparticles and nanosheets, respectively (44–46 μm film thickness). The variation in NA with different morphologies is explained using size-dependent scattering approach. The maximum NA (of 1.971) is achieved for a turbid film of ZnO nanosheets. This will result in higher value of NA of objective lens with ZnO nanosheets based turbid films. The observed results also indicate that the NA of an objective lens can be further improved by fabricating thicker ZnO nanostructure film, however it will reduce the transmittance.

Chapter-5

Visible-light photodetectors based on ZnO nanostructures

This chapter starts with a brief introduction of photodetectors following by the experimental procedure for the fabrication and operation photodetector. In the next section, visible-light photodetector performances of the different nanostructures have been discussed. In next section, a brief description of the mechanism of photodetector is presented. Finally, the chapter concludes with a brief summary.

5.1. Introduction

A photodetector is a device which converts the energy of photons to electrical energy, usually expressed as a photocurrent or photovoltage. Depending upon the material properties of the photodetectors, it can be used for the detection of optical signals over a range of the electromagnetic spectrum. However, a detector is usually selected based on the requirements of a particular application. The general requirements include wavelength of light to be detected, sensitivity level, and the response speed of the detector. Most of the photodetectors respond uniformly within a specific range of the electromagnetic radiation. Therefore, the wavelength of light to be detected determines the selection of a photodetector material and the target application [292, 293].

The various applications where the photodetectors plays an important role are such as biological research, sensing, detection, and missile launch etc. The nanomaterials as an active light collection region in photodetectors have become an attractive research topic due to their high surface-to-volume ratio and also more freedom in the design of material properties [294]. However, there are a number of photodetector materials depending upon the applications but ZnO based photodetectors have become popular in recent years particularly due to its low cost, non-toxicity, and stability against photocorrosion. Furthermore, ZnO nanostructures have very high internal photoconductivity gain due to the surface-enhanced electron-hole separation efficiency [295]. The interest is also because it is a rich family of nanostructures, versatile and low cost synthesis processes large excitonic binding energy [295-298]. The ZnO as a photodetector is used in the form of single crystals ZnO [299], polycrystalline ZnO films [300], and nanostructures of ZnO [153, 301-304]. Generally, the performance of ZnO based photodetector depends upon the deposition techniques, growth conditions, measurement ambient, structure, porosity, presence of defects, and orientation of the crystallites [305-307] etc.

The ZnO based photodetectors are inclusive of photoconductors, metal-semiconductor metal (MSM) photodetectors, schottky photodiodes, *p-n* junction photodiodes. In the past few years, MSM photodiodes have become increasingly popular in the research field due to their advantages: (1) simple structure, (2) ease of fabrication and integration and (3) low capacitance per unit area [308, 309]. The MSM photodiodes are two back-to-back schottky diodes by using an interdigitated electrode configuration on top of an active light collection region. This type of photodetector cannot work at a zero bias. The MSM photodiodes are fast usually due to their low capacitance per unit area and limited transit time. The biggest drawback of MSM photodetectors is their intrinsic low responsivity. MSM detectors show quite a low photoresponsivity, it is mainly because the metallization used for the electrodes shadows the active light collecting region. This drawback can be overcome by using sensing material of high surface to volume ratio and with surface defects to expand active light collecting region and electrodes of less width in pattern form [310].

One of the most promising semiconductor materials is ZnO because of its wide band gap (≈ 3.3 eV), restricts its performance to UV region. To expand its performance to visible region, many strategies have been reported such as creation of oxygen vacancy defects [311], doping with metals [312], and nonmetals [313, 314], cations [315], anions [316], and combining with another semiconductor material [317]. However, most of these methods often need a higher process temperature and pressure, complicated and expensive equipments. Among these strategies, the creation of oxygen defects states in the synthesized ZnO nanostructures is an efficient way to fabricate ZnO nanostructure based photodetector. Once the oxygen defects are created, the ZnO nanostructures due to their high surface area exhibit higher photoresponse due to extended absorption in the visible region. We know that the oxygen vacancy defects are kind of self-doping without addition of external impurities which enhances the visible photocatalytic activity by narrowing the bandgap [173]. Identifying the importance of oxygen vacancy defects, it is important to find a simple method to create oxygen vacancies inside synthesized ZnO nanostructures in order to work them in the visible region [311]. The undoped ZnO is an n-type semiconductor due to the presence of donor centers like zinc interstitials and oxygen vacancies. The dangling bonds due to a breaking of the periodicity of ZnO lattice on its surface induce acceptor-type surface states which served as charge traps and electron barriers. Therefore, the

surface states of ZnO nanostructures play a crucial role in the optical properties of ZnO nanostructures [318-323].

In many reported studies [294, 324-326], the ZnO has been used as a visible-light photodetector by doping with some suitable dopant material or combining it with a material having low band gap. However, to the best of our knowledge, there are few studies which report the photodetection property of ZnO in visible range without modifications. Herein, we report visible-light photoresponse of different nanostructures morphologies of ZnO with defects synthesized by a facile solution method. The oxygen vacancy defects effectively extend the absorption of ZnO nanostructures to the visible light range. The distinct and fast photoresponse of the device is a direct result of enhanced charge transfer between surface defects and ZnO nanostructures in visible region. This work will provide a new perspective on preparation and utilization of ZnO semiconductor for energy applications in visible region.

5.2. Experimental

In order to achieve uniformity in the deposited films, the ZnO structures: nanosheets, flower-like and nanoparticles were dispersed in C_2H_5OH solution and sonicated for 30 min to achieve good dispersion of ZnO structures inside of the solution. First, to fabricate thin film of ZnO, the glass substrate was cleaned by immersing it in acetone for 10 min, and then in isopropyl alcohol for 10 min. The chemically cleaned substrate was then rinsed in deionized water and baked at 100 °C for 30 min. Spray coating was used for the deposition of ZnO films of optimum thickness on glass slides. During spraying, the substrate temperature was kept at 150 °C and the heater with substrate was kept inside a fume hood to remove vapors of the solvent. The carrier gas N_2 and the ZnO solution were fed into the spray nozzle at a constant spray rate of 1 ml /min. The carrier gas flow rate was maintained at 2×10^4 kg/cm^2. The thickness of each film was controlled by the number of spraying cycles. Finally, using thus obtained ZnO films, experiments were performed to estimate photovoltage with a mercury lamp of 150 W powers as light source. Silver (Ag) contacts, were printed on top of the ZnO nanostructures, and were patterned as interdigitated fingers. Finally, the photodetector was mounted and wire bonded using silver paste. For the measurement of photovoltage, the digital multimeter (DT9205A, accuracy 0.05% ± 1 in the voltage range 200 mV to 200 V, input impedance: 10 MΩ on all ranges) and digital clock (least count: 0.01 s) was used. The 2D view of the fabricated photodetector is shown in Fig. 5.1. Also,

the schematic layout of the experimental set-up for the measurement of photovoltage with time is shown in the Fig. 5.1.

5.3. Result and discussion

5.3.1. Experimental setup

The metal-semiconductor-metal (MSM) is a type of photodetector which is can be used for both the UV to IR detection. In MSM, the photodetector consist of two interdigitated contacts which are called fingers. The fingers are deposited on top of an active ZnO layer as shown in Fig. 5.1. Since the interdigitated structure in these devices reduces carrier transit time through close spacing of the electrodes while maintaining the large surface, these devices show fast response as compared to other photodetectors of the same active area.

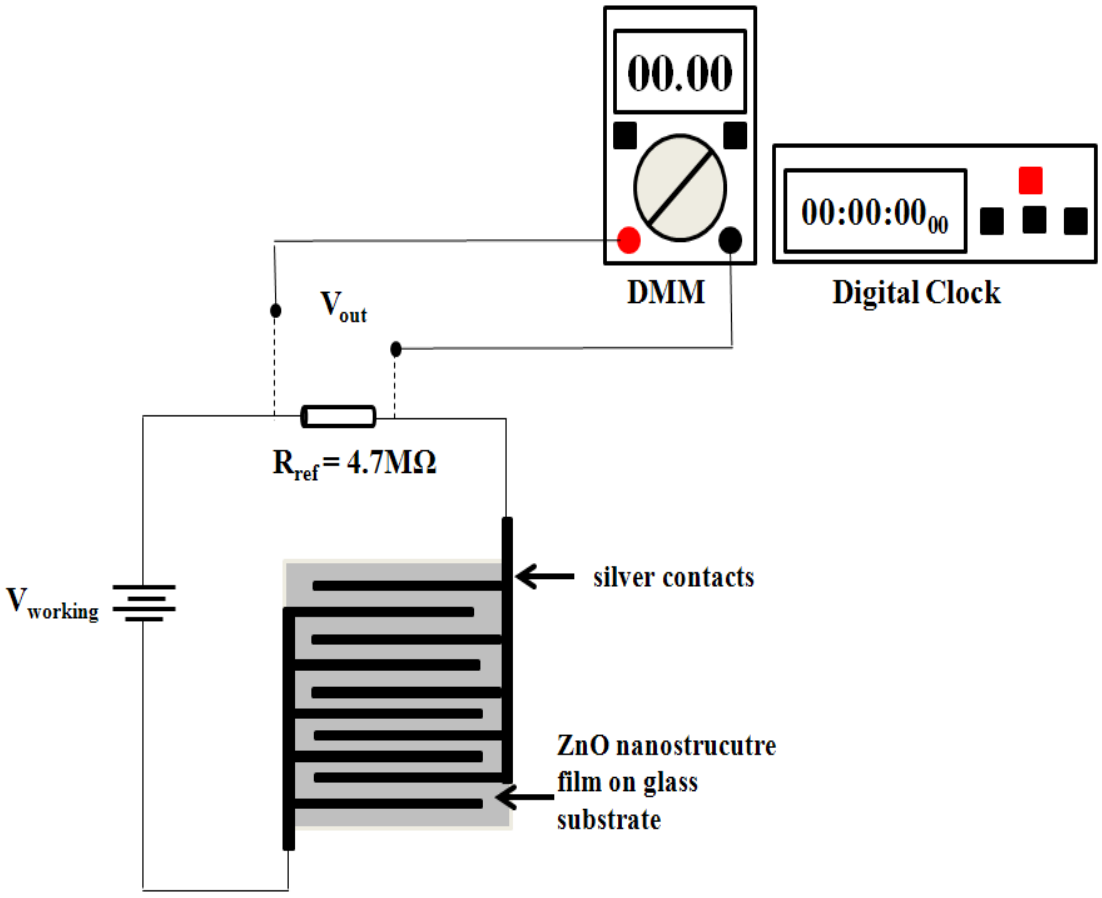

Figure 5.1: Schematic diagram for the measurement of photovoltage with time of visible-light photodetector.

The MSM photodetector operates when the light is illuminated on the surface of the semiconductor (ZnO in this case) material between the fingers. The electrons will be generated in the conduction band by creating the holes in the valance band of the ZnO. This results in creating a photocurrent which is determined by the magnitude of the incident photon energy (hν) relative to the band gap energy (E_g) of the ZnO and the work function of the metal (Ag) (Φ). When $E_g > h\nu$ and $h\nu > \Phi$, the photoelectric emission of electrons from the metal to the semiconductor would occurs. In another case, when $h\nu > E_g$ then photoconductive electron-hole pairs are would be generated in the ZnO. Thus generated electrons and holes are separated by an electric field intrinsically formed between the fingers which lead to photocurrent or photovoltage [293].

5.3.2. Performance of ZnO nanostructure-based photodetector

Figure 5.2 shows the photoresponse of the ZnO nanosheets-based photodetector under different color light illumination (White light intensity= 37000 flux, Violet and Green light intensity = 16700 flux). We can see that there is an initial fast rise in the photovoltage with light illumination (Fig. 5.2(a)). The rise in the photovoltage with light illumination can be explained by the release of the surface-adsorbed oxygen molecules to the air, which results in a sharp increase in carrier concentration and thus the ZnO conductivity. With the time the oxygen desorption process will slow down because the density of surface adsorbed oxygen decrease with time and leads to a slow increase in the photovoltage. In the figure, there is an initial fast decay in the photovoltage when the light is turned off, which is reverse to the process which occurs when the light is on. In the process when the light is turned off, the re-adsorption of oxygen to the surface takes place and it captures the electrons from the nanostructures surfaces, leading to the reduction of photovoltage. The similar type of changes occurs in photoresponse of the all three viz. nanosheets, nanoparticles and flower-like structures-based ZnO photodetectors under different color light illumination as shown in Figs. 5.2, 5.3 and 5.4, respectively.

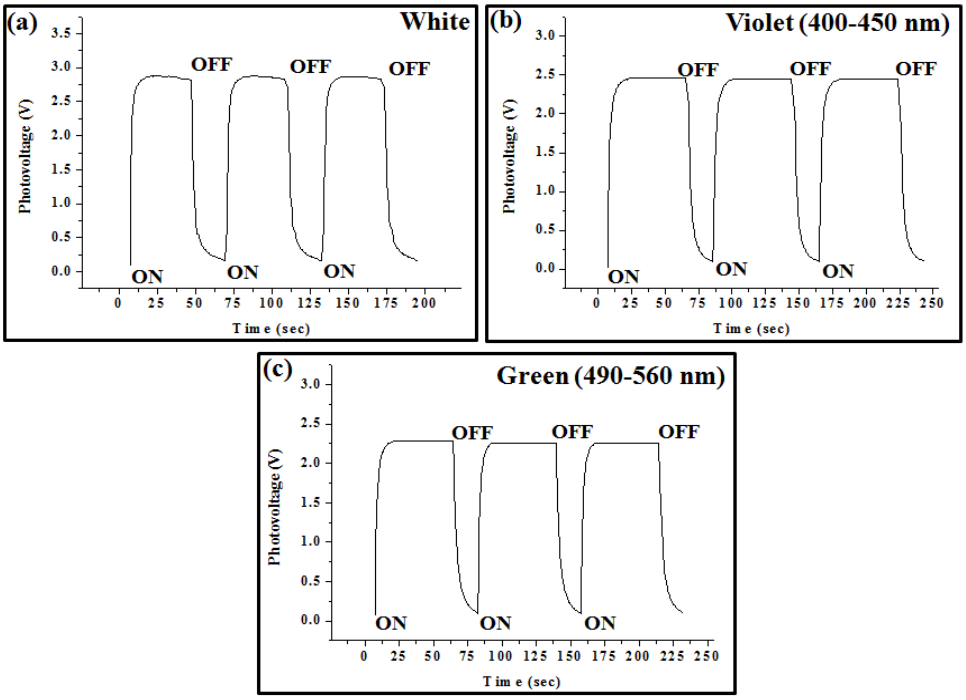

Figure 5.2: Photovoltage versus time plots of ZnO nanosheets-based photodetector using 3V bias under different color light illumination.

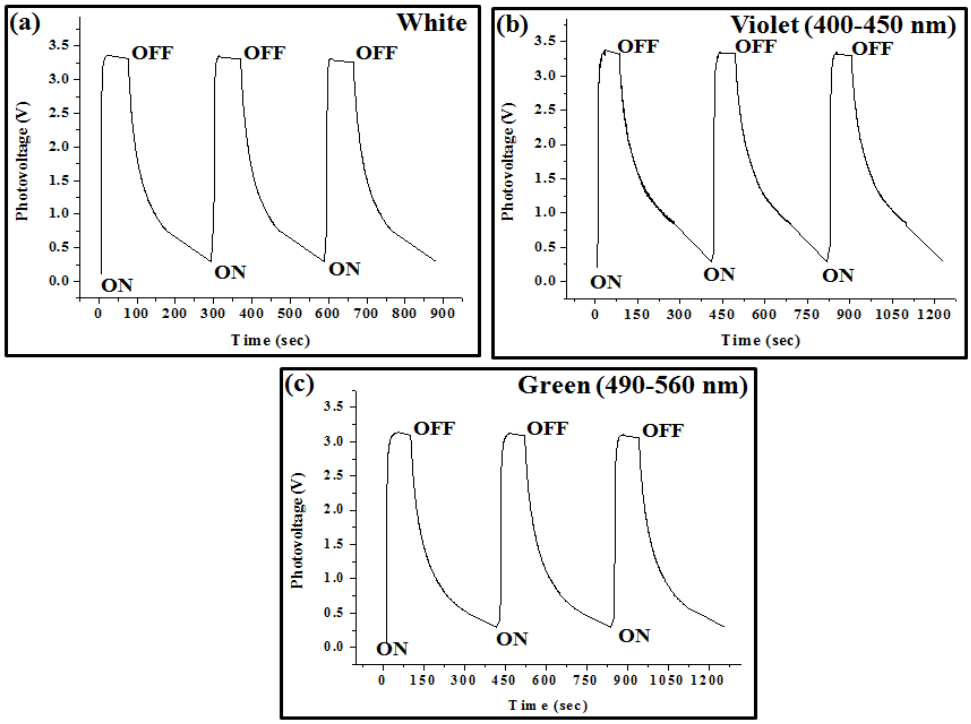

Figure 5.3: Photovoltage versus time plots of ZnO nanoparticles-based photodetector using 3V bias under different color light illumination.

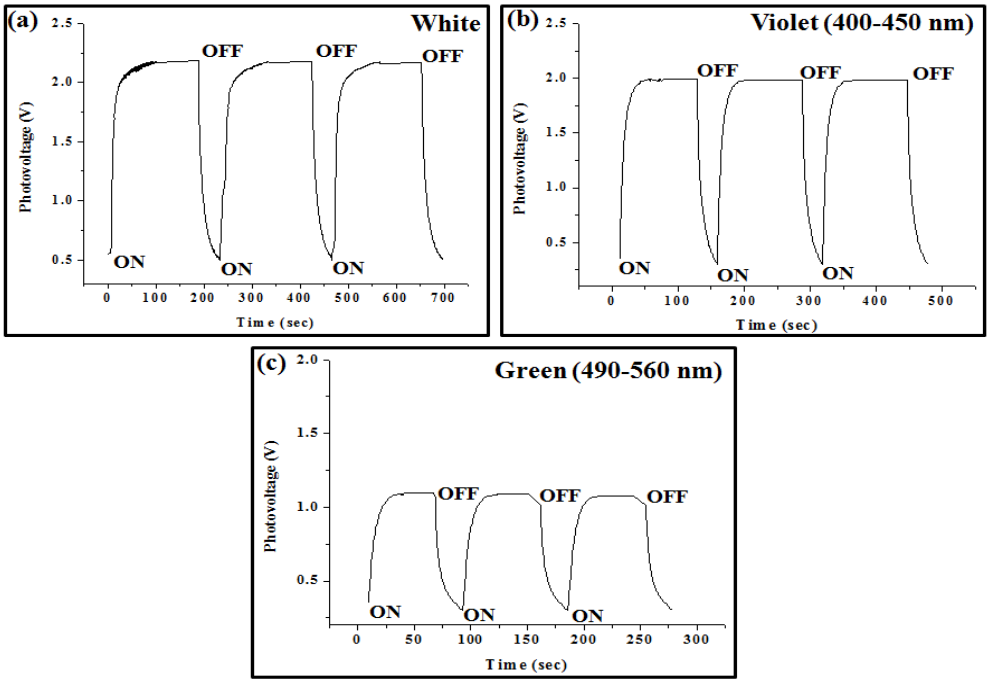

Figure 5.4: Photovoltage versus time plots of ZnO flower-like structures-based photodetector using 3V bias under different color light illumination.

5.3.3. Photodetector mechanism

The schematic for the working of photodetector in dark as well as in light illumination is shown in Fig. 5.5. The mechanisms of the ZnO based-photodetector is explained earlier [153, 295 and 327-329] as follows. The transport and photoconduction properties are mainly affected by surface morphology, trapping at surface states, and O_2 is responsible for the increased voltage intensity. In dark, O_2 molecules adsorbed on the oxide surface and capturing the free electrons [$O_2(g) + e^- \rightarrow O_2^-(ad)$], increases the holes concentration. Therefore, a low-conductivity depletion layer is formed near the samples surface as shown in Fig. 5.5(a). Now, when this oxide layer is illuminated by visible light, electron-hole pairs are generated [$h\nu \rightarrow e^- + h^+$] because of the surface defects states. The generated holes migrate towards the surface and discharge the negatively charged adsorbed oxygen ions combine with oxygen, which induces the desorption of oxygen from the surface of nanostructure [$h^+ + O_2^-(ad) \rightarrow O_2(g)$]. The remaining unpaired holes are either collected at the electrode or recombine with the electrons. Due to the conversion of O_2^- back to the O_2, the thickness of the low-conductivity depletion layer decreased as shown in Fig. 5.5(b). The reduction in the thickness of the depletion layer leads to the increase of the carrier

concentration which results an enhancement in the photovoltage. In the second step, when the light is turned off again, oxygen re-adsorbed on the nanostructure surfaces takes place, which results in the returning to its initial state (Fig. 5.5(c)).

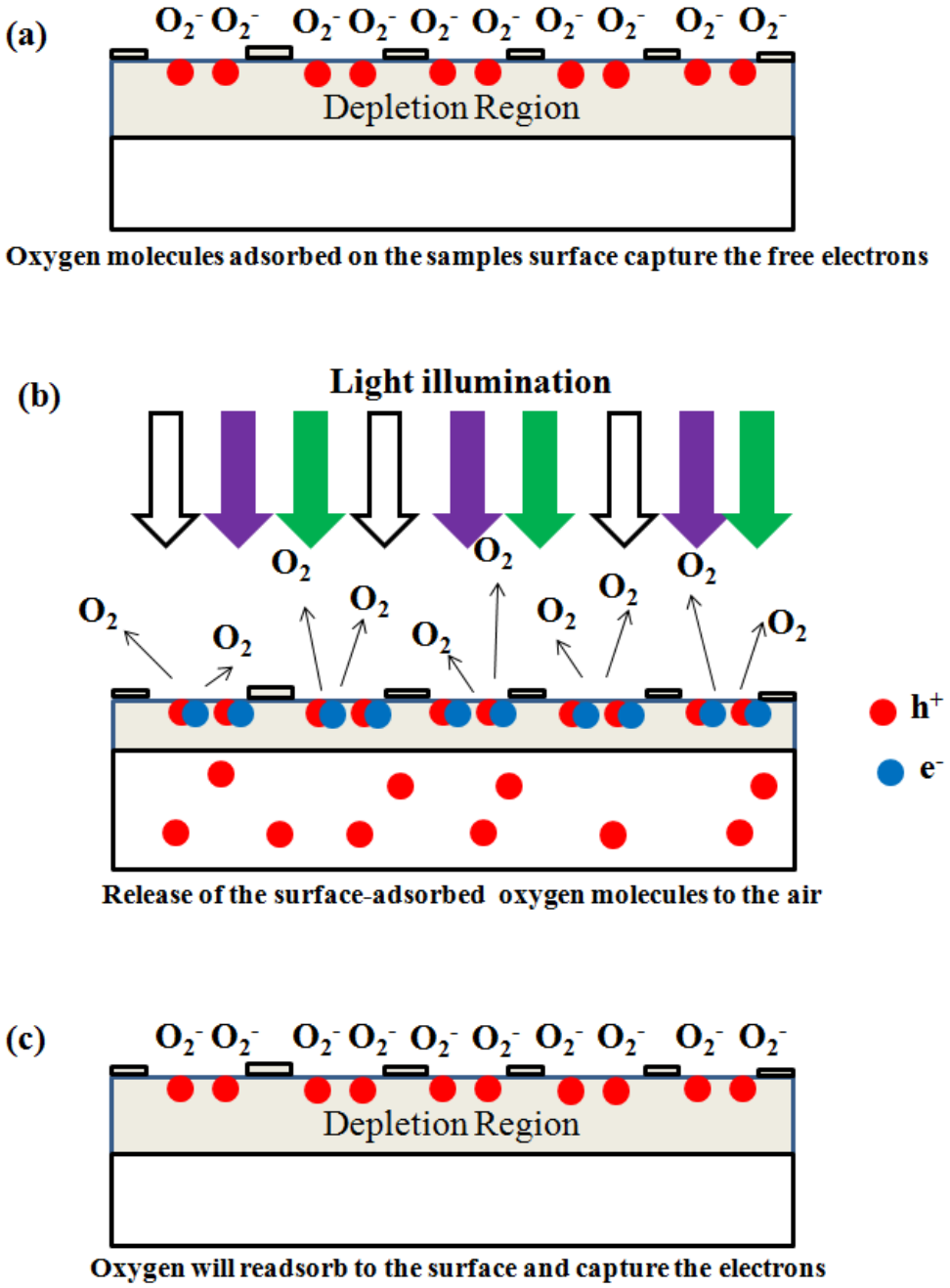

Figure 5.5: Schematic representation of photodetector working for the performance of ZnO nanostructures under dark and visible light illumination.

Based on the above explanation the results are summarized in Table 5.1. It can be seen that the photoresponse/performance of ZnO nanosheets and nanoparticles is better than that of flower-like structure. The ZnO nanoparticles having higher surface area (20.523 m^2/g) would enhance the oxygen adsorption/desorption process, which leads to an enhancement of carrier injection and transport. In addition the surface area for this high photoresponse, the surface states must be taken into consideration. The surface states which act as trap sites capture free electrons leading to a surface-depletion with a band bending upwards towards the surface [330]. When the holes are generated by light illumination they will be migrated along the bending and get trapped at the negatively charged oxygen molecules, and lower the barrier height. Therefore, the increase in the photovoltage is due to both the photogenerated electrons and the lowering of the barrier height [331]. The observed higher value of photovoltage in case of nanoparticles can also be explained on the basis of the surface states as the surface states are proportional to the surface area. From the BET measurements, we observed that the surface area of nanoparticles is higher than the nanosheets and then the flower-like structures. The photovoltage according to the surface area will follow the trend $V_{nanoparticles} > V_{nanosheets} > V_{flower\text{-}like}$, which are in accordance of the observed results as indicated in table 5.1.

Table 5.1: Table shows comparison of the performance of ZnO nanostructures-based photodetector under different color light illumination using 3V bias.

Structures	**Surface area (m^2/g)**	**Intensity of photovoltage with color (V)**	**Growth time with color (s)**	**Decay time with color (s)**
Nanosheets	11.765	White: 2.87 Violet: 2.45 Green: 2.27	White ~ 2 Violet ~ 4 Green ~ 4	White ~ 10 Violet ~ 10 Green ~ 10
Nanoparticles	20.523	White: 3.37 Violet: 3.27 Green: 3.13	White ~ 2 Violet ~ 4 Green ~ 4	White ~ 210 Violet ~ 310 Green ~ 310
Flower-like structures	10.247	White: 2.21 Violet: 1.98 Green: 1.08	White ~ 20 Violet ~ 25 Green ~ 25	White ~ 30 Violet ~ 40 Green ~ 40

The existence of surface states was confirmed by using PL spectra. The PL spectra corresponding to the nanosheets, flower-like structures and nanoparticles are already shown in chapter 2. The PL spectra of nanosheets, flower-like structures and nanoparticles show similar UV as well as visible emissions at 390 nm (UV), 420 nm (violet), 466 nm (blue), 485 nm (blue-green) and 520 nm (green).

The growth time of photovoltage in case of nanoparticles and nanosheets is almost same; this may be attributed to the combined effect of surface area and surface defects. In case of nanoparticles, the surface area is more as compared to the nanosheets, whereas the nanosheets have more surface defects (PL intensity is related to the surface states) [193], therefore in the photoresponse the surface defects predominates. In the case of decay, we observed that after switching off the light, the order of decay time in nanoparticles > flower-like structures > nanosheets i.e. the nanoparticles take around 210-310 s, flower-like structures take approximately 30-40 s, and nanosheets take around 10 s to decrease the photovoltage by same order of magnitude. Since the decay rate becomes faster with increasing adsorbed oxygen (O_2^-) concentrations on the surface [331]. Therefore, the nanoparticles owing to comparatively large surface area should have fast decay time but in our case they show slower decay time. However, the reason for observed decay time behavior is unclear but it may be due to the presence of more deep level defects [332] or surface modification due to light shining [333] in case of nanoparticles. In case of flower-like structures and nanosheets, there may be less deep level defects improving the decay time.

5.4. Summary

In summary, the existence of surface states and large surface area are responsible for the photodetection mechanism in the as synthesized ZnO nanostructured morphologies in visible region. The flower-like structures due to aggregation tendencies do not completely expose their surfaces when irradiated with visible light, resulting in less production of photogenerated electrons and hence a lower response as compared with the nanosheets and nanoparticles. Conclusively, the nanosheets showing good response to photovoltage, growth time and decay time under visible light illumination. It can be used as an efficient material for photodetector applications in visible region also.

Chapter-6

Summary and future suggestions

6.1. Summary and important findings

A facile solution method is used for the synthesis of ZnO nanostructures viz. nanosheets, flower-like structures and nanoparticles. The variety of ZnO nanostructures and their crystal structures were analyzed by using Scanning electron microscope and X-ray Diffraction studies. All the three morphologies of as synthesized ZnO structures possessed wurtzite-hexagonal structure as confirmed by XRD analysis. The studies of concentrations and molar ratios of $ZnAc_2$ and KOH solutions indicated that the thickness and roughness of ZnO structures decreases with the increasing concentration of precursor and alkali solution in the reaction chamber. In this study we used two different solvents i.e. water and ethanol. While varying the ratio OH^-/Zn^{2+} along with concentration of precursor and alkali solution, show an impact on the morphologies in both of the solvents cases. To analyzed the growth, we used Transmission electron microscopy which shows that the ZnO nanostructures viz. nanosheets and flower-like structures synthesized in ethanol and water as solvent, respectively have faceted edges, and grow via oriented attachment of the particles along the (002) direction. The observed similar growth direction (002) for both of the synthesized ZnO nanostructures indicates that the mediums affect the aggregation tendencies of initially formed nanocrystals only. All the synthesized ZnO morphologies have different band gap due to their different size range as observed by UV-Vis spectroscopy. The Fourier transform infrared spectroscopy shows that both the nanosheets and flower-like structures have hydroxyl (chemisorbed and/or physisorbed H_2O molecules) and carboxylate group of acetate coordinated to the surface of ZnO nanocrystals along with other remnant species.

The whole process of formation of ZnO nanostructures i.e. nanosheets and flower-like structures with reaction time may be described to proceed via the nucleation of ZnO nanocrystals and their different aggregation in respective mediums. After aggregation of nanocrystals, the anisotropic growth leading to the formation of nanosheets and flower-like structures may occur either by collision (due to random Brownian motion), oriented attachment of nanocrystals or Ostwald ripening. The reason behind the different aggregation tendencies of initially nucleated ZnO nanocrystals in H_2O and C_2H_5OH medium leading to the formation of nanosheets and flower-like structures with the reaction time is attributed to the extent of hydrogen bonding. The solvent facilitating the adhesion among the ZnO centres through hydrogen bonding leads into the complex interwoven morphologies like nanoflowers. Strong hydrogen bonding networking takes place between the adjacent ZnO

nuclei in water than alcohol medium due to the +I effect of the alkyl chain. Hydrogen bonding was confirmed by symmetry distortion in both of the mediums. And the symmetry distortion is found to be higher in case of nanocrystals from H_2O medium revealing the strong inter hydrogen bonding among these ZnO nanocrystals as compared to the nanocrystals obtained from C_2H_5OH medium. Therefore, the alcohol medium prevents nanoparticles from aggregation while water medium favors their aggregation.

We know that the wide band gap of ZnO restricts its use only in UV region, but in the present study we have used as synthesized ZnO structures in visible regime as well by creating the defects during synthesis at room temperature. The defects were created by fast addition of the precursor solutions, therefore during the reaction the precursor ions do not have sufficient time to orient themselves in completely oriented manner, and hence defects are created in the structures. The defects were confirmed by photoluminescence spectroscopy, which showed emissions peaks around 390 nm (UV), 420 nm (violet), 466 nm (blue), 485 nm (blue-green) and 520 nm (green) for all structures, confirming the visible emission. The observed emission in photoluminescence spectroscopy indicated the existence of oxygen and zinc vacancies which expands its use in UV as well as visible regions also. The existence of oxygen and zinc vacancies could be used for environmental and opto-electronics applications. Taking advantage of the induced defects, we applied ZnO structures for photocatalytic activities under sunlight illumination. However, both the nanosheets and flower-like structures performed the photocatalytic activity in sunlight irradiation but the nanosheets due to large surface area as compared with the flower-like structures showed better performance as a catalyst. In other words, the flower-like structures due to aggregation tendencies do not completely expose their surfaces when irradiated in sunlight irradiation, resulting in less production of $OH^{\cdot}$ and $O_2^{\cdot -}$ radicals and hence a lower degradation efficiency of dye as compared with the nanosheets. Therefore, nanosheets can be used as an efficient material for water purification in photocatalytic mechanism under sunlight irradiation.

The as synthesized ZnO structures due to the presence of oxygen and zinc vacancies show good opto-electronics properties in visible light. The photoresponse of these nanostructures was obtained under different color (white, violet and green) illumination using 3V bias voltage. The existence of surface states and large surface area are inferred to be responsible for the photodetection mechanism in the ZnO nanostructures in visible region. The nanosheets show good response to photovoltage, growth time and decay time under

different color light illumination as compared with nanoparticles and flower-like structures, which is attributed to the surface defects and surface area of nanosheets. However, the nanoparticles owing to comparatively large surface area should have fast decay time but in our case, they show slower decay time which is inferred due to the presence of deeper level defects in case of nanoparticles. In case of flower-like structures again due to their aggregated structure do not completely expose their surfaces when irradiated with visible light and hence result in less production of photogenerated electrons which leads to their lower photoresponse. The as synthesized nanosheets could be used as an efficient material for photodetector applications in visible region.

The ZnO being its negligible absorption in the visible region (red light) can be used as a turbid medium to bend the light in optical imaging applications. In our case, we used different ZnO morphologies to bend the light and increased the numerical aperture of an objective lens. We know that for better image resolution in optical microscopy using a turbid lens not only the numerical aperture but also the transmittance of the turbid lens should be high. The greater the transmittance and bending of a turbid medium, the higher the resolution achieved in optical microscopy. In our case, we enhanced both numerical aperture as well as transmittance of a turbid medium using different morphologies of ZnO. By applying ZnO turbid films, the numerical aperture of an objective lens with an initial value 0.906 has been increased to 1.861, 1.939 and 1.971 using the films composed of microstructures, nanoparticles and nanosheets, respectively (44–46 μm film thickness). The variation in NA with different morphologies is attributed to the size-dependent scattering approach. The maximum bending of light is achieved for a turbid film of ZnO nanosheets. ZnO nanosheets based turbid films shows higher value of numerical aperture of objective lens with suitable transmittance. Observed results indicate that the numerical aperture of an objective lens can be further improved by fabricating thicker ZnO nanostructure film, however it will reduce the transmittance.

This is the first report which highlights the creation of defects states during the synthesis of ZnO nanostructures viz. nanosheets, flower-like structures without addition of surfactant, directing agent or template. This approach offers several advantages because of control of synthesis parameters on the properties of the nanostructures. For the opto-electronic application, this is first time we report pure ZnO as a visible-light photodetector without doping, surface modifications, high temperature or expensive equipment. The ZnO

morphologies are firstly applied to enhance the numerical aperture as well as transmittance of turbid lens for improved optical microscopy. The changes observed in the optical and electrical properties of ZnO nanostructures with the variation of solvent suggest that this could be a very useful way to synthesize different morphologies with novel optical and opto-electronic properties.

Future suggestions

- In future attempts, this method could develop a synthesis procedure to obtain nanostructures with surface defects and of better quality in smaller time frames. This means these reaction methodologies can be utilized to produce surface defects in materials without doping and surface modifications, and without use of high temperature and expensive equipments.
- This synthesis method can be used for the formation of nanostructures of other metal oxide such as Fe_2O_3, NiO, Ce_2O_3, CoO, AZO etc and their properties can be controlled by changing the synthesis parameters.
- Further, the luminescence properties suggest that the visible emissions in ZnO nanostructures expand their use in visible region for the environmental and opto-electronics application.
- In this thesis, photocatalytic activity of ZnO nanostructures for the removal of organic dye: methylene blue is studied in detail. It would be interesting to study the utilize ZnO nanostructures for other hazardous pollutants such as phenols, malachite green, methyl orange, metronidazole, coliform, E. coli bacteria etc.
- Since ZnO thin film and its nanostructures have great application in lithium-ion batteries, sensors and in water purification, the as prepared pure ZnO nanostructures can be further studied for these applications. Also, due to their more surface area and visible emissions they can be used for solar cell, fuel cell, LED, LASER applications etc.

References

[1] Taniguchi N 1974 *On the Basic Concept of Nanotechnology* (Int. Conf. Prod. Eng. Tokyo, Part II, Japan Society of Precision Engineering).

[2] Barsotti R J, Fischer J E, Lee C H, Mahmood J, Adu C K W and Eklund P C 2002 *Appl. Phys. Lett*. **81** 2866.

[3] Hanrath T and Korgel B A 2003 *Adv. Mater.* **15** 437.

[4] Wang Z L and Pan Z W 2002 *Adv. Mater.* **14** 1029.

[5] Zhang H, Ma X Y, Xu J, Niu J J, Sha J and Yang D R 2002 *J. Cryst. Growth* **246** 108.

[6] Mayers B and Xia Y 2002 *Adv. Mater.* **14** 279.

[7] Gao M, Huang S M, Dai L M, Wallace G G, Gao R P and Wang Z L 2000 *Angrew. Chem. Int. Ed.* **39** 3664.

[8] Perez J M, Josephson L and Weissleder R 2002 *Eur. Cell. Mater.* **3** 181.

[9] Cowburn R P, Koltsov D K, Adeyeye A O and Welland M E 1998 *Appl. Phys. Lett.* **73** 28.

[10] Ailhas C F, Meyer A G, Rigler P, Mittelhozer C, Raman S, Aebi U and Burkhard P 2007 *Eur. Cell. Mater.* **14** 115.

[11] Weller D and Doerner M F 2000 *Annu. Rev. Mater. Sci.* **30** 611.

[12] Craddock P T *et al.* 1998 *2000 years of zinc and brass* (British Museum) p 27 ISBN 0-86159-124-0.

[13] Liedekerke M D 2006 Pigment, Inorganic, 2.3 Zinc oxide (zinc white) *Ullmann's Encyclopedia of Industrial Chemistry* (Wiley-VCH Verlag GmbH, Weinheim, Germany).

[14] Partington J R 1989 *A short history of chemistry* (Dover Publications, New York).

[15] Wold R 2013 "*Investigation of defect properties of Li in ZnO - A first-principles study of vibrational frequencies, transition rates and diffusion profiles of Li and Li-complexes in ZnO*" University of Oslo, Norway.

[16] Harte L B 2002 *When radio was the cat's whiskers* (Rosenberg Publications Pty. Ltd., Dural LSW, Australia) p 213.

[17] Bunn C W 1935 *Proc. Phys. Soc.* **47** 835.

[18] Clarke D R 1999 *J. Am. Ceram. Soc.* **82** 485.

[19] Wasa K, Kitabatake M and Adachi H 2004 *Thin Film Materials Technology: Sputtering of Compound Materials* (William Andrew Publications, New York).

[20] Strite S and Morkoc H 1992 *J. Vac. Sci. Technol. B* **10** 1237.

[21] Jagadish C and Pearton S 2006 *Zinc Oxide Bulk, Thin Films and Nanostructures: Processing, Properties, and Applications* (Amsterdam : Elsevier).

[22] Heo Y W, Norton D P, Tien L C, Kwon Y, Kang B S, Ren F, Pearton S J and LaRoche J R 2004 *Mater. Sci. Eng. R-Rep.* **47** 1.

[23] Mende L S and Driscoll J L M 2007 *Mater. Today* **10** 40.

[24] Wang Z L 2007 *Adv. Mater.* **19** 889.

[25] Zou C W, Yan X D, Han J, Chen R Q, Bian J M, Haemmerle E and Gao W 2009 *Chem. Phys. Lett.* **476** 84.

[26] Han J, Qiu W and Gao W 2010 *J. Hazard. Mater.* **178** 115.

[27] Han J and Gao W 2009 *J. Electron. Mater.* **38** 601.

[28] Law M, Greene L E, Johnson J C, Saykally R and Yang P 2005 *Nat. Mater.* **4** 455.

[29] Wang Z L and Song J 2006 *Science* **312** 242.

[30] Wang X, Song J, Liu J and Wang Z L 2007 *Science* **316** 102.

[31] Chen R 2011 "*Synthesis of zinc oxide nanostructures by wet oxidation process*" The University of Auckland, New Zealand.

[32] Ashrafi A B M A, Ueta A, Avramescu A, Kumano H, Suemune I, Ok Y W and Seong T Y 2000 *Appl. Phys. Lett.* **76** 550.

[33] Bates C H, White W B and Roy R 1962 *Science* **137** 993.

[34] Leszczynski M, Suski T, Perlin P, Teisseyre H, Grzegory I, Bockowski M, Jun J, Porowski S, Pakula K, Baranowski J M, Foxon C T and Cheng T S 1996 *Appl. Phys. Lett.* **69** 73.

[35] Kisi E and Elcombe M M 1989 *Acta Crystallogr. Sec. C* **45** 1867.

[36] Braekken H and Jore C 1935 Det Norske Videnskabers Skifter (*The Norwegian Science Scripts)* **NR8** 1 (in Norwegian).

[37] Heller R B, McGannon J and Weber A H 1950 *J. Appl. Phys.* **21** 1283.

[38] Rymer T B and Archard G D 1952 *Res.* **5** 292.

[39] Cimino A, Marezio M and Santoro A 1957 *Naturwissenschaften* **12** 348.

[40] Gray T J 1954 *J. Am. Ceram. Soc.* **37** 534.

[41] Mohatny G P and Azaroff L V 1961 *J. Chem. Phys.* **35** 1268.

[42] Khan A A 1968 *Acta Crystallogr. Sec. A* **24** 403.

[43] Reeber R R 1970 *J. Appl. Phys.* **41** 5063.

[44] Morkoc H and Özgür U 2009 *Zinc Oxide: Fundamentals, Materials and Device Technology* (WILEY-VCH Verlag GmbH & Co. KGaA, Weinheim) ISBN: 978-3-527-40813-9.

[45] Jaffe J E, Snyder J A, Lin Z and Hess A C 2000 *Phys. Rev. B* **62** 1660.

[46] Chelikowsky J R 1977 *Solid State Commun.* **22** 351.

[47] Rossler U 1969 *Phys. Rev.* **184** 733.

[48] Bloom S and Ortenburger I 1973 *Phys. Status Solidi.* B **58** 561.

[49] Usuda M, Hamada N, Kotani T and van Schilfgaarde M 2002 *Phys. Rev. B* **66** 125101.

[50] Ivanov I and Pollmann J 1981 *Phys. Rev. B* **24** 7275.

[51] Vogel D, Krüger P and Pollmann J 1995 *Phys. Rev. B* **52** R14316.

[52] Özgür U, Alivov Y I, Liu C, Teke A, Reshchikov M A, Doğan S, Avrutin V, Cho S J and Morkoc H 2005 *J. Appl. Phys.* **98** 041301.

[53] Djurišić A B, Chen X, Leung Y H and Ng A M C 2012 *J. Mater. Chem.* **22** 6526.

[54] Wang Z L 2004 *J. Phys.: Condens. Matter* **16** R829.

[55] Özgür U, Hofstetter D and Morkoc H 2010 *Proceed. IEEE* **98** 1255.

[56] Willander M 2014 *Zinc Oxide Nanostructures: Advances and Applications* (Pan Stanford Publishing, CRC Press, Florida) ISBN: 978-981-4411-34-9.

[57] Liu Y, Shi J, Peng Q and Li Y 2012 *J. Mater. Chem.* **22** 6539.

[58] Wang H, Li G, Jia L, Wang G and Tang C 2008 *J. Phys. Chem. C* **112** 11738.

[59] Barick K C, Singh S, Aslam M and Bahadur D 2010 *Micropor. Mesopor. Mater.* **134** 195.

[60] Wu Q, Chen X, Zhang P, Han Y, Chen X, Yan Y and Li S 2008 *Cryst. Growth Des.* **8** 3011.

[61] Kim D and Huh Y D 2011 *Mater. Lett.* **65** 2100.

[62] Li Y, Gong J and Deng Y 2010 *Sens. Actuators A* **158** 176.

[63] Ma X Y and Zhang W D 2009 *Polym. Degrad. Stab.* **94** 1103.

[64] Yang H, Liu C, Yang D, Zhang H and Xi Z 2009 *J. Appl. Toxicol.* **29** 69.

[65] Ohira T, Yamamoto O, Iida Y and Nakagawa Z 2008 *J. Mater. Sci.: Mater. Med.* **19** 1407.

[66] Barui A K, Veeriah V, Mukherjee S, Manna J, Patel A K, Patra S, Pal K, Murali S, Rana R K, Chatterjee S and Patra C R 2012 *Nanoscale* **4** 7861.

[67] Shi J, Hong H, Ding Y, Yang Y, Cai W and Wang X 2011 *J. Mater. Chem.* **21** 9000.

[68] Park J K, Kim Y J, Yeom J, Jeon J H, Yi G C, Je J H and Hahn S K 2010 *Adv. Mater.* **22** 4857.

[69] Vinod R, Sajan P, Achary S R, Tomas C M, Sanjosé V M and Bushiri M J 2012 *J. Phys. D: Appl. Phys.* **45** 425103.

[70] Liu J, Wei A, Zhao Y, Lin K and Luo F 2014 *J. Mater. Sci.: Mater. Electron.* **25** 1122.

[71] Umar A, Akhtar M S, Al-Hajry A, Al-Assiri M S and Almehbad N Y 2012 *Mater. Res. Bull.* **47** 2407.

[72] Kim Y J, Yoo J, Kwon B H, Hong Y J, Lee C H and Yi G C 2008 *Nanotechnology* **19** 315202.

[73] Guo X, Zhao Q, Li R, Pan H, Guo X, Yin A and Dai W 2010 *Opt. Express* **18** 18401.

[74] Qi L, Li H and Dong L 2013 *Mater. Lett.* **107** 354.

[75] Ahmad U, Chauhan M S, Chauhan S, Kumar R, Sharma P, Tomar K J, Wahab R, Al-Hajry A and Singh D 2013 *J. Biomed. Nanotechnol.* **9** 1794.

[76] Pawar R C, Shaikh J S, Suryavanshi S S and Patil P S 2012 *Curr. Appl. Phys.* **12** 778.

[77] Khan A, Abbasi M A, Wissting J, Nur O and Willander M 2013 *Phys. Status Solidi-RLL* **7** 980.

[78] Wang Y, Li X, Wang N, Quan X and Chen Y 2008 *Sep. Purif. Technol.* **62** 727.

[79] Chen S J, Liu Y C, Shao C L, Mu R, Lu Y M, Zhang J Y, Shen D Z and Fan X W 2005 *Adv. Mater.* **17** 586.

[80] Vempati S, Mitra J and Dawson P 2012 *Nanoscale Res. Lett.* **7** 470.

[81] Tan W K, Razak K A, Lockman Z, Kawamura G, Muto H and Matsuda A 2013 *Solid State Commun.* **162** 43.

[82] Umar A and Hahn Y B 2006 *Nanotechnology* **17** 2174.

[83] Kim K H, Kumar B, Lee K Y, Park H K, Lee J H, Lee H H, Jun H, Lee D and Kim S W 2013 *Sci. Rep.* **3** 2017.

[84] Wang J, Qu F and Wu X 2013 *Sci. Adv. Mater.* **5** 1052.

[85] An Q, Xin Y, Huo K, Cai X and Chu P K 2009 *Mater. Chem. Phys.* **115** 439.

[86] Hynek J, Kalousek V, Žouželka R, Bezdička P, Dzik P, Rathouský J, Demel J and Lang K 2014 *Langmuir* **30** 380.

[87] Wang H, Jiang H, Zhang H, Zhou Y, Wu C, Zhao J, Wu C, Ba L and Wang X 2011 *J. Nanosci. Nanotechnol.* **11** 1117.

[88] Zhang S L, Lim J O, Huh J S, Noh J S and Lee W 2013 *Curr. Appl. Phys.* **13** S156.

[89] Amini E, Dolatyari M, Rostami A, Shekari H, Baghban H, Rasooli H and Miri S 2012 *IEEE Photon. Technol. Lett.* **24** 1995**.**

[90] Costenaro D, Carniato F, Gatti G, Marchese L and Bisio C 2013 *New J. Chem.* **37** 2103.

[91] Liu B, Wang Z, Dong Y, Zhu Y, Gong Y, Ran S, Liu Z, Xu J, Xie Z, Chen D and Shen G 2012 *J. Mater. Chem.* **22** 9379.

[92] Bagabas A**,** Alshammari A**,** Aboud M F and Kosslick H 2013 *Nanoscale Res. Lett.* **8** 516.

[93] Hong R Y, Li J H, Chen L L, Liu D Q, Li H Z, Zheng Y and Ding J 2009 *Powder Technol.* **189** 426.

[94] Zheng Y, Li R and Wang Y 2009 *Int. J. Mod. Phys. B* **23** 1566.

[95] Xiong H M 2013 *Adv. Mater.* **25** 5329.

[96] Matsuyama K, Ihsan N, Irie K, Mishima K, Okuyama T and Muto H 2013 *J. Colloid Interf. Sci.* **399** 19.

[97] Rasmussen J W, Martinez E, Louka P and Wingett D G 2010 *Expert Opin. Drug Deliv.* **7** 1063.

[98] Al-Kahlout A 2012 *Thin Solid Films* **520** 1814.

[99] Smijs T G and Pavel S 2011 *Nanotechnol. Sci. Appl.* **2011** 95.

[100] Sun H, Tian H, Yang Y, Xie D, Zhang Y C, Liu X, Ma S, Zhao H M and Ren T L 2013 *Nanoscale* **5** 6117.

[101] Wang X, Zhuang J, Peng Q and Li Y D 2005 *Nature* **437** 121.

[102] Wang X D, Gao P X, Li J, Summers C J and Wang Z L 2002 *Adv. Mater.* **14** 1732.

[103] Yin Y D and Alivisatos A P 2005 *Nature* **437** 664.

[104] Xu L, Hu Y L, Pelligra C, Chen C H, Jin L, Huang H, Sithambaram S, Aindow M, Joesten R and Suib S L 2009 *Chem. Mater.* **21** 2875.

[105] Shi Z F, Zhang Y T, Cai X P, Wang H, Wu B, Zhang J X, Cui X J, Dong X, Liang H W, Zhang B L and Du G T 2014 *CrystEngComm* **16** 455.

[106] Fan Z and Lu J G 2005 *J. Nanosci. Nanotechnol.* **5** 1561.

[107] Udom I, Ram M K, Stefanakos E K, Hepp A F and Goswami D Y 2013 *Mat. Sci. Semicon. Proc.* **16** 2070.

[108] Zhang Y, Ram M K, Stefanakos E K and Goswami D Y 2012 *J. Nanomater.* **2012** 624520.

[109] Kossanyi J, Kouyate D, Pouliquen J, Ronfard-Haret J C, Valat P, Oelkrug D, Mammel U, Kelly G P and Wilkinson F1990 *J. Lumin.* **46** 17.

[110] Kouyate D, Ronfard-Haret J C and Kossanyi J 1991 *J. Lumin.* **50** 205.

[111] Bachir S, Sandouly C, Kossanyi J and Ronfard-Haret J C 1996 *J. Phys. Chem. Solids* **57** 1869.

[112] Lundblad A and Bergrnan B 1997 *Solid State Ionics* **96** 173.

[113] Fey G T K and Pemg W B 1997 *Mater. Chem. Phys.* **47** 279.

[114] Rockett A 2008 *The Materials Science of Semiconductors* (Springer XVII) ISBN: 978-0-387-25653-5.

[115] Gaikwad A B, Navale S C, Samuel V, Murugan A V and Ravi V 2006 *Mater. Res. Bull.* **41** 347.

[116] Zawrah M F, Hamaad H and Meky S 2006 *Cera. Inter.* **33** 969.

[117] Xu G, Zhang X, He W, Liu H, Li H and Boughton R I 2006 *Mater. Lett.* **60** 962.

[118] Carter C B and Norton M G 2007 *Ceramic Materials: Science and Engineering* (Springer, New York) p 400-411.

[119] Byrappa K and Yoshimura M 2001 *Handbook of Hydrothermal Technology* (Noyes Publications, New Jersey (USA)).

[120] Lonescu M 2005 *Chemistry and Technology of Polyols for Polyurethanes* (Rapra Technology Ltd., Shawbury, United Kingdom).

[121] Laudise R A and Ballman A A 1960 *J. Phys. Chem.* **64** 688.

[122] Li W J, Shi E W, Zhong W Z and Yin Z W 1999 *J. Cryst. Growth* **203** 186.

[123] Demianets L N, Kostomarov D V, Kuz'mina I P and Pushko S V 2002 *Crystallogr. Rep.* **47** S86.

[124] Demianets L N and Kostomarov D V 2001 *Ann. Chim. Sci. Mat.* **26** 193.

[125] Dem'yanets L N, Kostomarov D V and Kuz-mina I P 2002 *Inorg. Mater.* **38** 124.

[126] Xu S and Wang Z L 2011 *Nano Res.* **4** 1013.

[127] Zhang J, Sun L, Yin J, Su H, Liao C and Yan C 2002 *Chem. Mater.* **14** 4172.

[128] Cheng B and Samulski E T 2004 *Chem. Commun.* **2004** 986.

[129] Liu B and Zeng H C 2003 *J. Am. Chem. Soc.* **125** 4430.

[130] Cao H L, Qian X F, Gong Q, Du W M, Ma X D and Zhu Z K 2006 *Nanotechnology* **17** 3632.

[131] Hou X M, Zhou F, Sun Y B and Liu W M 2007 *Mater. Lett.* **61** 1789.

[132] Alammar T and Mudring A V 2009 *Mater. Lett.* **63** 732.

[133] Yamabi S and Imai H 2002 *J. Mater. Chem.* ***12*** 3773.

[134] Rao C N R, Müller A and Cheetham A K 2007 *Nanomaterials Chemistry: Recent Developments and New Directions* (Wiley-VCH Verlag GmbH & Co, KGaA, Weinheim, Germany) p 140,157.

[135] Cheng B, Shi W, Russell-Tanner J M, Zhang L and Samulski E T 2006 *Inorg. Chem.* **45** 1208.

[136] Thilagavathi T and Geetha D 2014 *Appl. Nanosci.* **4** 127.

[137] Pankove J I 1971 *Optical Processes in Semiconductors* (Prentice-Hall, Englewood Cliffs, New Jersey).

[138] Yu W, Li X and Gao X 2005 *Cryst. Growth Des.* **5** 151.

[139] Xu X L, Lau S P, Chen J S, Chen G Y and Tay B K 2001 *J. Cryst. Growth* **223** 201.

[140] Mahamuni S, Borgohain K, Bender B S, Leppert V J and Risbud S H 1999 *J. Appl. Phys.* **85** 2861.

[141] Xue Z Y, Zhang D H, Wang Q P and Wang J H 2002 *Appl. Surf. Sci.* **195** 126.

[142] Liu B, Fu Z and Jia Y 2001 *Appl. Phys. Lett.* **79** 943.

[143] Hu J Q, Ma X L, Xie Z Y, Wong N B, Lee C S and Lee S T 2001 *Chem. Phys. Lett.* **344** 97.

[144] Williams G and Kamat P V 2009 *Langmuir* **25** 13869.

[145] Suttiponparnit K, Jiang J, Sahu M, Suvachittanont S, Charinpanitkul T and Biswas P 2011 *Nanoscale Res. Lett.* **6** 27.

[146] Kar J P, Ham M H, Lee S W and Myoung J M 2009 *Appl. Surf. Sci.* **255** 4087.

[147] Pei L Z, Zhao H S, Tan W, Yu H Y, Chen Y W and Zhang W F 2009 *Mater. Charact.* **60** 1063.

[148] Qiu M, Ye Z, Lu J, He H, Huang J, Zhu L and Zhao B 2009 *Appl. Surf. Sci.* **255** 3972.

[149] Liang Y and Yoffe A D 1968 *Phys. Rev. Lett.* **20** 59.

[150] Huang M H, Wu Y, Feick H, Tran N, Weber E and Yang P 2001 *Adv. Mater.* **B13** 113.

[151] Gonzalez-Valls I and Lira-Cantu M 2009 *Energy Environ. Sci.* **2** 19.

[152] Lai E, Kim W and Yang P 2008 *Nano Res.* **1** 123.

[153] Jin Y Z, Wang J P, Sun B Q, Blakesley J C and Greenham N C 2008 *Nano Lett.* **8** *1649.*

[154] Zhang C, Zhang F, Xia T, Kumar N, Hahm J I, Liu J, Wang Z L and Xu J 2009 *Opt. Express* **17** 7893.

[155] Wei A, Wang Z, Pan L H, Li W W, Xiong L, Dong X C and Huang W 2011 *Chin. Phys. Lett.* **28** 080702.

[156] Frenzel H, Lajn A, Wenckstern H, Lorenz M, Schein F, Zhang Z and Grundmann M 2010 *Adv. Mater.* **22** 5332.

[157] Hillman T R, Yamauchi T, Choi W, Dasari R R, Feld M S, Park Y and Yaqoob Z 2013 *Sci. Rep.* **3** 1909.

[158] Choi Y, Yang T D, Fang-Yen C, Kang P, Lee K J, Dasari R R, Feld M S and Choi W 2011 *Phys. Rev. Lett.* **107** 023902.

[159] Dev A, Elshaer A and Voss T 2011 *IEEE J. Sel. Topics Quantum Electron.* **17** 896.

[160] Garcia M A, Merino J M, Fernandez E P, Quesada A and Venta J 2007 *Nano Lett*. **7** 1489.

[161] Lim J H, Kang C K, Kim K K, Park I K, Hwang D K and Park S J 2006 *Adv. Mater.* **18** 2720.

[162] Lansdown A B G and Taylor A 1997 *Int. J. Cosmet. Sci.* **19** 167.

[163] Mohammad M T, Hashim A A and Al-Maamory M H 2006 *Mater. Chem. Phys.* **99** 382.

[164] Wang J, Liu P, Fu X, Li Z, Han W and Wang X 2009 *Langmuir* **25** 1218.

[165] Guo M Y, Ng A M C, Liu F Z, Djurisic A B, Chan W K, Su H M and Wong K S 2011 *J. Phys. Chem. C* **115** 11095.

[166] Li G R, Hu T, Pan G L, Yan T Y, Gao X P and Zhu H Y 2008 *J. Phys. Chem. C* **112** 11859.

[167] Becker J, Raghupathi K R, St. Pierre J, Zhao D and Koodali R T 2011 *J. Phys. Chem. C* **115** 13844.

[168] McLaren A, Valdes-Solis T, Li G and Tsang S C 2009 *J. Am. Chem. Soc.* **131** 12540.

[169] Jang E S, Won J H, Hwang S J and Choy J H 2006 *Adv. Mater.* **18** 3309.

[170] Tian Z R, Voigt J A, Liu J, Mckenzie B, Mcdermott M J, Rodriguez M A, Konishi H and Xu H 2003 *Nat. Mater.* **2** 821.

[171] Wang L, Chang L X, Zhao B, Yuan Z Y, Shao G S and Zheng W J 2008 *Inorg Chem* **47** 1443.

[172] Zhang L, Yang H Q, Ma J H, Li L, Wang X W, Zhang L H, Tian S and Wang X Y 2010 *Appl. Phys. A* **100** 1061.

[173] Kong M, Li Y, Chen X, Tian T, Fang P, Zheng F and Zhao X 2011 *J. Am. Chem. Soc.* **133** 16414.

[174] Justicia I, Ordejon P, Canto G, Mozos J L, Fraxedes J, Battiston G A, Gerbasi R and Figueras A 2002 *Adv. Mater.* **14** 1399.

[175] Zuo F, Wang L, Wu T, Zhang Z Y, Borchardt D and Feng P Y 2010 *J. Am. Chem. Soc.* **132** 11856.

[176] Wan Q, Wang T H and Zhao J C 2005 *Appl. Phys. Lett.* **87** 083105.

[177] Koch U, Fojtik A, Weller H and Henglein A 1985 *Chem. Phys. Lett.* **122** 507.

[178] Hynek J, Kalousek V, Žouželka R, Bezdička P, Dzik P, Rathouský J, Demel J and Lang K 2014 *Langmuir* **30** 380.

[179] Bang S, Lee S, Ko Y, Park J, Shin S, Seo H and Jeon H 2012 *Nanoscale Res. Lett*. **7** 290.

[180] Guo L, Ji Y L, Xu H, Simon P and Wu Z 2002 *J. Am. Chem. Soc.* **124** 14864.

[181] Munoz-Espi R, Jeschke G, Lieberwirth I, Gomez C M and Wegner G 2007 *J. Phys. Chem. B* **111** 697.

[182] Pacholski C, Kornowski A and Weller H 2002 *Angew. Chem. Int. Ed.* **41** 1188.

[183] Taubert A, Glasser G and Palms D 2002 *Langmuir* **18** 4488.

[184] Tian Z R, Liu J, Voigt J A, Mckenzie B and Xu H 2003 *Angew. Chem. Int. Ed.* **42** 413.

[185] Umetsu M, Mizuta M, Tsumoto K, Ohara S, Takami S, Watanabe H, Kumagai I and Adschiri T 2005 *Adv. Mater.* **17** 2571.

[186] Zhang T, Dong W, Keeter-Brewer M, Konar S, Njabon R N and Tian Z R 2006 *J. Am. Chem. Soc.* **128** 10960.

[187] Zhang Y and Mu J 2007 *Nanotechnology* **18** 075606.

[188] Zou H, Luan Y, Ge J, Wang Y, Zhuang G, Li R and Li Z 2011 *CrystEngComm* **13** 2656.

[189] Zhang J, Wang J, Zhou S, Duan K, Feng B, Weng J, Tang H and Wu P 2010 *J. Mater. Chem.* **20** 9798.

[190] Kahn M L, Monge M, Colliere V, Senocq F, Maisonnat A and Chaudret B 2005 *Adv. Funct. Mater.* **15** 458.

[191] Monge M, Kahn M L, Maisonnat A and Chaudret B 2003 *Angew. Chem. Int. Ed.* **42** 5321.

[192] Antonietti M, Kuang D, Smarsly B and Zhou Y 2004 *Angew. Chem. Int. Ed.* **43** 4988.

[193] Zhang X, Qin J, Xue Y, Yu P, Zhang B, Wang L and Liu R 2014 *Sci. Rep.* **4** 4596.

[194] Yang H, Cai W and Guo X 2014 *Mater. Sci. Semiconductor Process* **24** 164.

[195] Liu D, Lv Y, Zhang M, Liu Y, Zhu Y, Zong R and Zhu Y 2014 *J. Mater. Chem. A* **2** 15377.

[196] Bai W, Zhu X, Zhu Z and Chu J 2008 *Appl. Surf. Sci.* **254** 6483.

[197] Cao B, Cai W, Li Y, Sun F and Zhang L 2005 *Nanotechnology* **16** 1734.

[198] Sun Y, Wang L, Yu X and Chen K 2012 *CrystEngComm* **14** 3199.

[199] Wang J, Hou S, Zhang L, Chen J and Xiang L 2014 *CrystEngComm* **16** 7115.

[200] Ma J, Su S, Fu W, Yang H, Zhou X, Yao H, Chen Y, Yang L, Sun M, Mu Y and Lv P 2014 *CrystEngComm* **16** 2910.

[201] Xingfu Z, Zhaolin H, Yiqun F, Su C, Weiping D and Nanping X 2008 *J. Phys. Chem. C* **112** 11722.

[202] Khoa N T, Kim S W, Thuan D V, Yoo D H, Kim E J and Hahn S H 2014 *CrystEngComm* **16** 1344.

[203] Kawska A, Duchstein P, Hochrein O and Zahn D 2008 *Nano Lett.* **8** 2336.

[204] Mo M, Yu J C, Zhang L Z and Li S K A 2005 *Adv. Mater.* **17** 756.

[205] Liu Y, Wang D, Peng Q, Chu D, Liu X and Li Y 2011 *Inorg. Chem.* **50** 5841.

[206] Layek A, Mishra G, Sharma A, Spasova M, Dhar S, Chowdhury A and Bandyopadhyaya R 2012 *J. Phys. Chem. C* **116** 24757.

[207] Zhang D F, Sun L D, Yin J L, Yan C H and Wang R M 2005 *J. Phys. Chem. B* **109** 8786.

[208] Vinogradov S N and Linnell R H 1971 *Hydrogen bonding* (Van Nostrand Reinhold Co, New York).

[209] Philp R B 1995 *Environmental hazardous and human health* (CRC Press, Inc.) p 73-75.

[210] Borker P and Salker A V 2006 *Mater. Sci. Eng. B* **133** 55.

[211] Zollinger H 1991 *Color Chemistry: Synthesis, Properties and Applications of Organic Dyes and Pigments* 2nd ed. (VCH, New York).

[212] Prado A G S, Bolzon L B, Pedroso C P, Moura A O and Costa L L 2008 *Appl. Catal. B: Environ.* **82** 219.

[213] Olak F C, Atar N and Olgun A 2009 *Chem. Eng. J.* **150** 122.

[214] Bayramoglu G, Altintas B and Arica M Y 2009 *Chem. Eng. J.* **152** 339.

[215] Merzouk B, Gourich B, Sekki A, Madani K, Vial Ch. and Barkaoui M 2009 *Chem. Eng. J.* **149** 207.

[216] Ahmad A L and Puasa S W 2007 *Chem. Eng. J.* **132** 257.

[217] Lei L C, Dai Q Z, Zhou M H and Zhang X W 2007 *Chemosphere* **68** 1135.

[218] Meng Z D and Oh W C 2011 *Asian J. Chem.* **23** 847.

[219] Zhu L, Meng Z D, Chen M L, Zhang F J, Choi J G, Park J Y and Oh W C 2010 *J. Photo. Sci.* **1** 69.

[220] Konstantinou I K and Albanis T A 2004 *Appl. Catal. B: Environ.* **49** 1.

[221] Ravelli D, Donde D, Fagnoni M and Albini A 2009 *Chem. Soc. Rev.* **38** 1999.

[222] Chong M N, Jin B, Chow C W K and Saint C 2010 *Water Res.* **44** 2997.

[223] Hoffmann M R, Martin S T, Choi W Y and Bahnemann D W 1995 *Chem. Rev.* **95** 69.

[224] Sahinkaya E, Uzal N, Yetis U and Dilek F B 2008 *J. Hazard. Mater.* **153** 1142.

[225] Abe R 2010 *J. Photochem. Photobiol. C* **11** 179.

[226] Chan S H S, Wu T Y, Juan J C and Teh C Y 2011 *J. Chem. Technol. Biotechnol.* **86** 1130.

[227] Yu H, Liu R, Wang X, Wang P and Yu J 2012 *Appl. Catal. B: Environ.* **111-112** 326.

[228] Zhang Z, Wang W, Gao E, Sun S and Zhang L 2012 *J. Phys. Chem. C* **116** 25898.

[229] Zhang X, Zhang T, Ng J, Pan J H and Sun D D 2010 *Environ. Sci. Technol.* **44** 439.

[230] Liao J, Lin S, Zhang L, Pan N, Cao X and Li J 2011 *ACS Appl. Mater.* **4** 171.

[231] Wang X, Li S, Yu H, Yu J and Liu S 2011 *Chemistry* **17** 7777.

[232] Wang P, Wang J, Wang X, Yu H, Yu J, Lei M and Wang Y 2013 *Appl. Catal. B: Environ.* **132-133** 452.

[233] Yu J and Yu X 2008 *Environ. Sci. Technol.* **42** 4902.

[234] Shamim N and Sharma V K 2013 *Sustainable Nanotechnology and the Environment: Advances and Achievements* (ACS Symposium Series; American Chemical Society: Washington, DC) p 201-229.

[235] Poulios I, Makri D and Prohaska X 1999 *Global Nest J.* **1** 55.

[236] Carraway E R, Hoffman A J and Hoffmann M R 1994 *Environ. Sci. Technol.* **28** 786.

[237] Baruah S, Rafique R F and Dutta J 2008 *Nano* **3** 399.

[238] Vanheusden K and Warren W L 1995 *Appl. Phys. Lett.* **67** 1280.

[239] Ullah R and Dutta J 2008 *J. Hazard. Mater.* **156** 194.

[240] Colis S, Bieber H, Bégin-Colin S, Schmerber G, Leuvrey C and Dinia A 2006 *Chem. Phys. Lett.* **422** 529.

[241] Wang R, Xin J H, Yang Y, Liu H, Xu L and Hu J 2004 *Appl. Surf. Sci.* **227** 312.

[242] Xu F, Shen Y, Sun L, Zeng H and Lu Y 2011 *Nanoscale* **3** 5020.

[243] Banfield J F, Welch S A, Zhang H, Ebert T T and Penn R L 2000 *Science* **289** 751.

[244] Liao Z M, Lu Y, Wu H C, Bie Y Q, Zhou Y B and Yu D P 2011 *Nanotechnology* **22** 375201.

[245] Zhang A Q, Zhang L, Sui L, Qian D J and Chen M 2013 *Cryst. Res. Technol.* **48** 947.

[246] Coronado J M, Fresno F, Hernández-Alonso M D and Portela R 2013 *Design of Advanced Photocatalytic Materials for Energy and Environmental Applications* (Springer, London) p 106.

[247] Miao T T, Guo Y R and Pan Q J 2013 *J. Nanopart. Res.* **15** 1725.

[248] Eskizeybek V, Sarı F, Gulce H, Gulce A and Avc A 2012 *Appl. Catal. B: Environ.* **119-120** 197.

[249] Seema H, Kemp K C, Chandra V and Kim K S 2012 *Nanotechnology* **23** 355705.

[250] Pons A J, Sagués F, Bees M A and Sørensen P G 2000 *J. Phys. Chem. B* **104** 2251.

[251] Dave M D and Pande U C 2013 *Chem. Sci. Trans.* **2** 749.

[252] Matsuoka M 1990 *Infrared Absorbing Dyes* (Plenum Press, New York) p 89.

[253] Salvador P, Garcia Gonzalez M L and Munoz F 1992 *J. Phys. Chem.* **96** 10349.

[254] Liu Y, Son W J, Lu J, Huang B, Dai Y and Whangbo M H 2011 *Chem. Eur. J.* **17** 9342.

[255] Warule S S, Chaudhari N S, Kale B B and More M A 2009 *CrystEngComm* **11** 2776.

[256] Lu Y, Wang L, Wang D, Xie T, Chen L and Lin Y 2011 *Mater. Chem. Phys.* **129** 281.

[257] Umar A, Chauhan M S, Chauhan S, Kumar R, Kumar G, Al-Sayari S A, Hwang S W and Al-Hajry A 2011 *J. Colloid. Interface Sci.* **363** 521.

[258] Tong Y, Cheng J, Liu Y and Siu G G 2009 *Scr. Mater.* **60** 1093.

[259] Sun L, Shao R, Chen Z, Tang L, Dai Y and Ding J 2012 *Appl. Surf. Sci.* **258** 5455.

[260] Conkey D B, Caravaca-Aguirre A M and Piestun R 2012 *Opt. Express* **20** 1733.

[261] Van Putten E G, Lagendijk A and Mosk A P 2011 *J. Opt. Soc. Am. B* **28** 1200.

[262] Lerosey G, De Rosny J, Tourin A and Fink M 2007 *Science* **315** 1120.

[263] Vellekoop I M and Aegerter C M 2010 *Opt. Lett.* **35** 1245.

[264] Cui M, McDowell E J and Yang C 2009 *Appl. Phys. Lett.* **95** 123702.

[265] Aulbach J, Gjonaj B, Johnson P M, Mosk A P and Lagendijk A 2011 *Phys. Rev. Lett.* **106** 103901.

[266] Vellekoop I M, Lagendijk A and Mosk A P 2010 *Nature Photon* **4** 320.

[267] Sebbah P 2001 *Waves and Imaging Through Complex Media* (Kluwer Academic Publishers, The Netherlands).

[268] Goodman J W 2007 *Speckle Phenomena in Optics: Theory and Applications* (Roberts & Company Publishers, Englewood).

[269] Vellekoop I M and Mosk A P 2007 *Opt. Lett.* **32** 2309.

[270] Vellekoop I M, Van Putten E G, Lagendijk A and Mosk A P 2008 *Opt. Express* **16** 67.

[271] Lee J Y, Hong B H, Kim W K, Min S K, Kim Y, Jouravlev M V, Bose R, Kim K S, Hwang I C, Kaufman L J, Wong C W, Kim P and Kim K S 2009 *Nature* **460** 498.

[272] Mason D R, Jouravlev M V and Kim K S 2010 *Opt. Lett.* **35** 2007.

[273] Kim M S, Scharf T, Haq M T, Nakagawa W and Herzig H P 2012 *Proc. SPIE* **8249** 82491B.

[274] Reihani S N S, Charsooghi M A, Khalesifard H R and Golestanian R 2006 *Opt. Lett.* **31** 766.

[275] Ippolito S B, Goldberg B B and Ünlü M S 2001 *Appl. Phys. Lett.* **78** 4071.

[276] Kim M S, Scharf T, Haq M T, Nakagawa W and Herzig H P 2011 *Opt. Lett.* **36** 3930.

[277] Wiersma D, Bartolini P, Lagendijk A and Righini R 1997 *Nature* **390** 671.

[278] Kop R H J, De Vries P, Sprik R and Lagendijk A 1997 *Phys. Rev. Lett.* **79** 4369.

[279] Van Soest G 2001 "*Experiments* on *Scattering Lasers*" University of Amsterdam, Amsterdam, Netherlands.

[280] Bret B 2005 "*Multiple light scattering in porous gallium phosphide"* University of Twente, Enschede, Netherlands.

[281] Popoff S M, Lerosey G, Carminati R, Fink M, Boccara A C and Gigan S 2010 *Phys. Rev. Lett.* **104** 100601.

[282] Vellekoop I M and Mosk A P 2008 *Phys. Rev. Lett.* **101** 120601.

[283] Choi Y, Kim M, Yoon C, Yang T D, Lee K J and Choi W 2011 *Opt. Lett.* **36** 4263.

[284] Workman Jr. J and Springsteen A W 1998 *Applied Spectroscopy: A Compact Reference for Practitioners* (Academic Press, San Diego) p 401.

[285] Bohren C F and Huffman D R 1998 *Absorption and Scattering of Light by Small Particles* (Wiley Science Paperback Series, Chichester, UK) p 8-10.

[286] Craig F, Bohren C F and Huffman D R 1983 *Absorption and Scattering of Light by Small Particles* (Wiley, New York) p 132-134.

[287] Cox A J, DeWeerd A J and Linden J 2002 *Am. J. Phys*. **70** 620.

[288] Bohren C F 2001 *Clouds in a Glass of Beer: Simple Experiments in Atmospheric Physics* (Dover Publications, Inc., New York) p 271-275.

[289] Stojanovic Z and Markovic S 2012 *Tech.–New Mater.* **67** 11 (Special Edition).

[290] Backman V, Gurjar R, Badizadegan K, Itzkan I, Dasari R R, Perelman L T and Feld M S 1999 *IEEE J. Sel. Topics Quantum Electron.* **5** 1019.

[291] Stuer M, Bowen P, Cantoni M, Pecharroman C and Zhao Z 2012 *Adv. Funct. Mater.* **22** 2303.

[292] Sze S 2002 *Semiconductor devices, physics and technology 2nd ed.* (John Wiley & Sons, New York, USA).

[293] Gateva S 2012 *Photodetectors* (InTech, Europe, China) p 6, ISBN: 978-953-51-0358-5.

[294] Zhan Z, Zheng L, Pan Y, Sun G and Li L 2012 *J. Mater. Chem.* **22** 2589.

[295] Soci C, Zhang A, Xiang B, Dayeh S A, Aplin D P R, Park J, Bao X Y, Lo Y H and Wang D 2007 *Nano Lett.* **7** 1003.

[296] Pan Z W, Dai Z R and Wang Z L 2001 *Science* **291** 1947.

[297] Lao C S, Liu J, Gao P X, Zhang L Y, Davidovic D, Tummala R and Wang Z L 2006 *Nano Lett.* **6** 263.

[298] Korotcenkov G 2008 *Mater. Sci. Eng.* R **61** 1.

[299] Seager C H and Myers S M 2003 *J. Appl. Phys.* **94** 2888.

[300] Sharma P, Sreenivas K and Rao K V 2003 *J. Appl. Phys.* **93** 3963.

[301] Arnold M S, Avouris P, Pan Z W and Wang Z L 2003 *J. Phys. Chem. B* **107** 659.

[302] Cheng B C, Ouyang Z Y, Chen C, Xiao Y H and Lei S J 2013 *Sci. Rep.* **3** 3249.

[303] Lai W C, Chen J T and Yang Y Y 2013 *Opt. Express* **21** 9643.

[304] Chen C Y, Huang J H, Lai K Y, Jen Y J, Liu C P and He J H 2012 *Opt. Express* **20** 2015.

[305] Zhang D H and Brodie D E 1994 *Thin Solid Films* **251** 151.

[306] Yeong K S, Maung K H and Thong J T L 2007 *Nanotechnology* **18** 185608.

[307] Mridha S and Basak D 2006 *Chem. Phys. Lett.* **427** 62.

[308] Gao W, Khan A, Berger P R, Hunsperger R G, Zydzik G, O'Bryan H M, Sivco D and Cho A Y 1994 *Appl. Phys. Letts.* **65** 1930.

[309] Su Y K, Chiou Y Z, Juang F S, Chang S J and Sheu J K 2001 *Jpn. J. Appl. Phys.* **40** 2996.

[310] Liu K, Sakurai M and Aono M 2010 *Sensors* **10** 8604.

[311] Lv Y, Pan C, Ma X, Zong R, Bai X and Zhu Y 2013 *Appl. Catal. B: Environ.* **138– 139** 26.

[312] Subramanian V, Wolf E and Kamat P V 2001 *J. Phys. Chem. B* **105** 11439.

[313] Asahi R, Morikawa T, Ohwaki T, Aoki K and Taga Y 2001 *Science* **13** 269.

[314] Liu J C, Bai H W, Wang Y J, Liu Z Y, Zhang X W and Sun D D 2010 *Adv. Func. Mater.* **20** 4175.

[315] Sibu C P, Kumar S R, Mukundan P and Warrier K G K 2002 *Chem. Mater.* **14** 2876.

[316] Padmanabhan S C, Pillai S C, Colreavy J, Balakrishnan S, McCormack D E, Perova T S, Gunko Y, Hinder S J and Kellys J M 2007 *Chem. Mater.* **19** 4474.

[317] Mane R S, Lee W J, Pathan H M and Han S H 2005 *J. Phys. Chem. B* **109** 24254.

[318] Cheng B C, Xiao Y H, Wu G S and Zhang L D 2004 *Adv. Funct. Mater.* **14** 913.

[319] Hao Y F, Meng G W, Ye C H and Zhang L D 2005 *Appl. Phys. Lett.* **87** 033106.

[320] Zeng H B, Duan G T, Li Y, Yang S K, Xu X X and Cai W P 2010 *Adv. Funct. Mater.* **20** 561.

[321] Cheng B C, Tian B X, Sun W, Xiao Y H, Lei S J and Wang Z G 2009 *J. Phys. Chem. C* **113** 9638.

[322] Zeng H B, Cai W P, Hu J L, Duan G T, Liu P S and Li Y 2006 *Appl. Phys. Lett.* **88** 171910.

[323] Cheng B C, Zhang Z D, Liu H J, Han Z H, Xiao Y H and Lei S J 2010 *J. Mater. Chem.* **20** 7821.

[324] Nayak J, Son M K, Kim J K, Kim S K, Lee J H and Kim H J 2012 *J. Electr. Eng. Technol.* **7** 965.

[325] Hu L, Zhu L, He H, Guo Y, Pan G, Jiang J, Jin Y, Sun L and Ye Z 2013 *Nanoscale* **5** 9577.

[326] Gogurla N, Sinha A K, Santra S, Manna S and Ray S K 2014 Sci. Rep. **4** 6483.

[327] Kind H, Yan H Q, Messer B, Law M and Yang P D 2002 *Adv. Mater.* **14** 158.

[328] Ok J G, Tawfick S H, Juggernauth K A, Sun K, Zhang Y Y and Hart A J 2010 *Adv. Funct. Mater.* **20** 2470.

[329] Liu S, Ye J F, Cao Y, Shen Q, Liu Z F, Qi L M and Guo X F 2009 *Small* **5** 2371.

[330] Wan Q, Li Q H, Chen Y J, Wang T H, He X L, Li J P and Lin C L 2004 *Appl. Phys. Lett.* **84** 3654.

[331] Li Q H, Gao T, Wang Y G and Wang T H 2005 *Appl. Phys.Lett.* **86** 123117.

[332] Ghosh T and Basak D 2009 *J. Phys. D: Appl. Phys.* **42** 145304.

[333] Feng X, Feng L, Jin M, Zhai J, Jiang L and Zhu D 2004 *J. Am. Chem. Soc.* **126** 62.